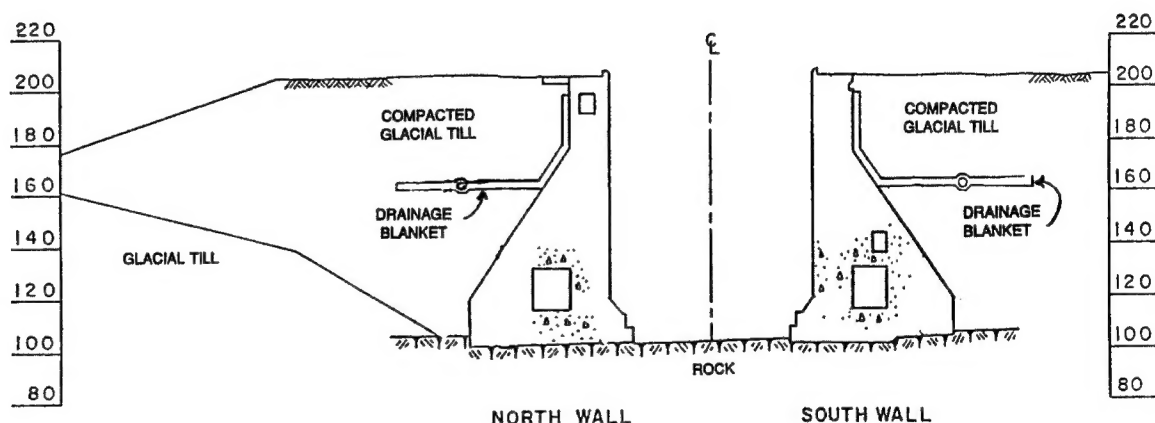Information Technology Laboratory

US Army Corps of Engineers®
Engineer Research and Development Center

Computer Aided Structural Engineering Project

Smeared and Discrete Crack Evaluations of a Lock Exhibiting Earth Pressure-Induced Cracking

Robert M. Ebeling, Robert C. Patev, and Guillermo A. Riveros

December 2001

NORTH WALL   SOUTH WALL

20020129 096

PRINTED ON RECYCLED PAPER

Smeared and Discrete Crack Evaluations of a Lock Exhibiting Earth Pressure-Induced Cracking

by   Robert M. Ebeling

Information Technology Laboratory
U.S. Army Engineer Research and Development Center
3909 Halls Ferry Road
Vicksburg, MS 39180-6199

Robert C. Patev

U.S. Army Engineer District, New England
696 Virginia Road
Concord, MA 01742-2751

Guillermo A. Riveros

Information Technology Laboratory
U.S. Army Engineer Research and Development Center
3909 Halls Ferry Road
Vicksburg, MS 39180-6199

Final report

Contents

List of Figures

List of Tables

Preface

The work described herein was sponsored by Headquarters, U.S. Army Corps of Engineers (HQUSACE), as part of the Civil Works Research and Development program on Structural Engineering (CWR&D). The research was initiated under Civil Works Unit 32837, "Computer-Aided Fracture Analysis of Concrete Gravity Structures" for which Dr. Robert M. Ebeling, Computer-Aided Engineering Division (CAED), Information Technology Laboratory (ITL), U.S. Army Engineer Research and Development Center (ERDC), was the Principal Investigator. The report was published under Civil Works Work Unit 31589, the "Computer-Aided Structural Engineering (CASE)" Project for which Dr. Stanley C. Woodson, Geosciences and Structures Laboratory (GSL), ERDC, is Problem Area Leader and Mr. H. Wayne Jones, Chief, CAED, is the Principal Investigator. The HQUSACE Technical Monitor is Mr. Jerry Foster, CECW-ED.

The research was performed at ITL by Dr. Ebeling and Mr. Guillermo A. Riveros, CAED, and by Mr. Robert C. Patev, U.S. Army Engineer District, New England. The report was written by Dr. Ebeling and Mr. Patev. Dr. Ebeling was the author of the scope of work for the original Civil Works Research Unit 32837, "Computer-Aided Fracture Analysis of Concrete Gravity Structures." This report was prepared under the direct supervision of Mr. Jones and Mr. Timothy D. Ables, Acting Director, ITL.

The authors are grateful to Mr. Anthony A. Bombich, Concrete and Materials Branch, Engineering Systems and Materials Division, GSL, and Dr. Barry Fehl, GEI Consultants, for discussions regarding the thermal material properties of the mass concrete used in Snell Lock.

At the time of publication of this report, Dr. James R. Houston was Director of ERDC, and COL John W. Morris III, EN, was Commander and Executive Director.

1   Introduction

The U.S. Army Corps of Engineers is responsible for designing and maintaining a large number of navigation and flood-control structures. Massive unreinforced concrete gravity walls serve many uses at many of these hydraulic structures. These concrete gravity structures are used as lock walls, are typically founded on rock, and are subjected to large differential water and earth loadings. These structures must maintain their internal structural integrity and be stable with respect to sliding and overturning. However, some rock-founded, unreinforced concrete gravity lock walls have experienced cracking as a result of earth loadings in excess of those anticipated during structural design. Examples of four such locks are discussed in Ebeling, Patev, and Mosher (1996). The objective of this study is to appraise two analytical procedures used to evaluate the potential for and/or the extent of cracking within massive concrete structures. The case history of Snell Lock on the St. Lawrence Seaway is used in this study. Snell Lock was chosen because it is one of the lock case histories in Ebeling, Patev, and Mosher (1996) for which the earth and water loadings and the engineering properties for the unreinforced mass concrete are well defined. A few years after the lock was put in service, a crack was found to extend from the landward-ceiling corner of the filling and emptying culvert through the mass concrete to the exterior backfilled face of the lock wall.

The two analytical procedures available for use in analyzing hydraulic structures that may exhibit cracking during loading are formulated based on either the smeared crack theory or the discrete crack theory. One procedure is based on the smeared crack theory and has been implemented in the computer program ANACAP (ANATECH Corporation 1997). The second procedure uses the discrete crack theory and has been implemented in the computer program MERLIN (Reich, Cervenka, and Saouma 1995).

Chapter 2 discusses the material specifications and design mixes for the mass concrete, the construction history, the loading history, and engineering material properties for Snell Lock and its backfill.

Chapter 3 discusses the results of a complete evaluation of crack potential of Snell Lock using smeared crack theory. Cracking potential and crack extent for the lock are assessed for both short-term end-of-construction earth loading and long-term earth and water loadings.

Chapter 4 discusses the results of an application of discrete crack theory to the evaluation of Snell Lock for both short-term earth loading and long-term earth and water loadings.

Chapter 5 summarizes the results of this research study and the application of both smeared crack theory and discrete crack theory to the case history of Snell Lock.

Appendix A presents the results of equilibrium calculations used to transform the earth (both horizontal and vertical shear) and water loadings from those acting along a plane extending vertically from the heel of the lock wall up through the backfill to those forces acting along the backfill-to-lock interface of the lock.

Appendix B summarizes the results from a limited literature survey of the results for unreinforced concrete laboratory specimens tested to failure. These test results are interpreted using discrete crack theory.

Appendix C presents figures showing the variations of the compressive strength results with time using data reported by Buck, Mather, and Thorton (1967) and by Mosher, Bevins, and Neeley (1991) for tests conducted on Snell Lock concrete specimens.

2 Snell Lock

2.1 Introduction

The Snell Lock was constructed between 1955 and 1958 as part of an international cooperative effort between the United States and Canada to build the Saint Lawrence Seaway. The project was placed in service in the spring of 1959. The U.S. portion of the project was authorized by the Wiley-Dondero Act of 13 May 1954. This act also created the Saint Lawrence Seaway Development Corporation (SLSDC) to construct, operate, and maintain the lock. SLSDC contracted with the U.S. Army Corps of Engineers to design and construct Snell Lock and its sister lock, Eisenhower.

The Snell and Eisenhower Locks are located in the Wiley-Dondero Canal portion of the Saint Lawrence River just north of Massena, NY. The locks are about 4 miles (6.4 km) apart, and together they allow vessels to transit around the Saint Lawrence Power Project.

The Snell and Eisenhower Locks have lifts of 45 to 49 ft (13.73 m to 14.95 m) and 38 to 42 ft (11.59 to 12.81 m), respectively. The chambers are 80 ft (24.4 m) wide and 860 ft (262.13 m) long from upstream miter gate to downstream miter gate, and the locks have 30 ft (9.15 m) of water depth over the sills.

2.2 The Lock Wall and Concrete Design Mixtures

Figure 2-1 shows a typical cross section through the chamber at Snell Lock. These two rock-founded gravity retaining structures composing the lock were designed in 1942 by the U.S. Army Corps of Engineers using then-state-of-the-art practices (U.S. Army Corps of Engineers 1942). The lock walls were designed as mass concrete structures. Buck, Mather, and Thorton (1967) and Mather (1967) provide details regarding the concrete mixtures and construction specifications for the lock walls. The following information is taken from these reports.

Each monolith is composed of about 40 percent interior grade concrete and 60 percent exterior grade concrete. Typical concrete mixtures are given in Table 2-1. The concrete mixtures for exterior grade concrete differ according to
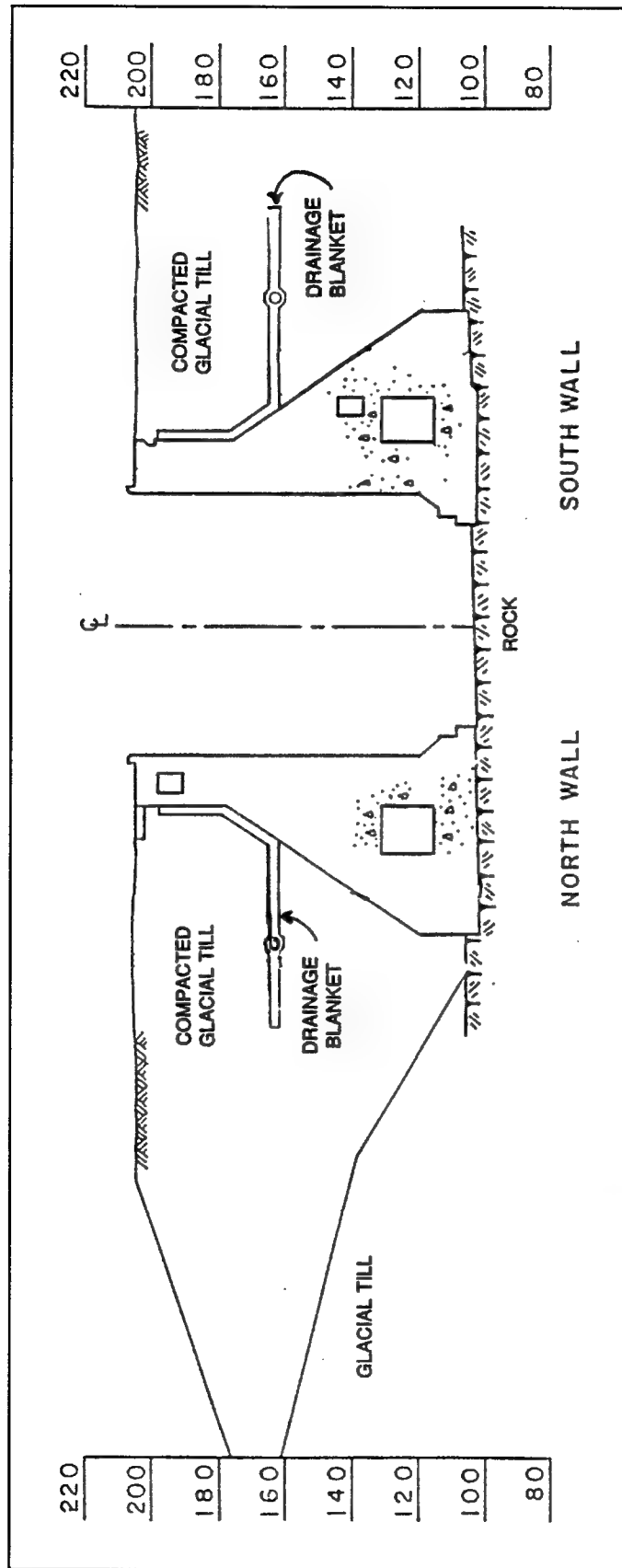
Figure 2-1. Typical cross section through the chamber at Snell Lock (elevations are in feet referred to the National Geodetic Vertical Datum. To convert to meters, multiply by 0.305 m)

Table 2-1
Typical Concrete Mixtures for Snell and Eisenhower Locks
(from Buck, Mather, and Thorton 1967)

Use	Exterior	Exterior	Interior
Maximum size aggregate, in.	6	3	6
Water-cement ratio, wt	0.49	0.49	0.64
Cement factor, bags/cu yd	3.80 to 3.88	4.20	2.75
Ratio of fine to total aggregrate, % by vol	23	28	23
Air, %[1]	6.1	5.7	6.2
Slump, in.	1-1/2 to 2-1/2	1-1/2 to 2-1/2	1-1/2 to 2-1/2

Note: 1 in. = 25.4 mm.
[1] In portion of concrete mixture smaller than the 1-1/2-in. sieve.

the maximum size aggregate being used, 6 in. (152.4 mm) or 3 in. (76.2 mm). More than 80 percent of the concrete contained 6-in. (152.4-mm) aggregate. Type II portland cement (moderate heat of hydration) was obtained from a number of sources. The specifications permitted the use of natural cement as a replacement for 25 percent by weight of the portland cement. The contractor for the Eisenhower Lock elected to use natural cement as a replacement for portland cement while the contractor for Snell Lock did not.

The use of interior concrete resulted in a reduction in heat evolution and ultimately a cost savings. Layers of concrete were required to be 20 in. (0.51 m) thick, and lifts were restricted to a height of 5 ft (1.52 m) in monoliths more than 16 ft (4.88 m) wide. It was required that 120 hours elapse between lifts. Concrete was required to be moist-cured 14 days, except in isolated cases where membrane-forming curing compounds were permitted. During cold weather the concrete was to be maintained at a temperature above 40 °F (4 °C) for at least 5 days and above freezing for the remaining 9 days of the 14-day curing period. Concrete was required to be at a temperature of at least 40 °F (4 °C) and not more than 60 °F (16 °C) when placed.

All concrete was air-entrained (Table 2-1). The coarse aggregate was crushed stone, and the fine aggregate was either crushed stone or natural sand or a combination of both. The crushed stone was dolomite from Beekmantown formation produced near Helena, NY, about 12 miles (19.3 km) from the jobsite. A natural sand was blended with manufactured sand during much of the work to facilitate compliance with grading requirements. The proportion of natural sand varied from 0 to 25 percent, and was greater near the completion of the work.

2.3 Dates of Construction of Lock Walls and Backfilling

Snell Lock was constructed during 1956 and 1957. The first construction season (1956) ended with the onset of winter and saw concrete placement for the two lock walls to within the region defined by the floor of the culverts. The last lift was placed on 9 November. No construction took place during the winter due to temperature restrictions on the curing of concrete imposed by the Corps of Engineers. Construction of the lock walls started again in the spring of 1957, and the last lift was placed 23 July. The remaining 90 to 95 percent of backfilling (in elevation) of the two lock walls commenced about this time.

2.4 Concrete Deterioration at Eisenhower Lock

The concrete deterioration problem at Eisenhower Lock has been linked to the natural cement used in the concrete mix. Recall that the mix at Eisenhower contained 25 percent by weight natural cement and 75 percent by weight portland cement. Based on a review of the available data and reports on the concrete deterioration, the mechanism of the concrete deterioration is freezing of water in the pores of the concrete. While the mechanism of the concrete deterioration is clear, the reason the concrete at Eisenhower Lock is less resistant to deterioration than the concrete at Snell Lock is less clear.

The concrete mixture at both Eisenhower and Snell Locks varies throughout the structures depending on the locations. The concrete mix design was the same at both locks except for the 25 percent by weight of natural cement. A detailed investigation of concrete at the two locks was conducted by the U.S. Army Engineer Waterways Experiment Station (Buck, Mather, and Thorton 1967).

Both the Corps (Buck, Mather, and Thorton 1967) and Harza Engineering Company (1981) cited the slow development of the strength of the concrete at Eisenhower Lock as the most plausible reason for the lower resistance to frost damage. The available evidence from the construction records and laboratory experiments shows that the Eisenhower concrete developed strength more slowly than did the Snell concrete. Based on the construction data, it would have taken about 12 and 37 days, respectively, for the Snell and Eisenhower exterior grade concrete made in 1956 to reach a strength of 3,000 psi (20.68 MPa) (Buck, Mather, and Thorton 1967).

It was required that the concrete be kept at a temperature above 40 °F (4 °F) for 5 days and above freezing for 14 days. Buck, Mather, and Thorton (1967) reported that climatological data at Eisenhower and Snell Locks show that the cores for the concrete placed 24-27 September and 2-26 October 1956 would have been subject to freezing at an age between 14 and 18 days. The exterior concrete at Eisenhower Lock placed during 1956 had an average 28-day compressive strength of 2,812 psi (19.39 MPa) compared with a 28-day compressive strength at Snell Lock of 3,954 psi (27.26 MPa). The results of tests of cylinders made during construction showed significant differences that

persisted to the greatest age at which such tests were made. For example, the 6-month averages were 3,810 psi (26.27 MPa) for Eisenhower and 5,080 psi (35.03 MPa) for Snell. Yet by 1966, samples of nondeteriorated concrete from comparable locations within Eisenhower and Snell Locks had compressive strengths approaching one another, 5,160 psi (35.58 MPa) (range 4,190 to 5,860 psi; 28.89 to 40.40 MPa) and 5,550 psi (38.27 MPa) (range 4,760 to 6,450 psi; 32.82 to 44.47 MPa), respectively (Buck, Mather, and Thorton 1967).

Buck, Mather, and Thorton (1967) regarded the slow development of concrete strength as the most probable reason for the low durability of the concrete at Eisenhower Lock. If the concrete had matured enough, it should have been just as frost resistant as the Snell concrete has proven to be in service. The freezing of the concrete with low frost resistance introduced additional void space, such as microcracks, that would not otherwise be present. This additional void space, in excess of the entrained air-void system, which had been provided for protection, would provide the location in which additional water could freeze and produce progressive deterioration of the concrete.

A second study of Eisenhower and Snell Locks was conducted in 1991 by Mosher, Bevins, and Neeley (1991). Six-in.- (152.4-mm-) diameter concrete cores were recovered over the entire height of six lock monoliths (four at Eisenhower Lock and two at Snell Lock). Figure 2-2 shows the compressive strengths measured on 19 samples taken from Eisenhower Lock and on 10 samples taken from Snell Lock. The compressive strengths averaged 5,230 psi (36.06 MPa) (range 4,070 to 6,050 psi; 28.06 to 41.71 MPa) and 6,620 psi (45.64 MPa) (range 3,730 to 8,590 psi; 25.72 to 59.23 MPa), respectively. The average compressive strength for the 1991 tests of cylinders taken from Snell Lock was more than 1,000 psi (6.89 MPa) greater than the average compressive strength measured in 1966. (The time-dependent variations of compressive strength for Snell Lock exterior and interior concrete mixes are presented in Appendix C.) However, the average compressive strengths were nearly the same in the 1966 and 1991 studies for Eisenhower Lock.

The lower average value for compressive strength at Eisenhower from the Mosher, Bevins and Neeley (1991) study is biased because of the larger number of test specimens from the lower portion of the wall compared with specimens from Snell, i.e., six from Eisenhower and only one from Snell. Comparing the average compressive strength from specimens taken from the upper portion of Eisenhower borings with the Snell average gives a difference of only 9 percent, which is approximately the same difference reported by Buck, Mather, and Thorton (1967).

Extensive concrete repairs have been made to the chamber faces, filling and emptying culverts, gate recesses, pintle bases, and sills at Eisenhower Lock. SLSDC has had an aggressive program to repair and replace deteriorated concrete. Mosher, Bevins, and Neeley (1991) concluded that the concrete deterioration at Eisenhower Lock will be a continuing problem.

Figure 2-2. Variation of concrete compressive strengths with depth (from Mosher, Bevins, and Neeley 1991) (1 ft = 0.305 m, 1 psi = 0.00689 MPa)

2.5 Culvert Cracks at Eisenhower and Snell Locks

In January 1967, during inspections of the Eisenhower Lock filling and emptying culverts by SLSDC and Corps of Engineers personnel immediately after winter dewatering, a continuous crack was observed along the landward-ceiling corner of the culvert in the north wall. Further investigation revealed that these cracks were continuous from the culvert through to the exterior backfilled face of the lock wall. At the time, the crack leaked water in varying amounts along its entire length, and fresh spalls of concrete were found lying on the culvert floor beneath it. Subsequent detailed inspections and other pertinent investigations revealed that the crack extended along the culvert between the upper and lower valve monoliths.

After initial discovery of the crack in the north culvert, a close inspection was made in the south culvert. The same kind of crack that existed in the north culvert was present in the south culvert, at its landward-ceiling corner, as shown in Figure 2-3. Its longitudinal extent was the same as that of the north culvert
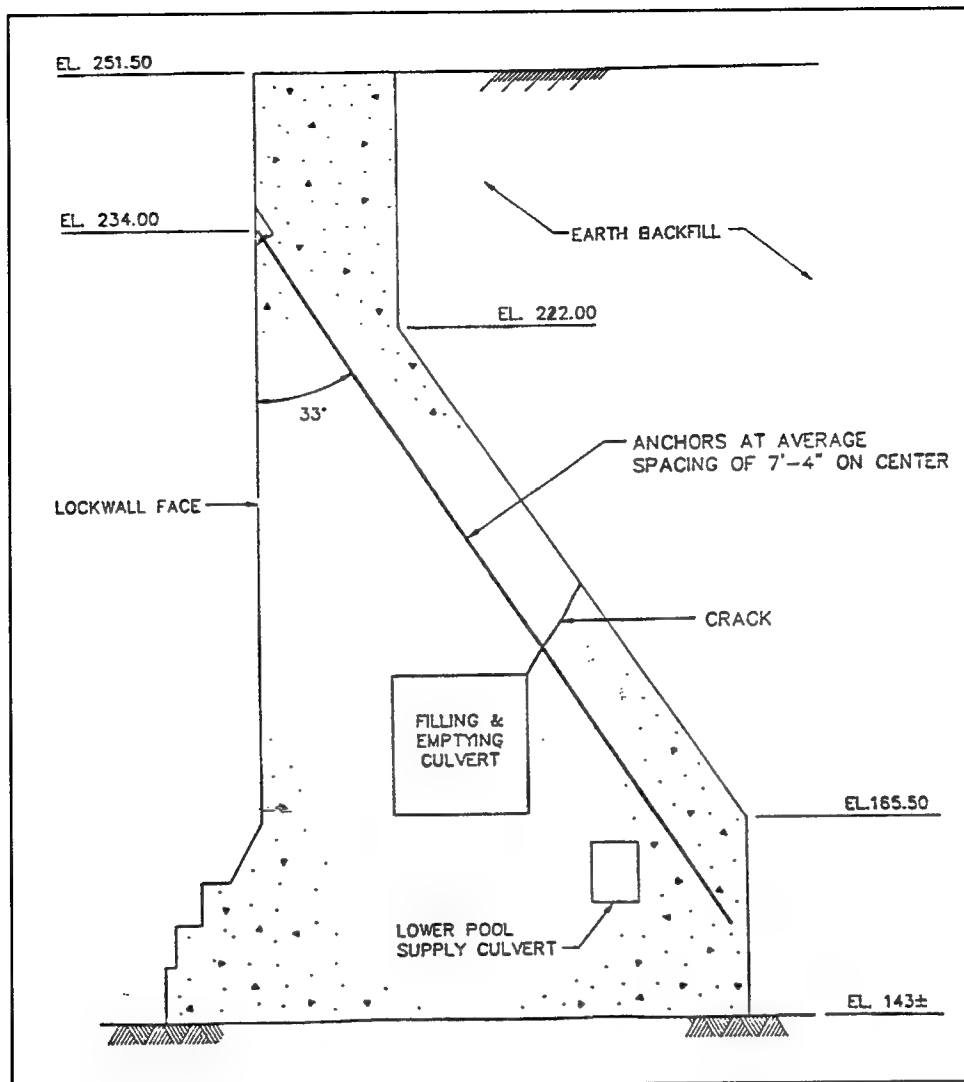
Figure 2-3. Typical section through south wall chamber monoliths at
Eisenhower Lock (from Mosher, Bevins, and Neeley 1991)
(1 ft = 0.305 m) (not to scale)

crack. Examination of the Snell Lock culverts revealed similar cracks in that
lock.

With these cracks extending through to the backfill, the overall stability of
the lock walls became a matter of serious concern. Under certain conditions, all
wall loads must be taken on the 15-ft- (4.57-m-) thick section (approximate
dimension) between the culverts and the faces of the lock chambers. This was
thought to be especially serious at Eisenhower Lock where portions of this
section were deteriorated and, thus, less capable of supporting the imposed loads.
The core boring program underway concerning the problem of deterioration was
enlarged to include exploration of these cracks. To obtain additional data on the
extent of the cracks and condition of the surrounding concrete, joint meters were
installed across the cracks to measure changes in the size of the cracks during

lock operations. Bar joints were installed across the lock chambers to measure relative movements of the lock walls, and an inclinometer was used to measure tilting of the lock walls during operation. Alignment control was set up to measure any lateral displacement of the wall, and piezometers were installed in the backfill areas to provide information on saturation levels and drainage patterns. Correlated flow measurements were taken of flows in the backfill drains.

Based on this information and the information gained by the 1966-67 concrete survey, a determination was made by an SLSDC-convened Board of Consultants that a complete rehabilitation program was necessary to guarantee continued structural integrity and stability and to assure ability to operate the locks. In a letter of June 26, 1967, from the Administrator, the Corps of Engineers was requested to perform the necessary design and contracting services concerning the proposed rehabilitation program for the Eisenhower and Snell Locks to restore the locks to a condition of full stability.

Priority was given to Eisenhower Lock. The rehabilitation work for the crack consisted of placing post-tensioned anchors across the culvert crack (both walls). This was accomplished during the winter shutdown of 1967-68 by contract with Peter Kiewit and Sons. Similar post-tensioned anchors were placed across the culvert cracks at Snell Lock during the winter of 1968-69 under contract with Morrison-Knudsen.

2.6 Rehabilitation of Eisenhower and Snell Locks Using Post-Tensioned Anchors

The north and south walls of the Eisenhower and Snell Locks have 14 monoliths with narrow tops and sloping backs. Figure 2-1 shows a typical section for Snell Lock. These walls in the chamber portion of the locks are 606 ft (184.7 m) long. Eighty-two and eighty-three anchors were installed in the north and south walls, respectively, of each lock (Figure 2-3). Six 636-kip (2,829-kN) anchors were installed in each monolith at an average spacing of 7.33 ft (2.23 m).

Review of data and stability analyses shows that the saturation level in the backfill was at el[1] 221.0 ft (67.36 m) at the time of anchor installation. This elevation is 16 ft (4.88 m) higher than was designed for originally. A field inspection of drainage pipe and dye tracing study of the drainage blanket conducted in 1986 by Gannett Fleming Geotechnical Engineering, Inc. (1986), Harrisburg, PA, shows the drainpipe to be operational and continuous. From historical data and recent observations it was determined that the static groundwater level is at the drain invert in the drainage blanket for the soil below the blanket. These data also show that the soil is saturated up to 18 ft (5.49 m) above the drain in the same locations. These high piezometer levels observed in the upper portion are the result of a perched water table fed by the water level in

---

[1] All elevations (el) cited herein are in feet referred to the National Geodetic Vertical Datum (NGVD). To convert elevations to meters, multiply by 0.305.

the natural soil. While the drainage blanket and pipe are functioning, they are not connected to the soil above the drainage blanket.

In February 1989, SLSDC and the Corps of Engineers conducted an anchor investigation program at Eisenhower Lock. The objective of the investigation was to determine whether the post-tensioned anchors in the chamber monoliths at Eisenhower Lock had sustained any significant corrosion due to water leakage through the existing culvert cracks. Of the 165 anchors in Eisenhower Lock, two anchors were examined, one in Monolith N-51 and one in Monolith S-17, at locations near the greatest amount of leakage through the existing culvert cracks. Significant corrosion was considered to have the greatest potential at these locations. The investigation consisted of excavating the concrete from inside the culvert to expose a short section of each anchor for visual inspection and dimensional measurements.

Results of the anchor investigation showed that the grout was intact and completely surrounded with the anchor strands in the exposed areas. The anchor strands were observed to be as shiny as new and there was no evidence of any surface corrosion or pitting. The results of this investigation showed that the anchors were in excellent condition. It was further concluded that post-tensioned anchors in Eisenhower Lock should remain structurally sound and should adequately serve the anticipated life expectancy of the lock. It was concluded that in any future structural evaluation of the lock, the existing anchors should be assumed 100 percent effective.

2.7 Splitting Tensile Test Measurements

Thirty-one of the 6-in.- (152.4-mm-) diameter concrete cores recovered in the 1991 study by Mosher, Bevins, and Neeley were used to measure the splitting tensile strength of the concrete that composes the Eisenhower and Snell Locks. Figure 2-4 shows the distribution with elevation of the tensile splitting strengths measured on 21 samples taken from Eisenhower Lock and on 10 samples taken from Snell Lock. The tensile splitting strengths averaged 581 psi (4.01 MPa) (range 390 to 790 psi; 2.69 to 5.45 MPa) and 650 psi (4.48 MPa) (range 495 to 930 psi; 3.41 to 6.41 MPa), respectively.

2.8 In-Place Backfill Densities and Design Earth Pressures

The four rock-founded, massive gravity retaining structures composing the two locks were designed in 1942 by the U.S. Army Corps of Engineers using then-state-of-the-art practices (U.S. Army Corps of Engineers 1942). The horizontal earth pressures used in the designs assumed an equivalent fluid pressure of 33 psf and 93 psf per foot (5.18 and 14.6 kPa per m) of depth for the moist and submerged glacial till, respectively (U.S. Army Corps of Engineers 1942 or Diviney 1990).
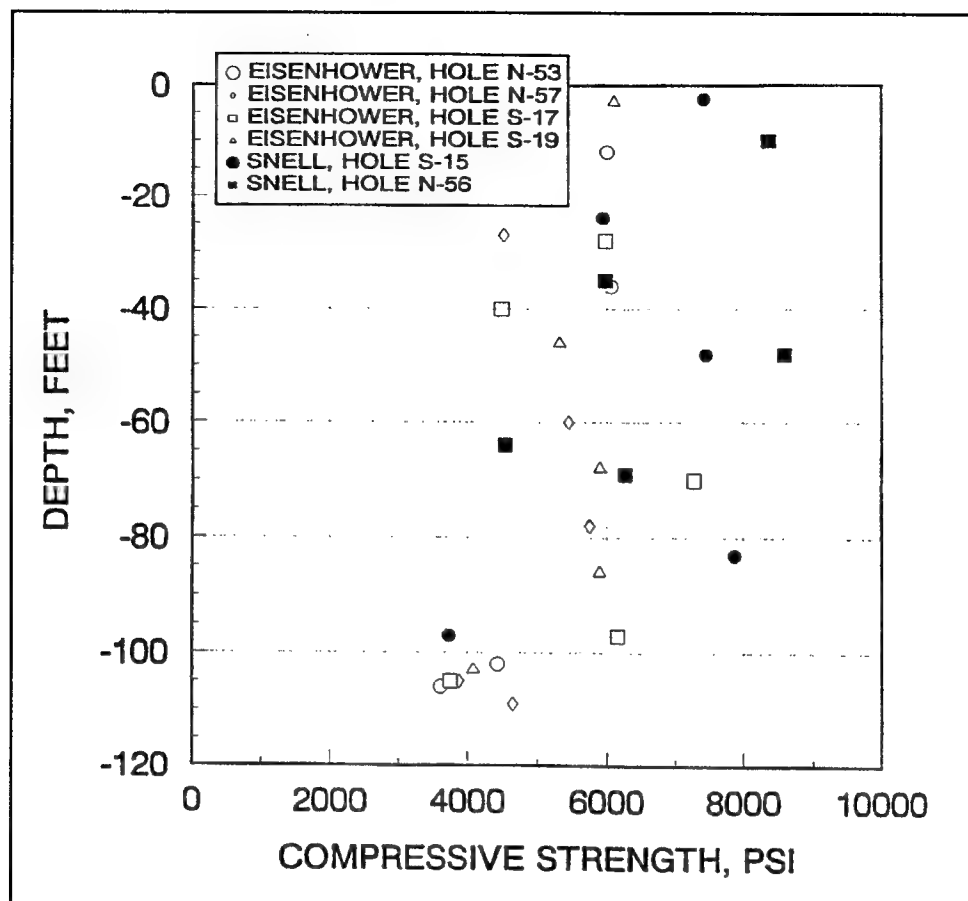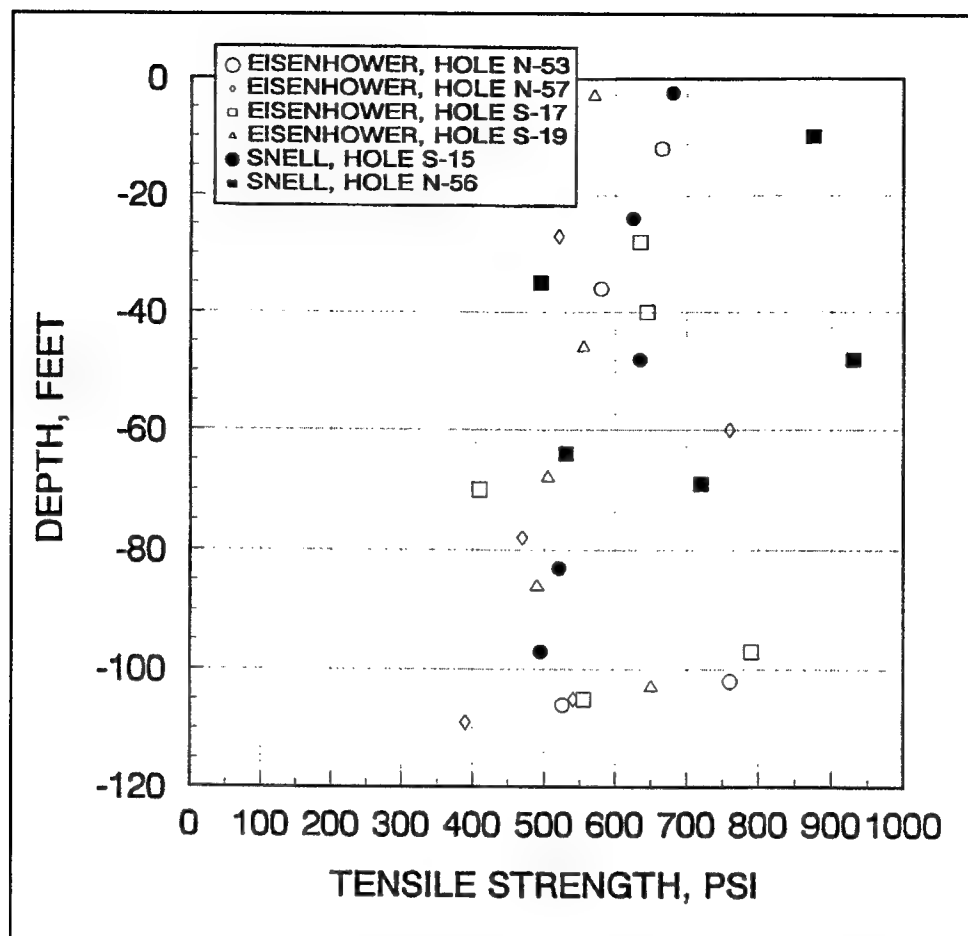
Figure 2-4. Variation of concrete tensile strengths with depth (from Mosher, Bevins, and Neeley 1991) (1 ft = 0.305 m, 1 psi = 0.00689 MPa)

The size of the excavations during construction of the locks was significant given the size of the monoliths (Figure 2-1). The excavated glacial till, consisting of fine to coarse gravel and fine to coarse sand with some silt, was stockpiled at the respective sites. The glacial till at Snell Lock is more fine grained than the till at Eisenhower Lock (gradation curves in Figure 2, Diviney (1990)). Backfilling commenced immediately after construction of the monoliths was completed. Large off-road dump trucks and heavy, self-propelled and dozer-drawn compactors were used to place and compact the backfill (Diviney 1990).

The in-place density of the backfill soil has been a point of controversy for some time because of the high values measured by in situ tests. Assumed moist densities from previous studies have ranged from 125 pcf (2,002.3 kg/m^3) in the 1957 Corps Design Memorandum (U.S. Army Engineer District, Buffalo, 1957a, 1957b) to 140 pcf (2,242.6 kg/m^3) used in the Harza Engineering Company (1981) study. Measured backfill density values from in-place tests range from a low of 135.5 pcf (2,170.5 kg/m^3) to a high of 150.6 pcf (2,412.4 kg/m^3) (e.g., Empire Soils Investigation, Inc., 1985). Mosher, Bevins, and Neeley (1991) evaluated all available information on density measurements at both locks and

assigned total unit weights of 140 pcf (2,242.6 kg/m^3) and 148 pcf (2,370.7 kg/m^3) to the backfill soils of Eisenhower and Snell Locks, respectively, for their soil-structure interaction analyses of the two locks. When these values are used for the unit weights of soil backfill, the equivalent fluid pressures used in the design of the two locks correspond to horizontal earth pressure coefficient K_h values between 0.21 and 0.24 for moist and submerged backfill soils. A total unit weight equal to 148 pcf (2,370.7 kg/m^3) is used in this analytical study of Snell Lock.

2.9 In Situ Horizontal Earth Pressure Investigations

In 1986 an in situ testing program was conducted using pressure meter testing (PMT) and hydrofracture testing (HF) in the backfill of the two locks to determine the state of horizontal (total) stress. Piezometers were also installed during the field investigations to determine the pore-water pressures within the backfills. Forty-three successful PMT tests were conducted in eight boreholes (four at each lock) made to 60-ft (18.3-m) depths through the backfill over the heel of the monoliths. Twenty HF tests were conducted in seven of the PMT test boreholes. Details regarding the tests, measurements, and their interpretation are described in Schmertmann (1986), Goldberg-Zoino and Associates (1986), Gannett Fleming Geotechnical Engineering, Inc. (1986), and Diviney (1990).

Figure 2-5 shows the variation in horizontal (total) stress σ_h with elevation from PMT and HF results for Snell Lock. The three dashed lines in this figure are the mean $\sigma_{h\,(mean)}$, mean plus standard deviation $\sigma_{h\,(mean+\sigma)}$, and mean minus standard deviation $\sigma_{h\,(mean-\sigma)}$ computed from the PMT data. The dashed line labeled σ_v shows the variation in total overburden pressure with elevation and is included for reference. The solid line designated as best estimate was reported in Diviney (1990), after Schmertmann (1986). (A companion figure showing the data from PMT and HF testing conducted at Eisenhower Lock is Figure 6 in Ebeling, Patev, and Mosher (1996).)

An independent statistical evaluation of the PMT test data shown in Figure 2-5 was made by Ebeling, Patev, and Mosher (1996) using weighting factors based on Schmertmann's interpretation of the data. Schmertmann's interpretation of the test data included a qualitative evaluation of each test (Schmertmann 1986 or Diviney 1990). He rated each data point as either very good, good, fair, or poor. A subjective weight equal to 1.0, 0.5, 0.25 or 0, respectively, was assigned to each data point according to Schmertmann's rating. Refer to Ebeling, Patev, and Mosher (1996) for details regarding the statistical approach and relationships used in this study.

The average, or more precisely, the expected value of the PMT data was computed and plotted in Figure 2-5 at each 10-ft (3.05-m) elevation increment, corresponding to the elevations at which the in situ tests were conducted. The standard deviation of the PMT data for Snell Lock is equal to 530 psf (25.3 kPa).
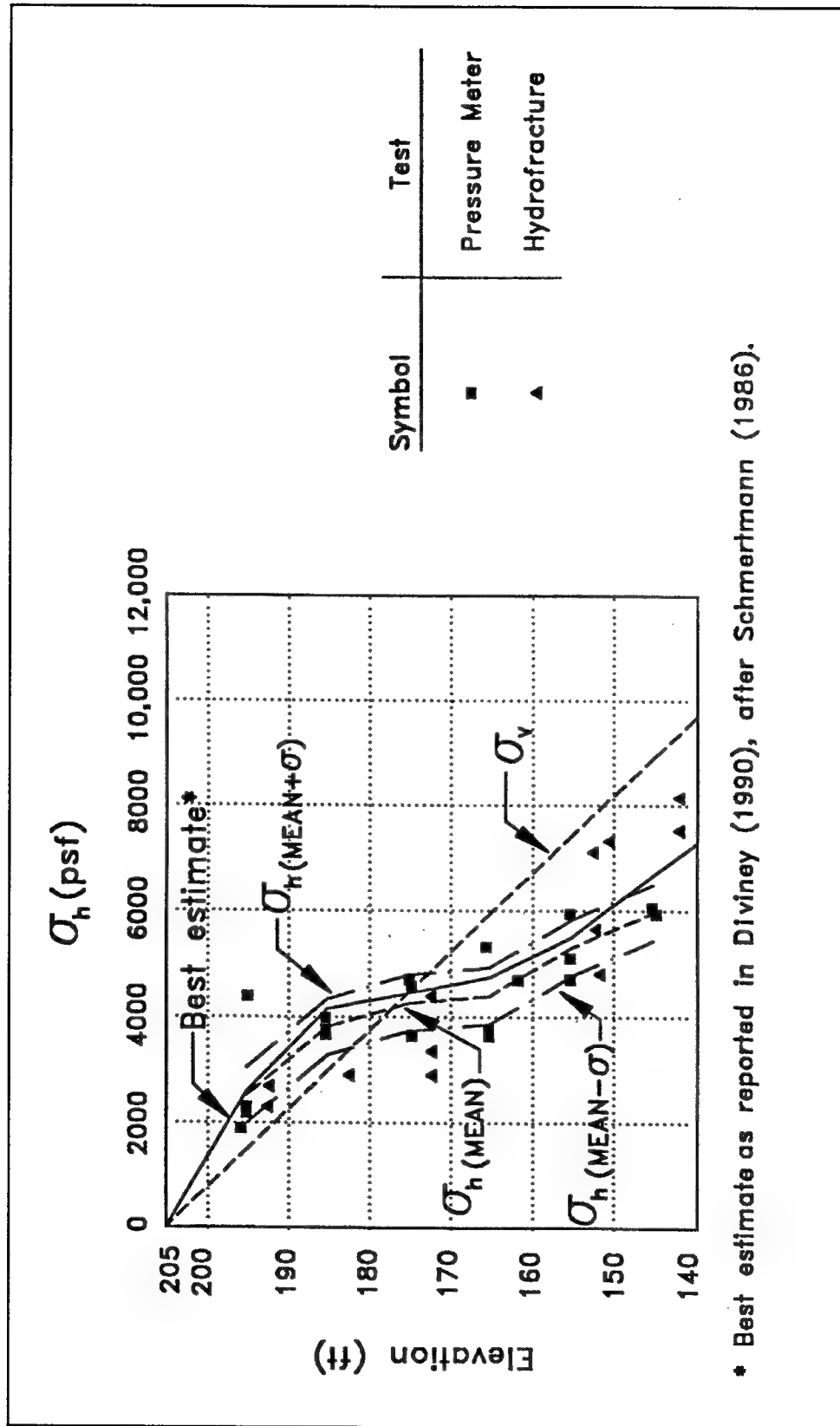
Figure 2-5. Horizontal stress from PMT and HT at Snell Lock (from Ebeling, Patev, and Mosher 1996) (1 ft = 0.305 m, 1 lbf/ft^2 = 0.00004788 MPa)

(The standard deviation of the PMT data was twice as large for Eisenhower Lock, 1,063 psf (50.9 kPa).)

Figure 2-5 shows the statistical evaluations made in the Ebeling, Patev, and Mosher (1996) study (with subjective weights assigned to each Snell Lock data point based on Schmertmann's qualitative evaluation of the test data) to be in agreement with the best estimate reported in Diviney (1990, after Schmertmann 1986). A similar conclusion was made by Ebeling, Patev, and Mosher for the Eisenhower lock data.

Twenty-eight vibrating wire piezometers were installed in selected boreholes at both locks. Data measured with this instrumentation were used to develop the distributions of pore-water pressures with elevation in the backfill of Eisenhower and Snell Locks (Ebeling, Patev, and Mosher 1996). Figure 2-6 shows the resulting distribution for Snell Lock. The piezometers indicated a perched water table approximately 30 ft (9.14 m) below the surface of the backfill at both locks. The water pressures are hydrostatic to the top of drains in the backfill at both locks. These drains, labeled as drainage blankets in Figure 2-1 for Snell Lock, are at midheight within the backfill (approximately). Hydrostatic water pressures were measured below the drains in the backfill.

The presence of the perched water table above the drains in the backfill was an unanticipated source of load on the two locks. However, the soil-structure interaction studies of the two locks by Mosher, Bevins and Neeley (1991) demonstrated that this factor alone could not have been responsible for the cracks in the four sections of lock walls.

Figure 2-6 shows the mean, mean plus standard deviation, and mean minus standard deviation of the horizontal total earth pressure σ_h computed from the PMT data by Ebeling, Patev, and Mosher (1996) for the two locks. The corresponding horizontal effective earth pressure σ'_h distributions are also shown in this figure.

Figure 2-7 (Ebeling, Patev, and Mosher 1996) shows the mean, mean plus standard deviation, and mean minus standard deviation of the horizontal effective earth pressure σ'_h for Snell Lock. The corresponding horizontal earth pressure coefficient K_h distributions are also shown in this figure. This figure also shows the distribution of vertical effective stress σ'_v used to calculate K_h values.

Figure 2-8 (Ebeling, Patev, and Mosher 1996) shows the statistical evaluations made in this study in terms of K_h for Snell Lock to be in agreement with the best estimate reported in Diviney (1990, after Schmertmann 1986).

In addition, Filz and Duncan (1992, 1996), using the Duncan and Seed (1986) compaction-induced earth pressure theory, applied their analytical model for simulating compaction-induced earth pressures to a model of Eisenhower and Snell Locks. Their results showed agreement with those PMT and HF test results when the heaviest compactor was used in the model.
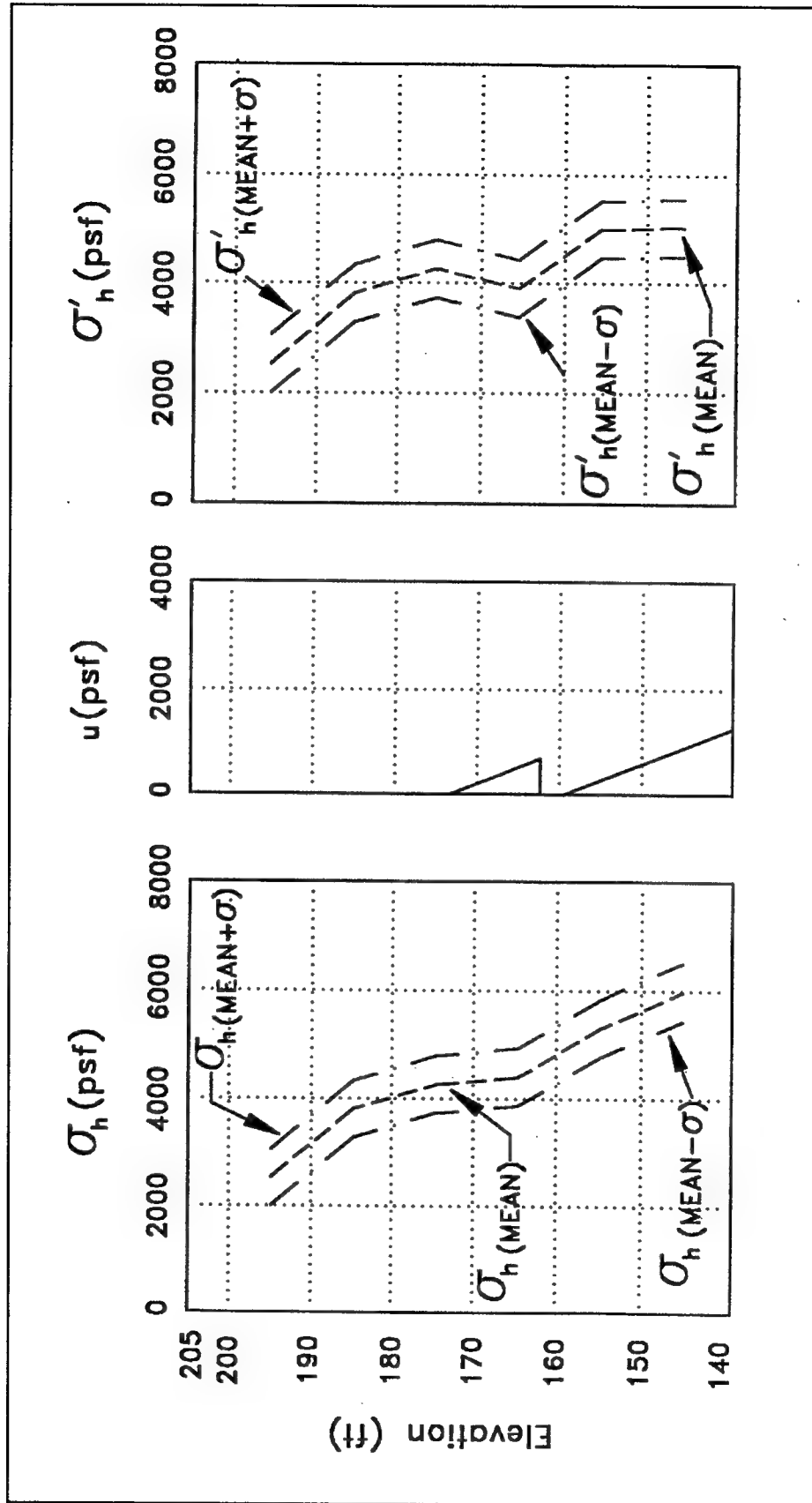
Figure 2-6. Distribution of σ_h, pore-water pressure u, and $\sigma_h{}'$ with elevation from statistical evaluation of PMT data at Snell Lock (from Ebeling, Patev, and Mosher 1996) (1 ft = 0.305 m, 1 lbf/ft^2 = 0.00004788 MPa)
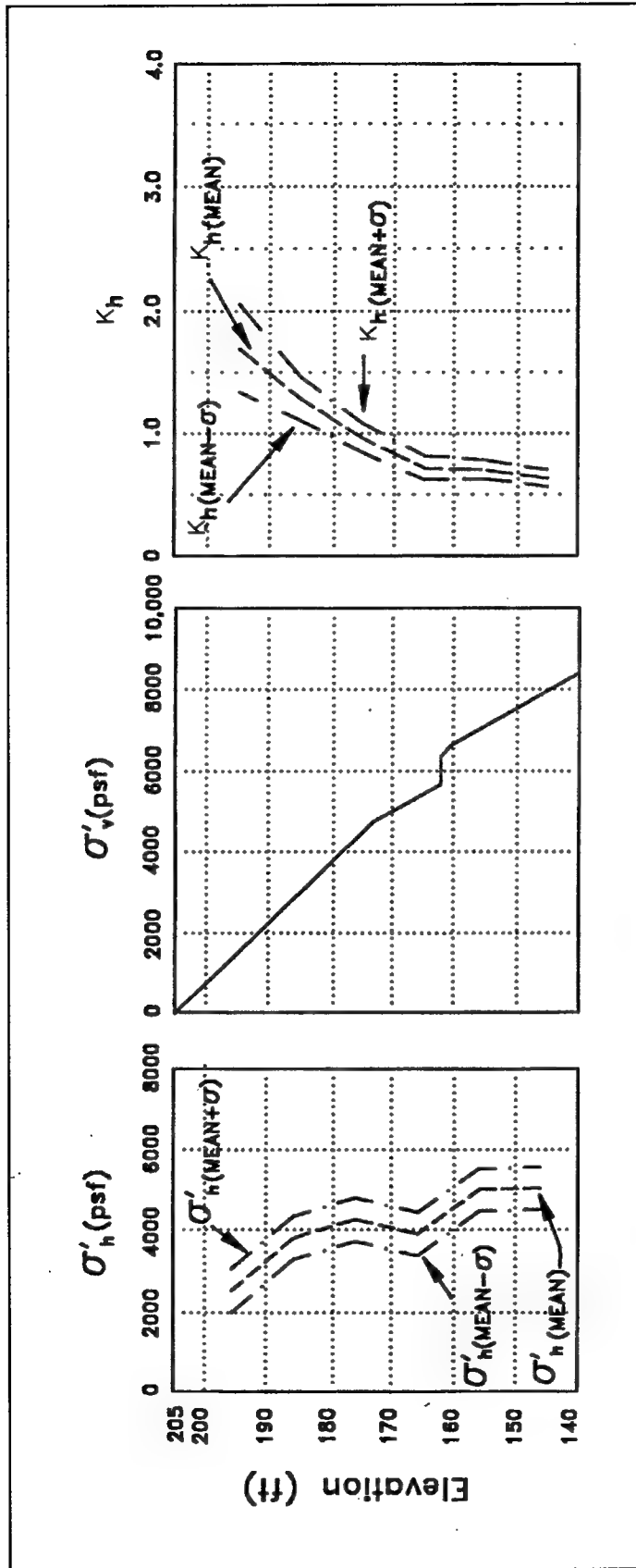
Figure 2-7. Distribution of σ_h', σ_v', and K_h with elevation from statistical evaluation of PMT data at Snell Lock (from Ebeling, Patev, and Mosher 1996) (1 ft = 0.305 m, 1 lbf/ft^2 = 0.00004788 MPa)
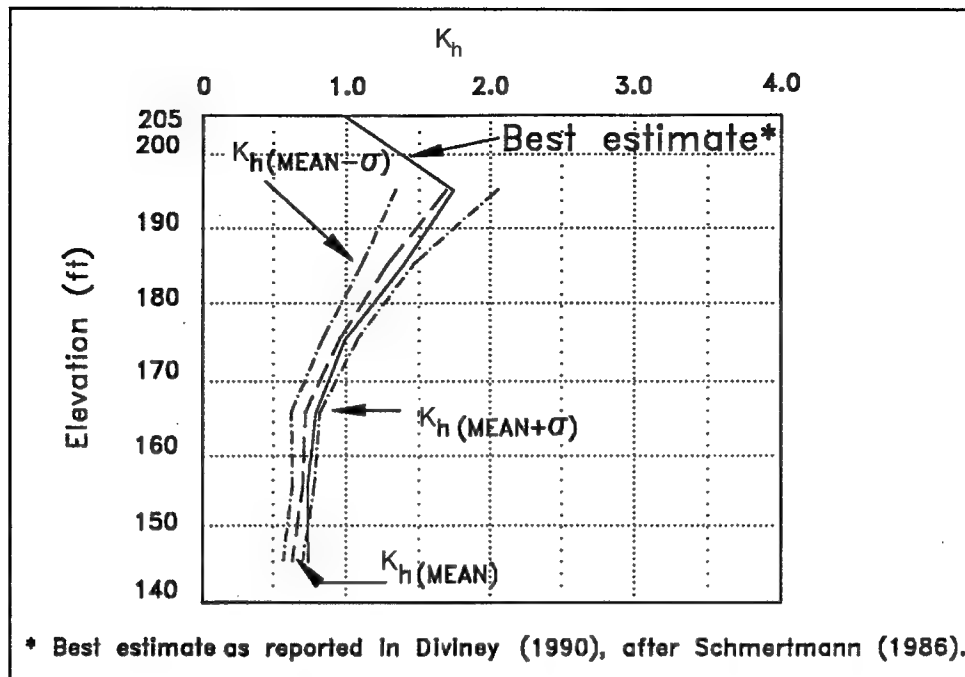
Figure 2-8. Distribution of K_h with elevation from statistical evaluation of PMT and HF data at Snell Lock (from Ebeling, Patev, and Mosher 1996) (1 ft = 0.305 m)

In summary, the statistical evaluations made of the PMT and HF data for Snell Lock by Ebeling, Patev, and Mosher (1996) show the best estimate of K_h reported in Diviney (1990, after Schmertmann 1986) to be a reasonable interpretation of the data. Thus the Diviney best estimate of K_h is used in the analyses to be discussed in subsequent chapters. The K_h profile exhibits high K_h values near the ground surface, which diminish with depth, reaching an asymptote of approximately 0.75 at depths of approximately 60 ft (18.29 m) in the Snell backfill and asymptotes to 0.71 in the Eisenhower backfill.

2.10 Conclusions of the Ebeling, Patev, and Mosher Study

Ebeling, Patev, and Mosher (1996) concluded that the primary means of loading that resulted in the cracking of the four culvert walls at Snell and Eisenhower Locks was the lateral earth loads. These structures were designed in the early 1940s as massive concrete structures using equivalent fluid pressures to account for the load imposed by the backfill. One index used by engineers to characterize the magnitude of earth pressures is the horizontal earth pressure coefficient K_h. The values for K_h corresponding to equivalent fluid pressure used in the design of the lock walls range from 0.21 to 0.24. The results from in situ testing (PMT and HF tests) at Snell Lock show K_h to range from 0.75 to 1.75, depending upon elevation within the backfill (Figure 2-8). (The results from in situ testing at Eisenhower Lock show K_h to range from 0.71 to 2.15.) The overcompaction of the backfill resulted in earth pressures larger than those

anticipated during the design of the lock walls by factors ranging from 3 to 10, depending on the elevation in the backfill.

Rehabilitation was accomplished using 165 post-tensioned anchors installed in all four walls of Snell and Eisenhower Locks. Six 636-kip (2,829-kN) anchors were installed in each monolith at an average spacing of 7.33 ft (2.23 m).

2.11 Cross-Section Used in the Smeared and Discrete Crack Analyses

Snell Lock Monolith N-56, approximately midway along the 860-ft- (262.13-m-) long lock chamber was selected for analysis. The geometry of this monolith is representative of those defining the lock chamber at Snell.

Figure 2-9 shows a cross section of Monolith N-56. Monolith N-56 is 101 ft (30.78 m) high and has a base width equal to 62 ft (18.9 m), corresponding to a base-to-height ratio of 0.61. The top of backfill is level with the top of the lock, el 205. The base of Monolith N-56 is at el 104. The backfill-to-monolith interface extends vertically from the heel of the monolith to el 120. Above this elevation the thickness of the monolith decreases with elevation. Starting at el 120 the monolith-to-backfill interface is inclined at an angle of 35.18 deg from vertical to el 176.75. Between el 176.75 and the top of backfill, el 205, the monolith-to-backfill interface is vertical and the thickness of the monolith is a constant 16 ft (4.88 m). The top of the 15-ft- (4.57-m-) wide by 16-ft- (4.88-m-) high culvert used for filling and emptying the lock chamber is at el 132. The closest distance from the landward-ceiling corner of the filling and emptying culvert through the mass concrete to the exterior backfilled face of the lock wall is 14.34 ft (4.37 m).

Figure 2-9. The cross section of Snell Lock Monolith N-56 (1 ft = 0.305 m)

3   Smeared Crack Analysis of Snell Lock and Dam

3.1 Introduction

This chapter discusses the smeared crack analysis of Snell Lock Monolith N-56. This analysis was performed to investigate if the cracking potential of the mass concrete was present during the placement of the monolith. The primary focus of the modeling effort was to determine if the thermal stress regime and lift placement sequence including the eventual backfilling of the structure created the cracking that was discovered in Monolith N-56. These cracks had formed from the inner corner of the lower culvert to the inclined face of the landward surface. The crack typically ran a distance across the throat of approximately 14.34 ft (4.37 m) across.

The smeared crack theory uses a strength-of-materials approach to evaluate crack initiation potential and/or crack propagation in a material. According to the theory, cracks may develop on planes on which tensile strain and tensile stress act. The largest tensile strain(s) and stress(es) will develop on principal planes. In ANACAP, the finite element (FE) program used for this analysis, the potential for cracking is evaluated on the three principal planes at each integration point within every element composing the mesh for each stage of loading. ANACAP uses the strains acting on an infinitesimal cube at an integration point to determine the orientation of the three principal planes. If the material is isotropic and there is no pre-existing crack, then the three principal planes of strain and stress are coincident and can be determined from the stresses acting on the faces of an infinitesimal cube at the integration point. The principal values for tensile strain and tensile stress on each of the three principal planes are then compared to the smeared crack criterion specified for the material. Figure 3-1 shows an example of the criterion used in ANACAP. The diagonal line distinguishes crack initiation potential in Figure 3-1 and is defined by the two concrete material properties, the tensile fracture strain ε_s and Young's modulus $E(t)$. If any of these three pairs of principal strains and stresses is tensile (i.e., tensile fracture strains and tensile fracture stresses) and exceeds the diagonal solid line in Figure 3-1, a crack develops on that plane. Otherwise, no cracking occurs on that plane. Unlike linear elastic fracture mechanics, to be discussed in Chapter 4, crack initiation is an explicit aspect of smeared crack theory.
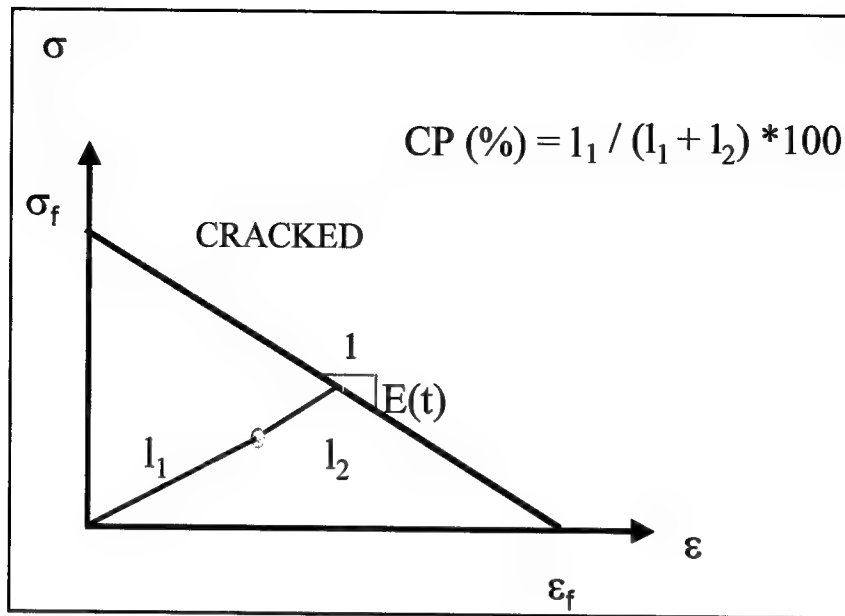
Figure 3-1. Cracking potential diagram

For this, a detailed two-dimensional FE model was developed that needed to account for both thermal and material properties of the concrete as well as the ambient air temperatures and form placement and removal at the monolith. The results from the FE model will focus on critical points during the construction sequence at Snell Lock: the end of construction season in 1956 and the winter of 1957, the final lift placement in June 1957, and placement and compaction of backfill in the fall of 1957. The cracking potential of mass concrete will be identified during these critical periods.

3.2 ANACAP Finite Element Program

The FE program utilized for the smeared crack analysis was the PC version of ANACAP (ANATECH 1997) developed by ANATECH Corporation of San Diego, CA. The ANACAP program is a specialized FE package that has been developed to perform thermal stress analysis with the capabilities to include nonlinear time rate for the modulus, creep, and shrinkage of young to mature mass concrete. Thermal stress analysis in ANACAP can be modeled using functions for ambient temperatures, volumetric heat generation, and convection boundary conditions.

Most important to this analysis, ANACAP calculates the cracking potential of the mass concrete. The principal tensile stress-tensile strain diagram for cracking potential is shown in Figure 3-1, and the formula for the cracking potential (CP) is determined by

$$CP \text{ (in percent)} = l_1 / (l_1 + l_2) * 100 \tag{3-1}$$

3.3 Finite Element Model of Snell Monolith N-56

The global FE mesh for Snell Monolith N-56 is shown in Figure 3-2. The two-dimensional model was developed with symmetry about the center line of the lock chamber. The model also includes sufficient foundation elements to reduce interference from the boundaries. In addition, the bottom and side edges of the FE model are restrained with a displacement boundary condition.
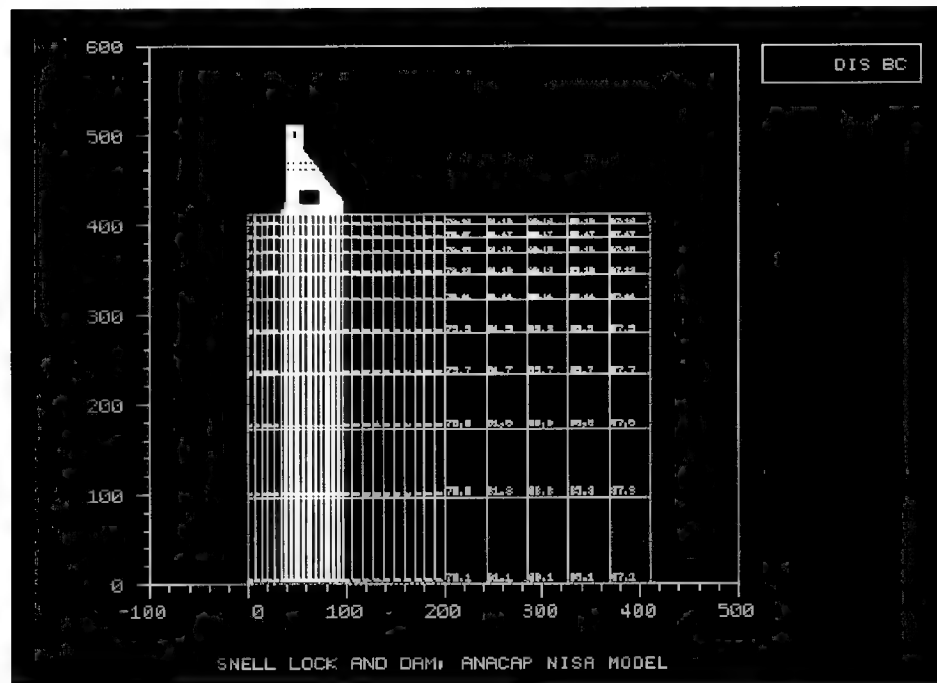
Figure 3-2. Global FE model for Snell Lock Monolith N-56

The local FE model of the lock Monolith N-56 is shown in Figure 3-3. The FE model accounts for thermal modeling in both the upper and lower culverts as well as exterior surfaces of the monolith. The FE model contains mainly quadilateral elements with height/width ratios of unity and a series of triangular elements on the inclined back slope of the monolith. In additon, the FE mesh has been refined in the area around the lower culvert to capture the stresses in the culvert region.

Figure 3-3 also shows the different concrete mixes that were used during construction. The green represents the placement of the 1956 concrete mix, and the blue represents the placement of the 1957 concrete mix.

3.4 Placement of Lifts

There were a total of 22 construction lifts in Snell Lock Monolith N-56. The average lift placement was 5 ft (1.5 m) in thickness. Table 3-1 describes the lift sequence number, lift height, and date of lift pour for Monolith N56. It is
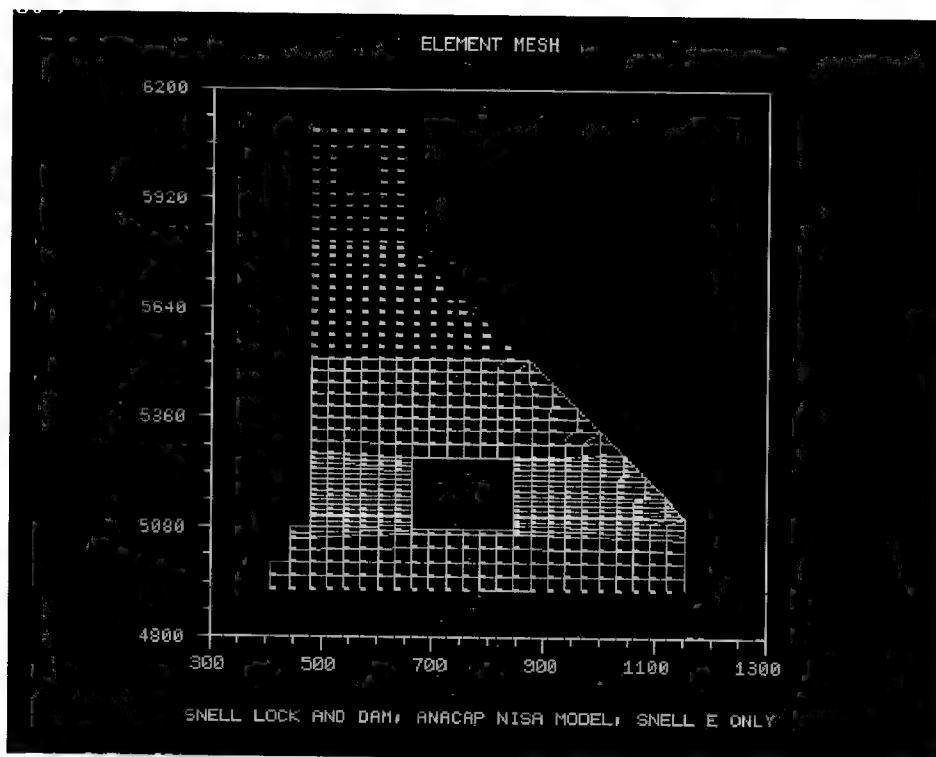
Figure 3-3. Local model of Snell Monolith N-56

interesting to note from Table 3-1 that the placement of concrete at the end of the 1956 construction season continued well into November. This might very well have played a large factor in leading to the cracking potential during the winter season.

Table 3-1 Lift Information for Snell Lock Monolith N-56		
Lift No. in FE Model (actual field lifts)	Lift Height, ft (m)	Date of Lift
1	6 (1.8)	8/7/56
2	5 (1.5)	8/10/56
3	4.5 (1.4)	9/15/56
4	4.5 (1.4)	9/20/56
5	4.5 (1.4)	10/3/56
6	4.5 (1.4)	10/08/56
7	5 (1.5)	10/17/56
8	5 (1.5)	11/02/56
9	5 (1.5)	11/07/56
10	5 (1.5)	11/21/56
11	5 (1.5)	4/08/57
12	5 (1.5)	4/12/57
13	5 (1.5)	4/17/57
14	5 (1.5)	4/23/57
15	5 (1.5)	4/29/57
16 (16,17)	10 (3)	5/03/57,5/8/57
17 (18,19)	10 (3)	5/17/57,5/24/57
18 (20, 21, 22)	7 (2.1)	6/11/57,6/15/57,6/18/57
Note: Top lifts where merged in FE model due to placement size limitations.		

The lifts of interest for the FE modeling were the completion of the construction season of 1956 and the winter of 1957 (August 1956 to April 1957), the end of final lift placement in 1957 (April 1957 to June 1957), and the compaction of the glacial till backfill in the summer of 1957. Figure 3-4 shows the first construction sequence with lift number, lift heights, and the number of hours between lifts. The final lift, Lift 10, was placed on 21 November 1956, and the partial monolith sat for a duration of 244 days until Lift 11 was poured.

el 153

Lift 10 (5 ft / 3312 hours)

Lift 9 (5 ft / 336 hours)

Lift 8 (5 ft / 120 hours)

Lift 7 (5 ft / 384 hours)

Lift 6 (4.5 ft / 216 hours)

Lift 5 (4.5 ft / 120 hours)

Lift 4 (4.5 ft / 312 hours)

Lift 3 (4.5 ft / 120 hours)

Lift 2 (5 ft / 864 hours)

Lift 1 (6 ft / 72 hours)
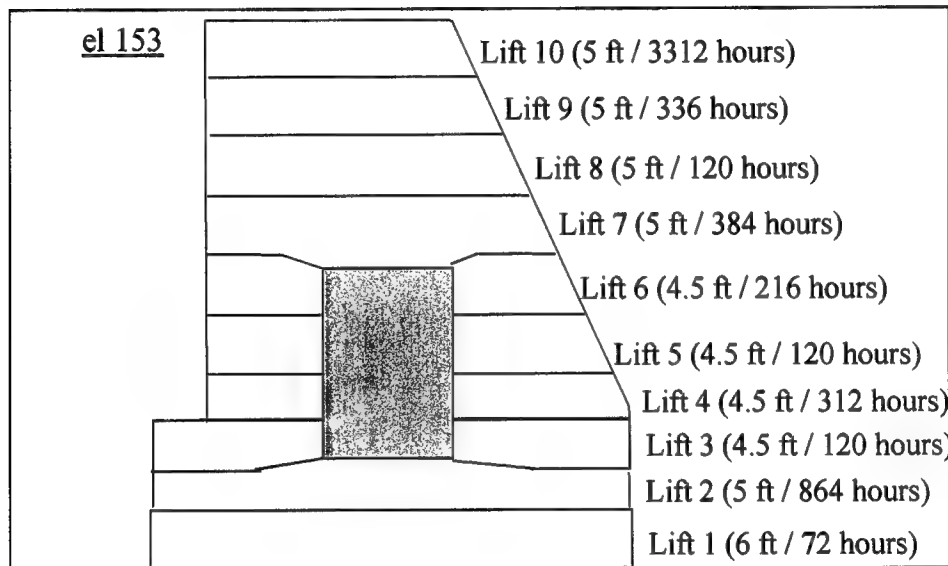
Figure 3-4. Construction sequence August 1956 - April 1957 (1 ft = 0.305 m)

Figure 3-5 shows the second construction sequence with lift number, lift heights, and the number of hours between lifts. The final lift, Lift 18 (actual lifts 20-22), was placed on 18 June 1956. The backfilling and compaction of the glacial tills were started right after final lift placement and completed before the fall of 1957. Figure 3-6 shows the completed Monolith N-56 with backfill.

3.5 Material Properties

The material properties for the concrete were determined from concrete mixture information and available design studies on Snell Lock. The concrete was a Type II cement with a dolomite aggregate and did not contain any pozzolans. The concrete at Snell Lock was batched into both an interior and exterior mix. The constituents for these mixes are shown in Table 3-2.

Compressive strength data over time were also available from construction records and testing and recent compressive tests performed by the U.S. Army Engineer Waterways Experiment Station in 1990 (Mosher, Bevins, and Neely 1991). From this information, a relationship for compressive strength for the concrete over time can be established for both mixes. Using the American Concrete Institute relationship (Equation C-2 multiplied by a scale factor of 1.49,
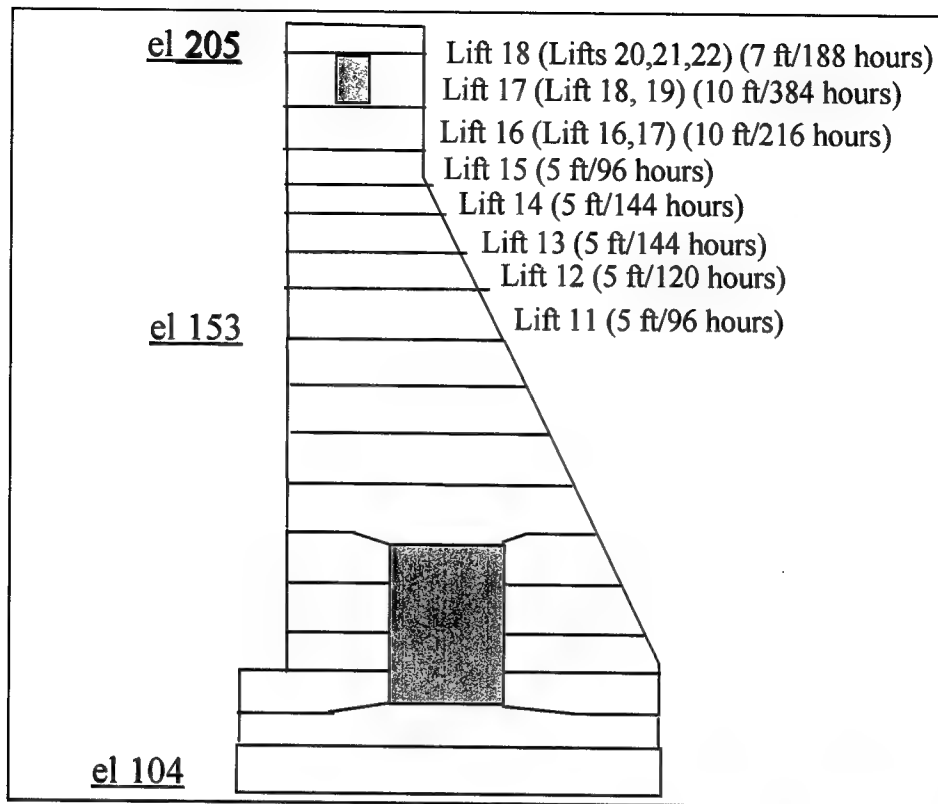
Figure 3-5. Construction sequence April 1957-June 1957 (1 ft = 0.305 m)
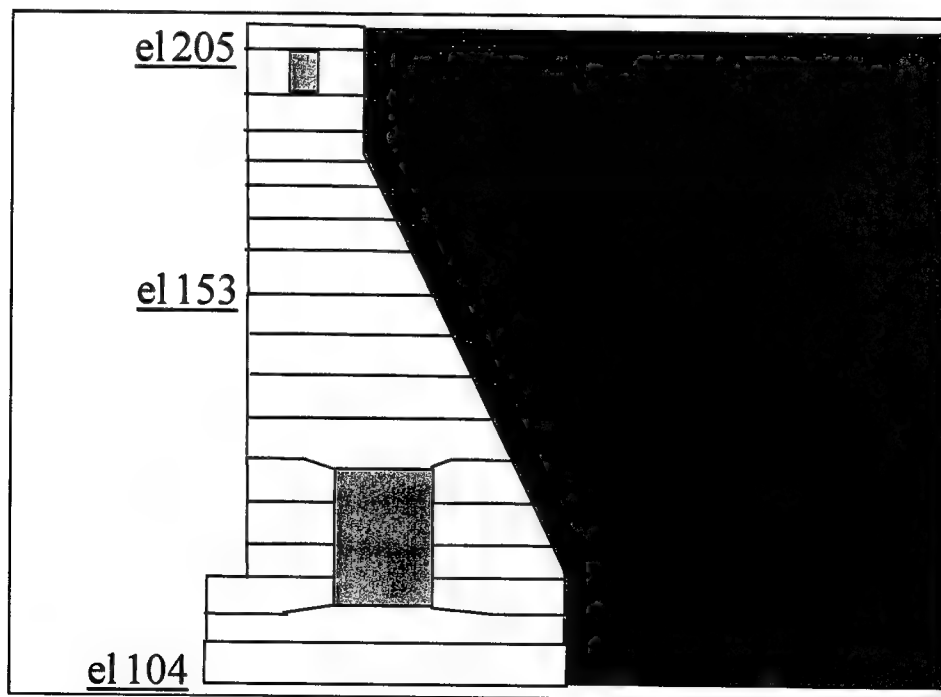
Figure 3-6. Construction sequence June 1957-Sept/Oct 1957

Table 3-2
Concrete Constituents for Snell Lock and Dam

Constituent	Exterior Mix	Interior Mix
Aggregate, maximum size, in.	6	6
Water-cement ratio, wt	0.49	0.64
Cement factor, bags/cu yd	3.8	2.75
Ratio of fine to total aggregate, % by volume	23	23
Air, %	6.1	6.2
Slump, in.	1.5 to 2.5	1.5 to 2.5
Coarse aggregate	Crushed stone	Crushed stone
Fine aggregate	Crushed or natural sand	Crushed or natural sand
Air-entraining mixture	Yes	Yes
Note: 1 in. = 25.4 mm		

as discussed in Appendix C) that estimates modulus of elasticity from compressive strength, the modulus values for the concrete mixes over time can be determined. These curves and the polynomial fits were used as functions in the FE model. These curves are shown in Figure 3-7 for the 1956 mix and Figure 3-8 for the 1957 mix. Also, for the simplification of the FE model, a 60/40 ratio of the mixes was assumed and calculated into the modulus curves.
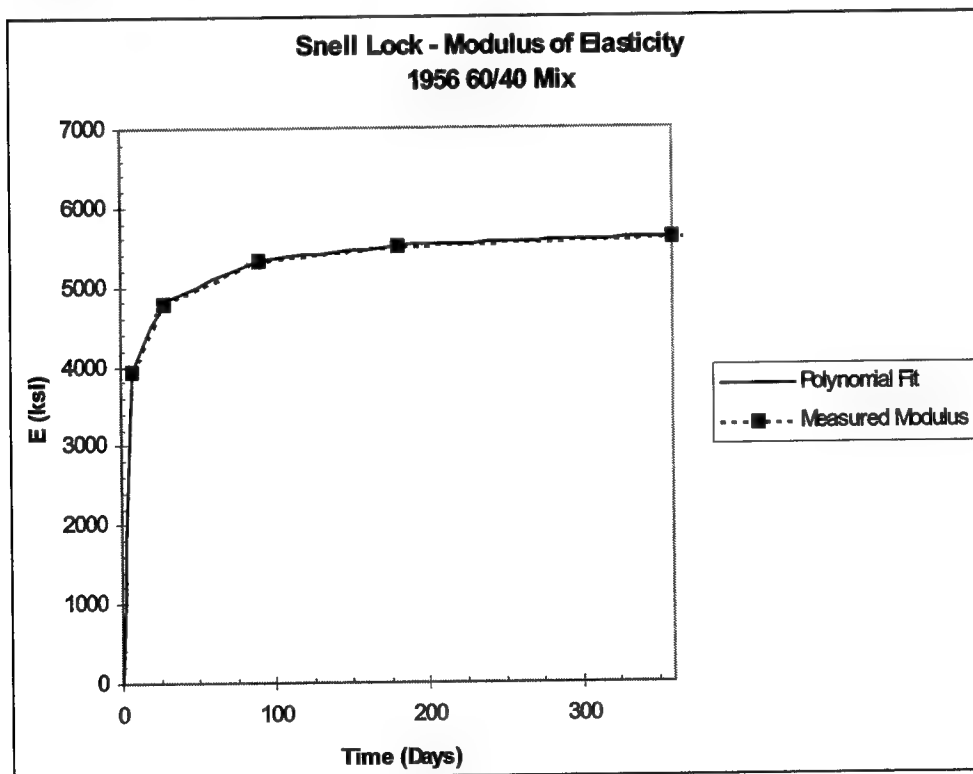
Figure 3-7. Modulus of elasticity curve for 1956 mix

Creep and shrinkage testing was not performed, and no information was available on the concrete mixes at Snell Lock. For these parameters, comparisons were made to previous Nonlinear Incremental Structural Analysis (NISA)
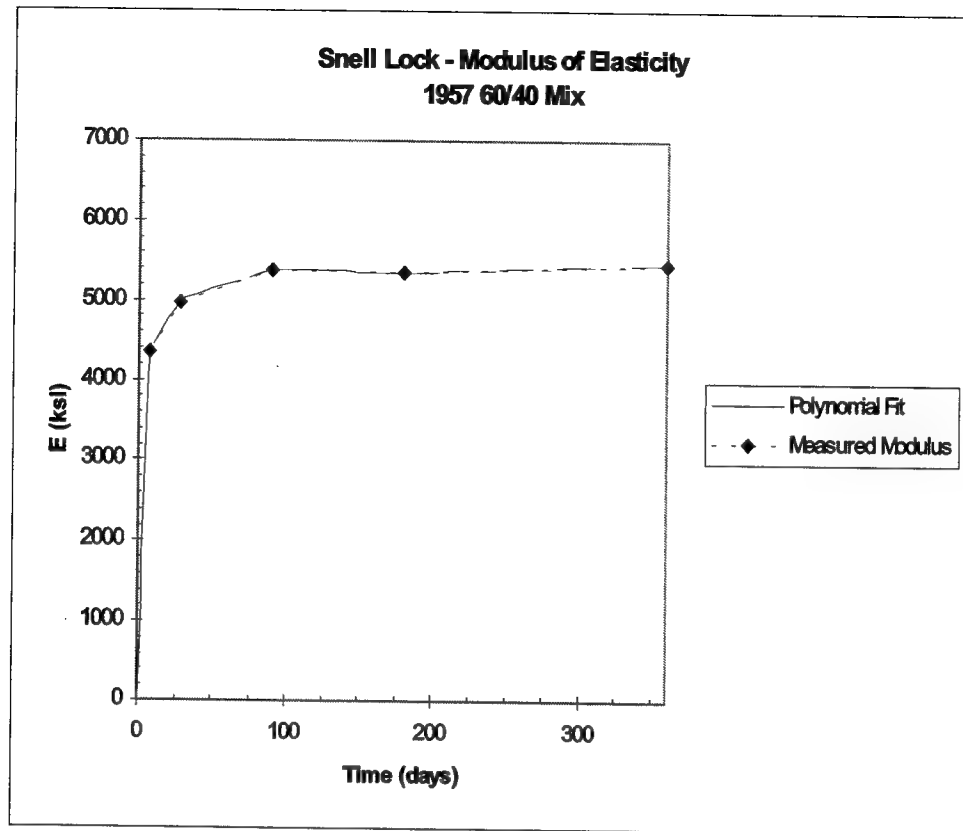
Figure 3-8. Modulus of elasticity curve for 1957 mix

modeling and laboratory testing on more recent lock construction projects. Based on the concrete type and constituents used at Snell Lock, the properties for creep and shrinkage in the FE model were based on the Olmsted 3- and 14-day mixes. In addition, variations to the creep and shrinkage were investigated and led to minimal varying of results. This information in conjunction with the modulus is incorporated in the ANACAP model through a **young.mix** file.

Density data were also available in Design Memorandum 7 for Snell Lock (U.S. Army Engineer District, Buffalo, 1955). The interior mixture had a density of 154.6 pcf (2,476.5 kg/cu m), and the exterior mix had a density of 156.4 pcf (2,505.3 kg/cu m). The FE model used a density of 0.0905 pci (2,505.03 kg/cu m) assuming the 60/40 mix.

3.6 Thermal Properties

3.6.1 Rock

The properties used for rock foundation in the FE model are shown in Table 3-3. It is assumed that these properties are not time-dependent and remain constant during the construction sequence at Snell Lock.

Table 3-3	
Properties for the Rock Foundation	
Property	Value
Density	0.1 pci (2,767.9 kg/cu m)
Specific heat	0.3 BTU/lb-°F (920.5 J/kg/°C)
Thermal conductivity	3.0 BTU/in.-day-°F (2.6 J/m-sec-°C)
Coeff. of thermal expansion	5.2E-06 in./in./°F (9.52 E-06 m/m/°C)
Modulus of elasticity	8.4E+06 psi (57,915.96 Mpa)
Poisson's ratio	0.22

3.6.2 Concrete

The thermal properties for the interior and exterior mixes is based on a previous thermal study done for Design Memorandum 7 for Snell Lock and laboratory testing performed at Ohio River Laboratory. Table 3-4 shows the properties used in the FE modeling for the concrete.

Table 3-4	
Thermal Properties for Mixes at Snell Lock	
Property	Value
Thermal diffusivity h	0.057 ft²/hr (5.295 m²/hr)
Specific heat s	0.22 Btu/lb-°F (920.5 J/kg/°C)
Thermal conductivity k	
Interior	1.939 Btu/day-°F-ft (3.35 J/m-sec-°C)
Exterior	1.961 Btu/day-°F-ft (3.39 J/m-sec-°C)
60/40 mix (used in FE model)	3.922 Btu/day-°F-in. (3.39 J/m-sec-°C)

Another important thermal property is the adiabatic temperature rise within the concrete. The temperature rise is a measure of the heat of hydration of the cementitious materials. This is an especially important factor when formwork is present on a mass concrete structure and heat from the hydration is contained internally within the lift and adjacent pours. Once the forms are removed, the heat can then be exchanged with the ambient air temperature. The adiabatic heat rise can be determined using the following equation:

$$T(n) = \{[1.8*C(e)*\Delta q(n)]/s\} + T(n-1) \qquad (3\text{-}2)$$

where

$T(n)$ = adiabatic heat rise in °F at heat of hydration

$C(e)$ = cement content in grams per gram of concrete

$\Delta q(n)$ = heat of hydration

s = specific heat of concrete

Based on this equation, the adiabatic temperature rise based on time in days for the 60/40 concrete mixes at Snell Lock are shown in Figure 3-9.
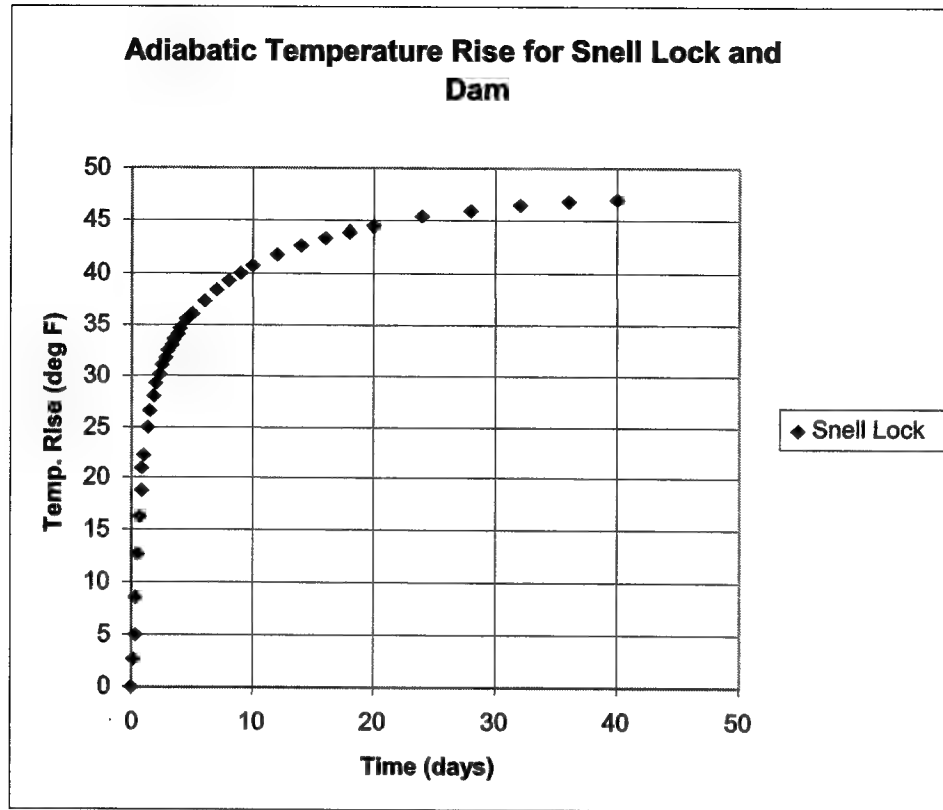
Figure 3-9. Adiabatic temperature rise for Snell concrete

3.7 Boundary Conditions

Ambient air temperatures were taken from temperature records recorded at Massena CAA Airport from 1956 to 1957. The minimum and maximum daily records were developed into temperature functions and incorporated in the FE model. The FE model was set up to interpolate the temperature records in quarter-day increments where the maximum temperatures were expected to occur at 2:00 p.m. and daily minimums at 6:00 a.m. The plots of the daily minimum and maximum temperatures are shown in Figures 3-10 and 3-11, respectively. These plots also show the end of 1956 construction, beginning of 1957 construction, and the 32-deg freezing mark. Interesting to note from these figures is the dramatic variation in temperatures during the period between 150 and 170 days.

3.7.1 Modeling of plywood forms

Additional modeling of the heat transfer through the plywood forms was accomplished using a convection boundary condition. According to the design specifications for lift control at Snell Lock, a minimum of 5 days was required between lifts and forms could not be removed before 14 days. Since no record of removal of forms exists for Snell Lock, this 14-day rule was adopted for form
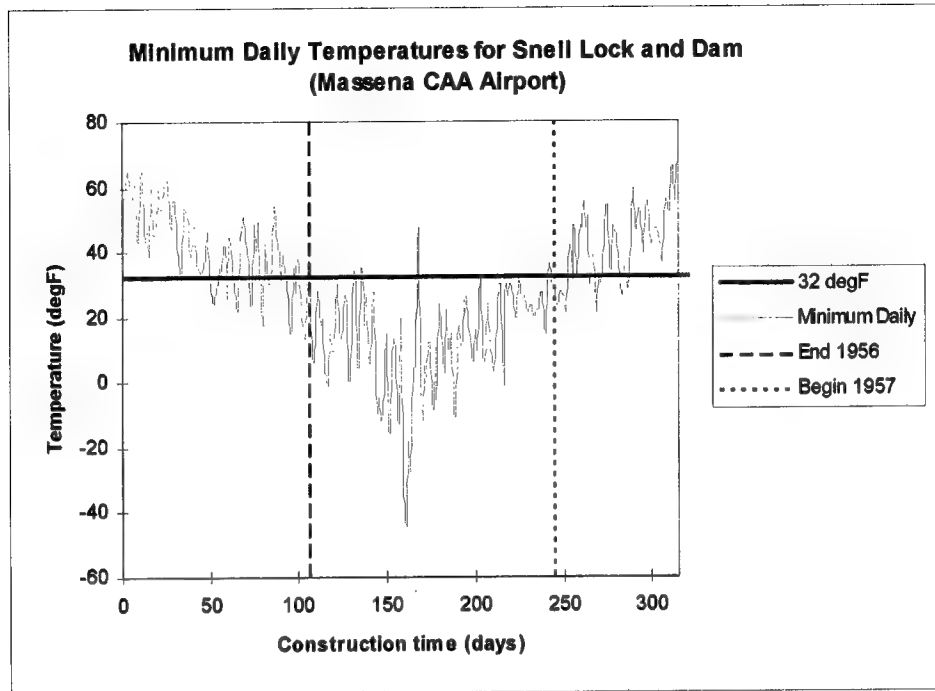
Figure 3-10. Minimum daily temperatures for Snell Lock
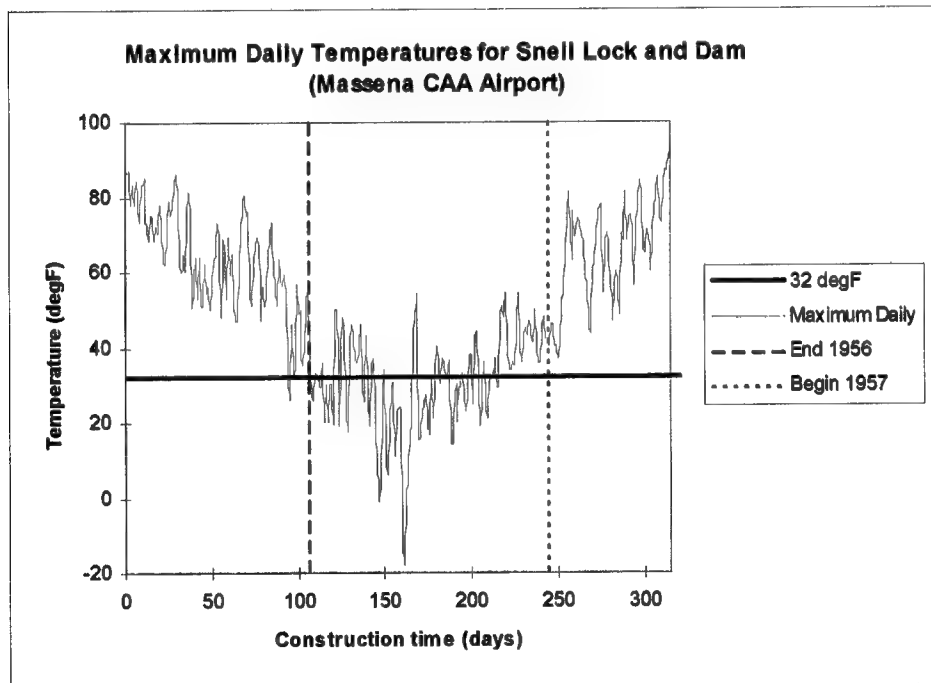
Figure 3-11. Maximum daily temperatures for Snell Lock

removal and was modeled into the FE model after each lift placement. Assuming an average 9-mph (14-km/hr) wind and formwork of ¾-in. (19-mm) plywood for insulation, the convection coefficient is 0.1176 Btu/day-in.^{2}-°F.

3.7.2 End of construction earth loading

The earth pressures were applied to the monolith after the final lift was placed in June 1957. Incremental application of the earth loads was not performed in the FE model. The loads were included into a boundary condition load step using both the pressure and shear (traction) components normal to the surface face of the lock wall.

The earth pressure forces applied to the back of the Snell Lock Monolith N-56 in the FE analyses are based on field instrumentation data, described in Chapter 2. Appendix A summarizes the results of equilibrium calculations used to transform the earth loading from those acting along a plane extending vertic-ally from the heel of the lock wall up through the backfill, shown in Figure 2-9, to those forces acting along the backfill-to-lock interface. Both horizontal and vertical shear resultant forces are included in these transformations. The horizon-tal earth pressures and downdrag, shear stresses acting along this vertical plane, are established using horizontal and vertical earth pressure coefficients. No water loading was applied in this end-of-construction load case.

Appendix A delineates the continuous effective earth pressure σ'_h distribu-tion with elevation as three discrete distributions, from el 104 to el 120, from el 120 to el 176.75, and from el 176.75 to el 205. The corresponding resultant horizontal effective forces F_{h1}, F_{h2}, and F_{h3} and points of action computed for each of the three pressure segments are identified in Figure A-2 and given in Table A-1. Values of the resultant water pressure forces shown in Figure A-2 are also given in Table A-1.

The applied loads are specified in the FE analyses in terms of surface tractions along the three lock-wall-to-soil-backfill interface regions. These surface tractions consist of both shear stresses τ and total stresses applied normal to the interface σ_n. Tables A-4, A-5, and A-6 list the values of the two surface tractions, σ_n and τ, specified in the FE analyses.

3.8 Results from FE Model

The results for the FE model are presented for three points in the construction sequence for Snell Lock Monolith N-56. The results presented focus on the cracking potential of mass concrete and not resultant stresses at the nodes or integration points. The results will be highlighted with plots of the monolith overlain by the cracking potential in percent. A legend is presented with the plots. The color red highlights the area with the highest potential for cracking.

32

3.8.1 Day 244 – Snell Lock

The first point during the construction history at Snell Lock is at Day 244 when the partially complete Monolith N-56 was ready for the placement of a new lift The cracking potential for Snell Lock at Day 244 is shown in Figure 3-12. This figure shows Monolith N-56 at a time in the sequence that is 138 days from the placement of Lift 10. Lift 10 was the last lift placed during the 1956 construction season.
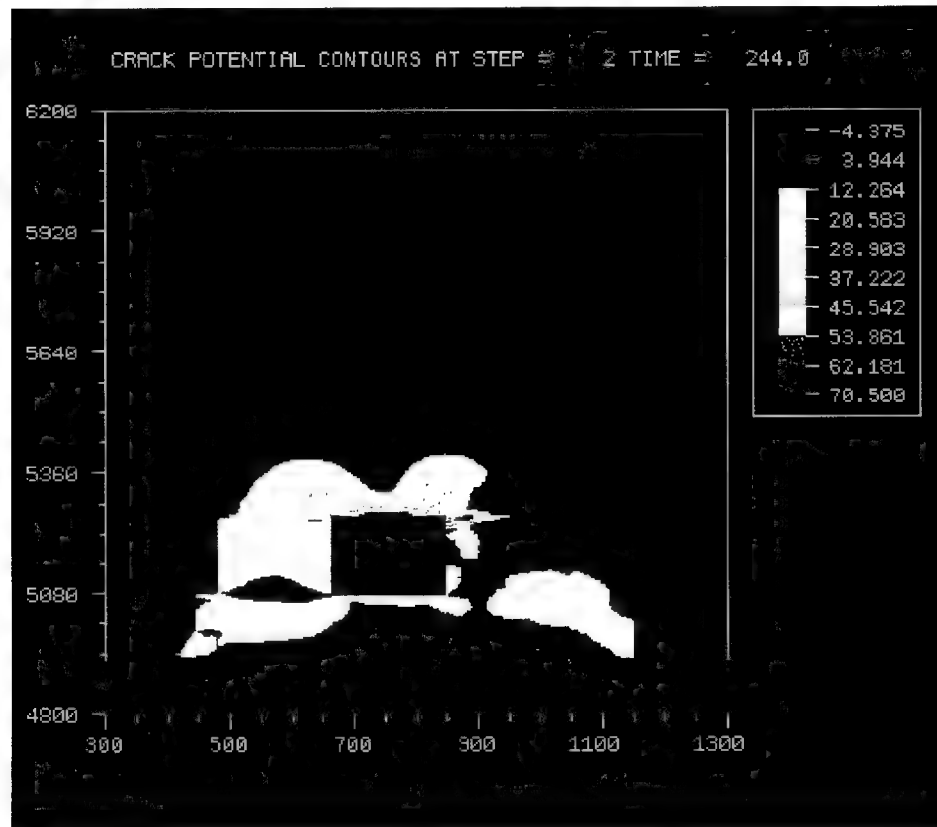
Figure 3-12.   Day 244 – end of 1956 construction and winter of 1956/1957

Also, at this point in time, the temperature extremes that occurred during the winter have subsided and the concrete has reached a mature age. From Figure 3-12, it appears that the highest potential for cracking exists around the top and side of the lower culvert. The cracking potential at Day 244 is in the order of 40 to 70 percent in the upper right corner of the culvert.

3.8.2 Day 315 – Snell Lock

The second point during the construction history at Snell Lock is at Day 315 when Monolith N-56 is completed. The cracking potential for Snell Lock at Day 315 is shown in Figure 3-13. This figure shows Monolith N-56 at a time that is 71 days from the placement of Lift 11 at Day 245. From Figure 3-13, it
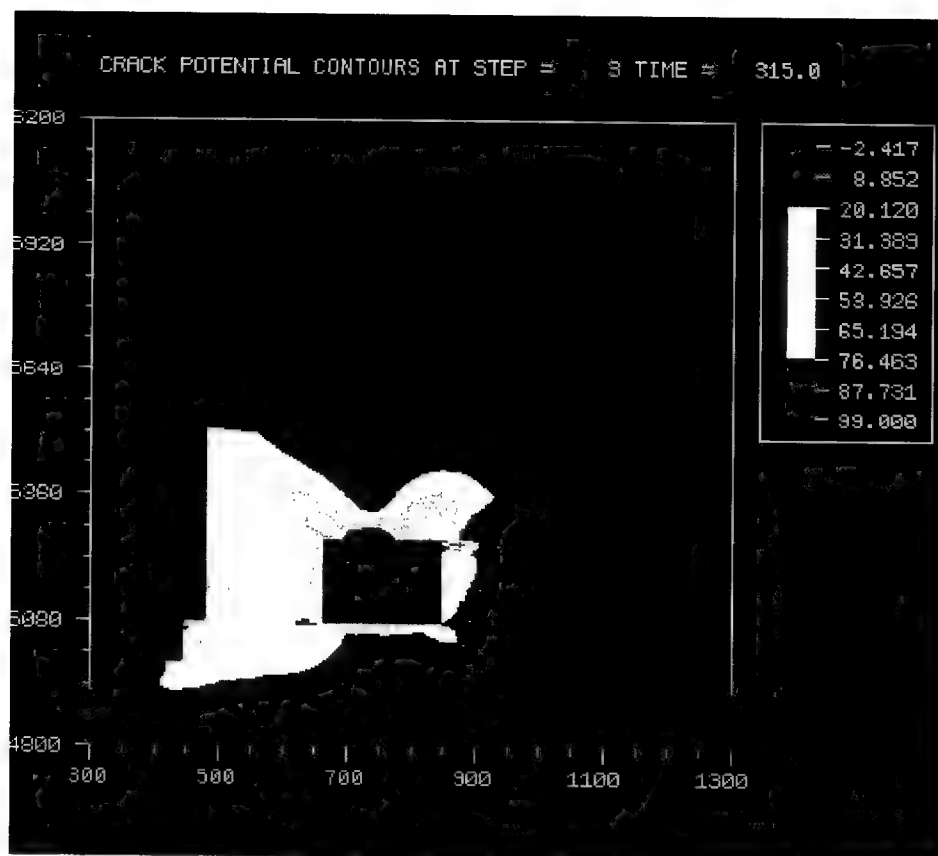
Figure 3-13.   Day 315 – end of 1957 construction

appears that the highest potential for cracking still exists at or around the culvert. The cracking potential at Day 315 is approximately 60 to 90 percent in the upper right corner of the culvert where the crack was formed.

3.8.3 Day 316 – backfilling at Snell Lock

The third point during the construction history at Snell Lock is assumed at Day 316. Day 316 is hypothetical and represents when Monolith N-56 was completed and backfilled with compacted glacial till. The cracking potential for Snell Lock at Day 316 is shown in Figure 3-14. This figure shows that the highest potential for cracking appears to be around the upper corners of the culvert toward the inclined back face of the lock wall. This was due primarily to the cantilever load effects from compacted fill. The cracking potential at Day 316 indicates that the potential is about 70 to 100 percent in the upper right corner of the culvert. This area of high potential correlates well with the location of the crack that was later found to exist in Monolith N-56.
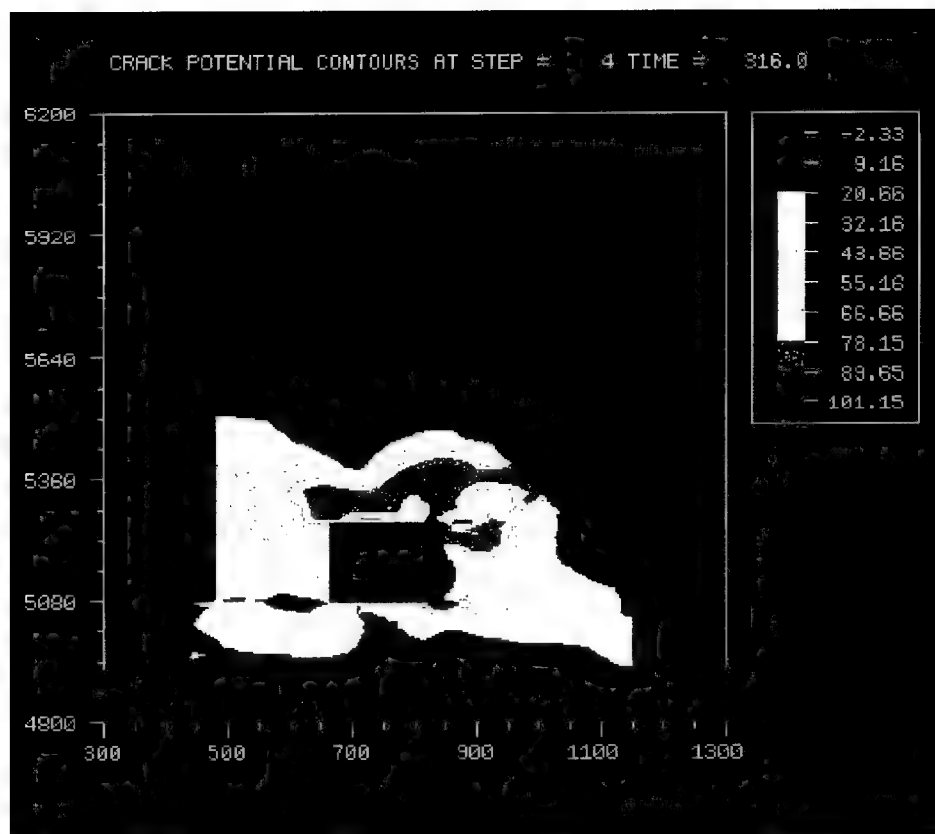
Figure 3-14. Day 316 – application of earth pressures to Monolith N-56

3.9 Conclusions

The FE thermal analysis performed on Snell Lock Monolith N-56 gives the strong indication that the potential for cracking in the upper right corner of the lower monolith did exist after the backfilling was complete in 1957. These results also indicate that microcracks in the mass concrete in the culvert area were created during the winter of 1956-1957. Upon an increase in stress intensity due to the backfilling and overcompaction of the glacial till, these cracks created an expansion of a crack to the inclined surface of the lock wall.

4 Discrete Crack Analyses of Snell Lock

4.1 Introduction

This chapter discusses the results of a crack propagation evaluation of Snell Lock using discrete crack theory, as given by Linear Elastic Fracture Mechanics (LEFM). A discrete crack model treats a crack as a geometrical entity (American Concrete Institute 1997 ACI (446.3R-97)). LEFM discrete crack analysis is used to assess if a crack will propagate or arrest for a given increment of loading.

Cracking potential and crack extent for the lock are assessed for both short-term, end-of-construction earth loading and long-term earth and water loading. The Snell Lock monolith selected for analysis is Monolith N-56, located approximately midway along the 860-ft- (262.13-m-) long lock chamber. The geometry of this monolith, which is shown in Figure 2-9 and described in Chapter 2, "Cross Section Used in the Smeared and Discrete Crack Analyses," is representative of those defining the lock chamber at Snell.

Figure 2-9 shows a cross section of Monolith N-56. Monolith N-56 is 101 ft (30.78 m) high and has a base width of 62 ft (18.9 m), corresponding to a base-to-height ratio of 0.61. The top of backfill is level with the top of the lock, el 205. The base of Monolith N-56 is at el 104. The backfill-to-monolith interface extends vertically from the heel of the monolith to el 120. Above this elevation the thickness of the monolith decreases with elevation. Starting at el 120 the monolith-to-backfill interface is inclined at an angle of 35.18 deg from vertical to el 176.75. Between el 176.75 and the top of backfill, el 205, the monolith-to-backfill interface is vertical and the thickness of the monolith is a constant 16 ft (4.88 m). The top of the 15-ft- (4.57-m-) wide by 16-ft- (4.88-m-) high culvert used for filling and emptying the lock chamber is at el 132. The closest distance from the landward-ceiling corner of the filling and emptying culvert through the mass concrete to the exterior backfilled face of the lock wall is 14.34 ft (4.37 m).

4.2 Earth and Water Pressure Loading

The earth and water pressure forces applied to the back of the Snell Lock Monolith N-56 in the FE analyses are based on field instrumentation data, described in Chapter 2. Appendix A summarizes the results of equilibrium calculations used to transform the earth and water loading from those acting along a plane extending vertically from the heel of the lock wall up through the backfill, shown in Figure 2-9, to those forces acting along the backfill-to-lock interface. Both horizontal and vertical shear resultant forces are included in these transformations. The horizontal earth pressures and downdrag, shear stresses acting along this vertical plane, are established using horizontal and vertical earth pressure coefficients. The water pressures acting normal to this vertical plane for the long-term load case are established based on a steady-state water table at el 160 and a perched water table at el 173 within the backfill.

Appendix A delineates the continuous effective earth pressure σ'_h distribution with elevation as three discrete distributions, from el 104 to el 120, from el 120 to el 176.75, and from el 176.75 to el 205. The corresponding resultant horizontal effective forces F_{h1}, F_{h2}, and F_{h3} and points of action computed for each of the three pressure segments are identified in Figure A-2 and given in Table A-1. Values of the resultant water pressure forces shown in Figure A-2 are also given in Table A-1.

The applied loads are specified in the FE analyses in terms of surface tractions along the three lock-wall-to-soil-backfill interface regions. These surface tractions consist of both shear stresses τ and total stresses applied normal to the interface σ_n. Tables A-4, A-5, and A-6 list the values of the two surface tractions, σ_n and τ, specified in the FE analyses.

4.3 Linear Elastic Fracture Mechanics Analysis

One analytical procedure available for use in analyzing hydraulic structures that may exhibit crack propagation during loading is formulated based on linear elastic fracture mechanics theory (LEFM). Discrete crack analysis is used to assess if a crack will propagate or arrest for a given increment of loading. This analytical procedure has been implemented in the computer program MERLIN (Reich, Cervenka, and Saouma 1995), which was used for the analyses of Snell Lock discussed in this chapter. This fracture mechanics method can be used in structures for which the area surrounding the crack tip is relatively large compared to the fracture process zone (FPZ) (American Concrete Institute 1997 (ACI 446.3R-97)). For normal-size building members (such as beams and columns), a nonlinear fracture mechanics is normally required.

The LEFM procedure is an FE method-based procedure to model the propagation of a discrete crack. Generally, LEFM relates the stress magnitude and distribution at the crack tip to the nominal stress applied to the structure; to the size, shape, and orientation of the crack or discontinuity; and to the material properties. The "demand" due to loading(s) applied to the retaining structure,

and specifically to the region of cracking, is represented by stress intensity factors K_I, K_{II}, and K_{III} for the three cracking modes. Cracking Mode I is an opening mode, Mode II is a shearing mode, and Mode III is a tearing mode. Conceptually, the stress intensity factors indicate the rate at which the stress approaches infinity ahead of the crack tip for each of the three displacement modes. The stress intensity factors characterize the magnitude of the crack tip stress field for the potential cracking modes. The "capacity" of the material is characterized by the fracture toughness K_{Ic}. (Values of K_{Ic} from select laboratory and in situ tests on concrete are discussed in Appendix B.) Crack advance is monitored in an LEFM analysis by comparing the demand to capacity (e.g., K_I to K_{Ic}). When the value for K_I is greater than the value for K_{Ic}, the crack advances. Otherwise, the crack will not advance.

No crack *initiation* aspect of LEFM is implemented in MERLIN (unlike the smeared crack theory). To circumvent this limitation, a strength-of-materials approach is first used *to assess the likely regions of potential cracking* within the monolith. The steps of the analyses proceed as follows: an initial FE mesh of the concrete monolith is *constructed with no discrete cracks* and subjected to gravity loading, followed by earth and water loading. In MERLIN, the gravity loading is applied as a body force within the elements that compose the lock model. (MERLIN does not have the capability to do an incremental construction analysis of the lock that models the placement of concrete in lifts and the maturation of the concrete with time.) The earth and water loading are then applied as surface tractions along the exterior faces of the lock model. The principal stresses computed within the monolith by MERLIN are then surveyed for region(s) of tensile stress using the contour plot capability of Post-MERLIN. If tensile stresses are to develop within the lock monolith, then these stresses will be largest normal to principal stress plane(s). If tensile stresses of significant magnitude are computed within the lock model in the linear FE analysis, a LEFM analysis of the lock is initiated. The initial FE mesh is then altered for subsequent LEFM analyses by introducing a discrete crack within the tensile stress region identified in the uncracked analysis of the lock monolith. The preprocessor for MERLIN is designed to facilitate remeshing of the lock model for the purpose of introducing (or extending) a discrete crack. The initial discrete crack is introduced in the mesh and oriented along the plane corresponding to the principal tensile stress identified in the first FE analysis. This initial LEFM analysis of the lock model is first subjected to gravity loading, followed by earth and water loading, and is used to assess if the discrete crack will propagate or arrest during loading. Recall that crack advance is determined in an LEFM analysis by comparing the demand to capacity (e.g., K_I to K_{Ic}). When the value for K_I is greater than the value for K_{Ic}, the crack advances. A second LEFM analysis is then initiated; and (a) the mesh is again altered by extending the crack further, (b) the gravity and earth and water loading are reapplied, (c) a new value of K_I is computed, (d) the newly computed value of K_I is then compared to the value of K_{Ic}. The analysis of crack propagation is terminated when the value of K_I is less than or equal to K_{Ic}.

4.4 LEFM Analysis of Snell Lock for End-of-Construction Loading

The first crack extent evaluation of Snell Lock Monolith N-56 is made for the short-term, end-of-construction earth loading. This load case occurred late in the fall of 1957, after the completion of lock construction and backfilling, and prior to flooding of the lock site. Figure 4-1 shows the load cases modeled through end of construction in the LEFM analyses. The model of the concrete monolith is first subjected to gravity loading followed by earth loading. No water pressures are applied to the lock model in this analysis.

a inches	$\frac{a}{L}$
8.6	0.05
34.4	0.2
60.2	0.35
86	0.5
120.5	0.7
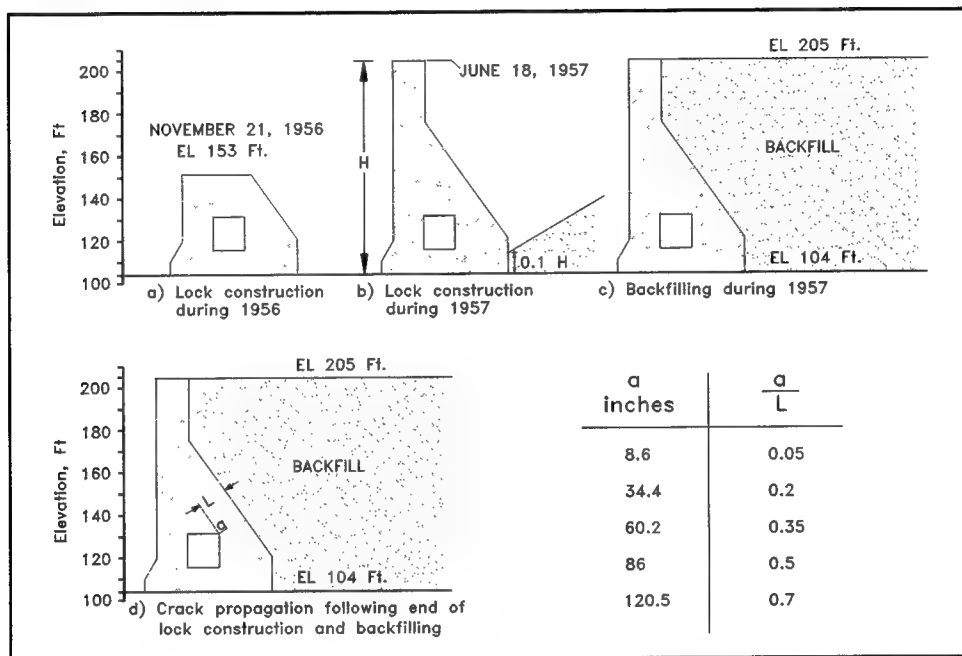
Figure 4-1. Load cases modeled in the FE analyses through end of construction (1 ft = 0.305 m) where *a* is the crack length and *L* is the closest distance from the landward-ceiling corner of the filling and emptying culvert through the mass concrete to the exterior backfilled face of the lock wall

4.4.1 Initial finite element analysis (no cracks)

Figure 4-2 outlines the boundaries of the FE model of Monolith N-56 and of the rock foundation. The lateral extent of the rock foundation for the FE model is defined using standard FE analysis criteria for rock-founded earth retaining structures: (a) by the center line of the lock chamber and (b) by the distance equal to three times the height of the backfill as measured from the heel of the lock wall. The horizontal movements along these two vertical boundaries are set equal to zero for all analyses. The base of the idealized model for the rock foundation is located at a depth below the base of the lock equal to five times the width of the lock base. Zero vertical and horizontal displacements are specified along this horizontal surface in all analyses. Full contact between the base of the
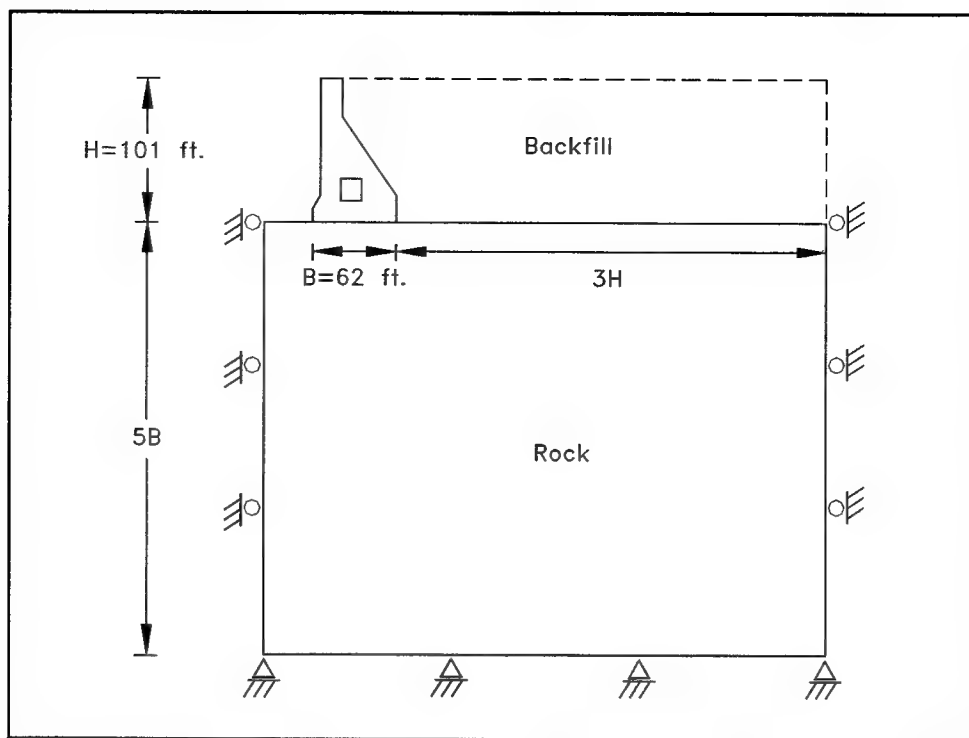
Figure 4-2. Snell Lock and elastic rock foundation model (1 ft = 0.305 m)

monolith and rock foundation is assumed in this analysis. MERLIN does not have the capability to do a nonlinear, incremental backfill placement method of analysis to develop the earth loading. Instead, the backfill is represented in the FE analyses by means of surface tractions applied along the back of the monolith and along the backfill-to-rock foundation interface. Appendix A outlines the calculations used to define the traction acting parallel and normal to the backfill-to-lock interface. Both horizontal and vertical shear (i.e., downdrag) earth forces are included in these transformations. Beyond the lock, total overburden pressure is applied to the top of rock below the backfill in the model.

Figure 4-3 shows the FE mesh used for the initial linear elastic response analysis of Monolith N-56. This mesh *contains no discrete cracks*. The FE mesh comprises 5,183 elements and 10,616 nodal points. Figure 4-4 shows the values assigned to the variable IMESH along various regions of the model in the MERLIN preprocessor. The parameter IMESH controls the sizing of the elements for the FE mesh generated using the preprocessor. Note that the mesh is finest within the lock region located between the landward-ceiling corner of the filling and emptying culvert and the exterior backfilled face of the lock wall. Smaller IMESH values are assigned to this region because of the presence of the sharp corner for the culvert. This is also the location where the crack formed in the actual lock structure. Six-noded, linear elastic/plane strain, triangular elements are used to model the monolith and the rock foundation. The values of Young's modulus E for concrete placed *below el 153* is assigned an E value of 4,600,000 psi (31,716 Mpa), while E is set equal to 4,200,000 psi (28,958 Mpa) for the concrete placed above this elevation. Elevation 153 delineates the end of

Chapter 4   Discrete Crack Analyses of Snell Lock
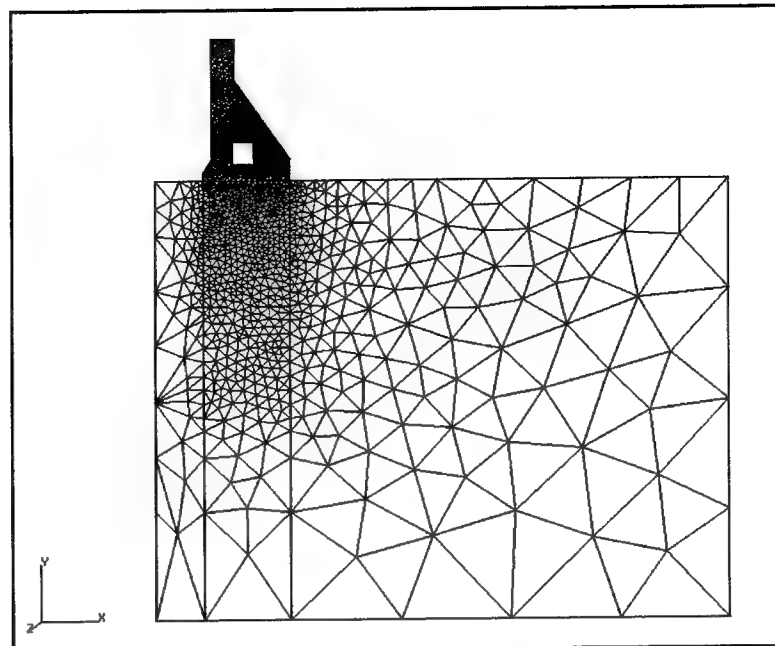
a. Monolith N-56 and its rock foundation
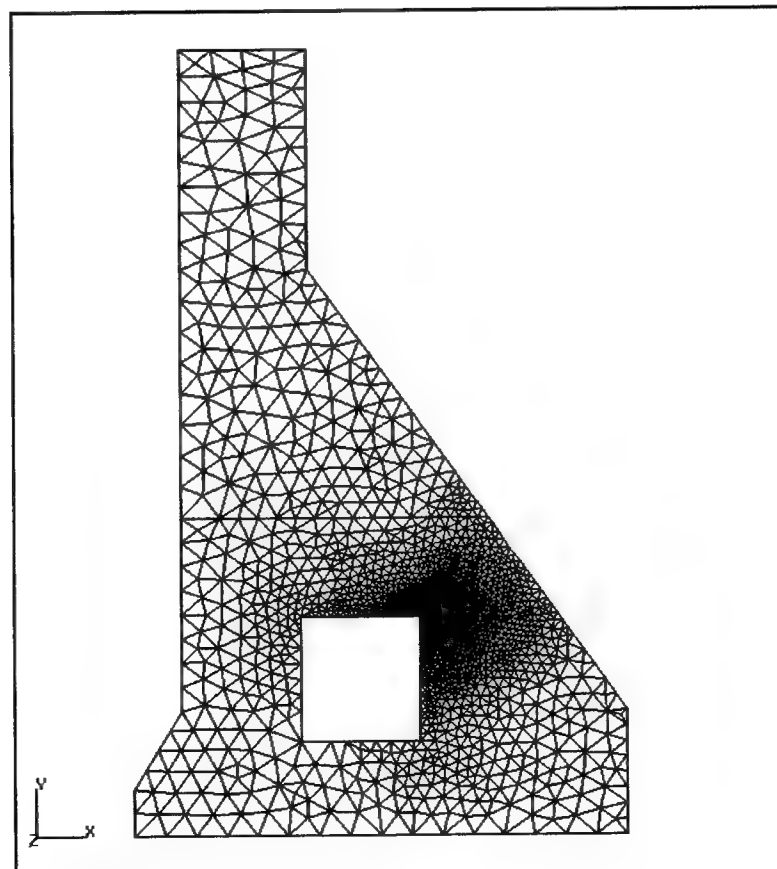
b. Monolith N-56

Figure 4-3.   FE mesh used for the linear elastic response analysis
of Monolith N-56 (Continued)
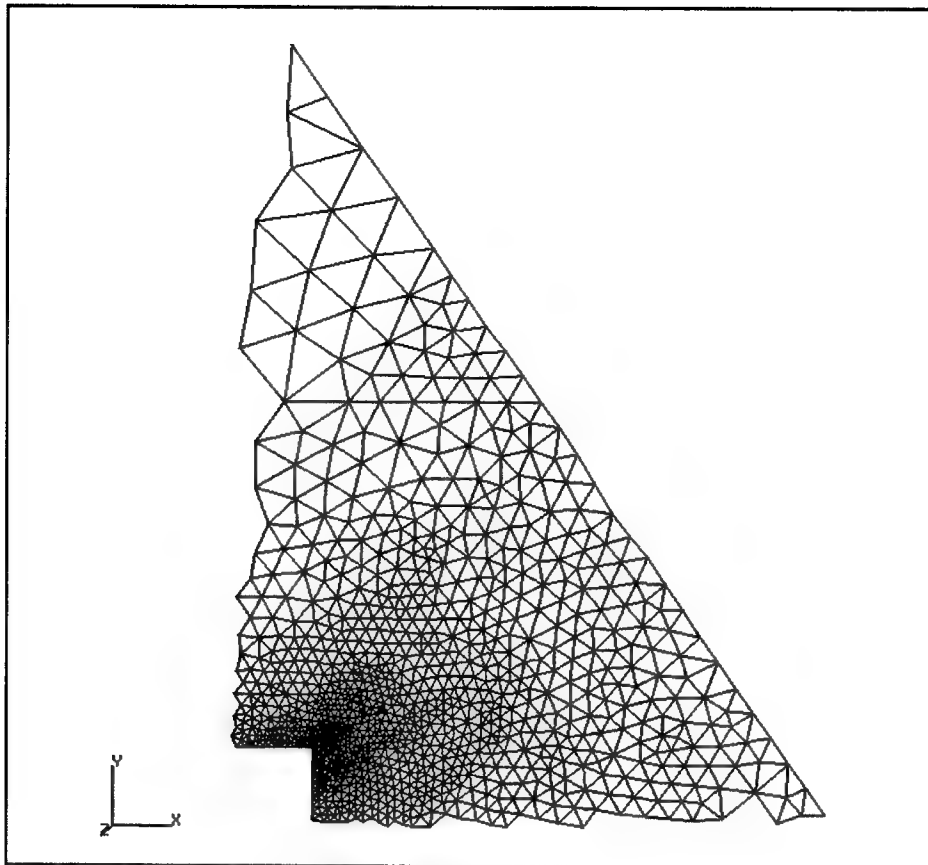
c. The region between the landward-ceiling corner of the filling and emptying culvert and the external backfilled face of the lock wall
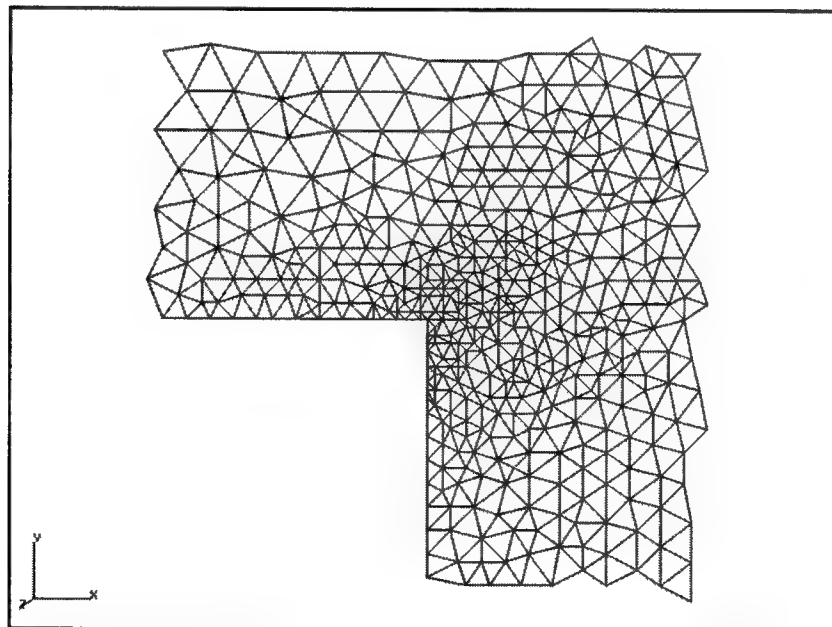
d. The region adjacent to the landward-ceiling corner of the filling and emptying culvert

Figure 4-3. (Concluded)
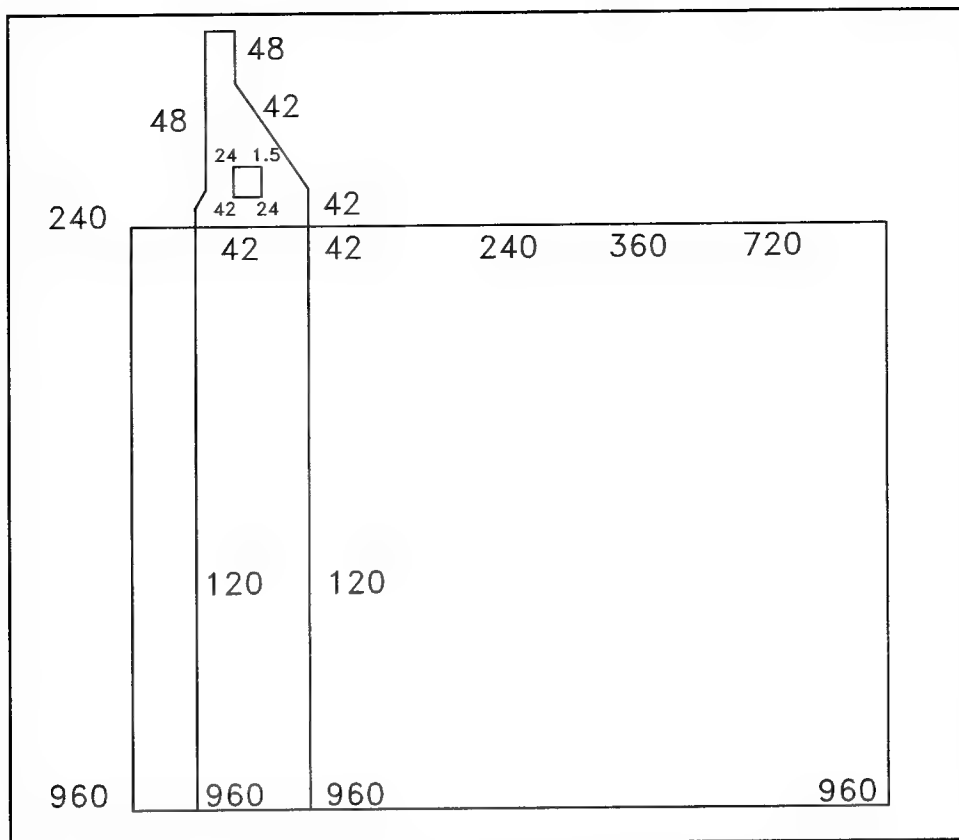
Figure 4-4.   IMESH values (in inches) assigned to MERLIN preprocessor
(1 inch = 25.4 mm)

Monolith N-56 construction in the fall of 1956 (Figure 4-1a). Construction of the
monolith resumed in the spring of 1957 and was completed by that summer.
These values for E reflect the maturation for the 1956 and 1957 concrete
specimens by the fall of 1957. Details regarding the maturation of concrete are
given in Section 3-5 and Appendix C. A value of Young's modulus E equal to
8.55×10^6 psi (58,950 Mpa) is assigned to the rock foundation. This value for E
is based on laboratory results on rock specimens recovered from the site in 1990
and tested by Mosher, Bevins, and Neeley (1991). Values for the Poisson's ratio
of the concrete and rock are set equal to 0.26 and 0.29, respectively.

The self-weight of the monolith is introduced into the FE model of the
monolith and the rock foundation using a gravity turn-on analysis. A unit weight
of concrete equal to 158.3 lb/ft^3 (2,535.7 kg/m^3) is assigned to the monolith. This
is followed by application of the short-term end-of-construction earth loading
given in Appendix A. In this first FE analysis of Monolith N-56 (with no
discrete cracks), tensile stresses are computed within the region adjacent to the
landward-ceiling corner of the filling and emptying culvert. The largest principal
(tensile) stress is computed by MERLIN to be equal to 769.43 psi (5,305 KPa) at
this culvert corner and normal to the plane oriented at 44.45 deg from horizontal.
(MERLIN extrapolates the stress values from the integration points within each
element to the nodal points defining the edge of the element and reports an
"averaged" stress value when nodes are shared by elements.) This value of

tensile stress is equal to approximately 15 percent of the unconfined compressive strength of 1-year-old concrete specimens cast in 1956 and representative of the concrete placed within the landward-ceiling corner of the culvert. Thus, the tensile stress is deemed of sufficient magnitude to warrant an LEFM analysis.

4.4.2 LEFM analysis with a/L = 0.05

The initial FE mesh (Figure 4-3) is then altered for the first LEFM analysis by introducing a discrete crack within the tensile stress region located at the landward-ceiling corner of the culvert. A discrete crack 8.6 in. (0.218 m) long and oriented at 44.45 deg from horizontal is introduced into the original (uncracked) mesh using the preprocessor of MERLIN. A crack length a of 8.6 in. (0.218 m) corresponds to 5 percent of the closest distance L from the landward-ceiling corner of the filling and emptying culvert through the mass concrete to the exterior backfilled face of the lock wall. This distance L equals 14.34 ft (4.37 m). Figure 4-5 shows the lock wall portion of the resulting FE mesh used for the first LEFM analysis of Monolith N-56. This figure shows the displaced mesh after loading is applied. These nodal point displacements have been multiplied by a factor of 2,000 to allow viewing of the discrete crack in these figures. This FE mesh comprises 5,669 elements and 11,684 nodal points. The values assigned to variable IMESH are the same as those given in Figure 4-4 with the exception that IMESH is set equal to 1 in. (25.4 mm) at the crack tip. (Recall from this figure that IMESH equals 1.5 in. (38.1 mm) at the landward-ceiling corner of the culvert.) Note the refinement of the resulting mesh within the lock region located between the landward-ceiling corner of the filling and emptying culvert and the exterior backfilled face of the lock wall. A very fine mesh in this region is important to capturing the flow of stresses/strains and displacements around the culvert corner and the discrete crack.

With a/L equal to 0.05, Figure 4-6 lists the computed values of stress intensity factors K_I and K_{II} as equal to $969.6 \, \text{psi} \sqrt{\text{in.}}$ (1,065.4 KN/m$^{3/2}$) and to $-3.08 \, \text{psi} \sqrt{\text{in.}}$ (-3.4 KN/m$^{3/2}$), respectively. The value for K_{II} is quite small relative to the value for K_I. This implies that the Mode I opening mode dominates the behavior at this crack tip. Recall that the demand due to loading(s) applied to the retaining structure to the region of cracking is represented by the stress intensity factor K_I. The capacity of the material is characterized by the fracture toughness K_{Ic}. There are no fracture toughness test results for the Snell concrete. (To date, fracture testing of concrete using discrete crack methodology is not routinely made on Corps projects. The engineering procedures and equipment for this type of advanced testing of concrete were not yet available at the time of Snell Lock construction (1956-57).) However, a limited review of the literature on this topic shows the values reported for K_{Ic} from appropriate laboratory and in situ tests on competent concrete typically range from approximately $850 \, \text{psi} \sqrt{\text{in.}}$ (934 KN/m$^{3/2}$) to $1,400 \, \text{psi} \sqrt{\text{in.}}$ (1,538 KN/m$^{3/2}$) (Appendix B). Recall that crack advance is monitored in an LEFM analysis by comparing the demand to capacity (e.g., K_I to K_{Ic}). With the computed value for K_I being within the range of likely values for K_{Ic}, crack advance is deemed likely in this numerical analysis.
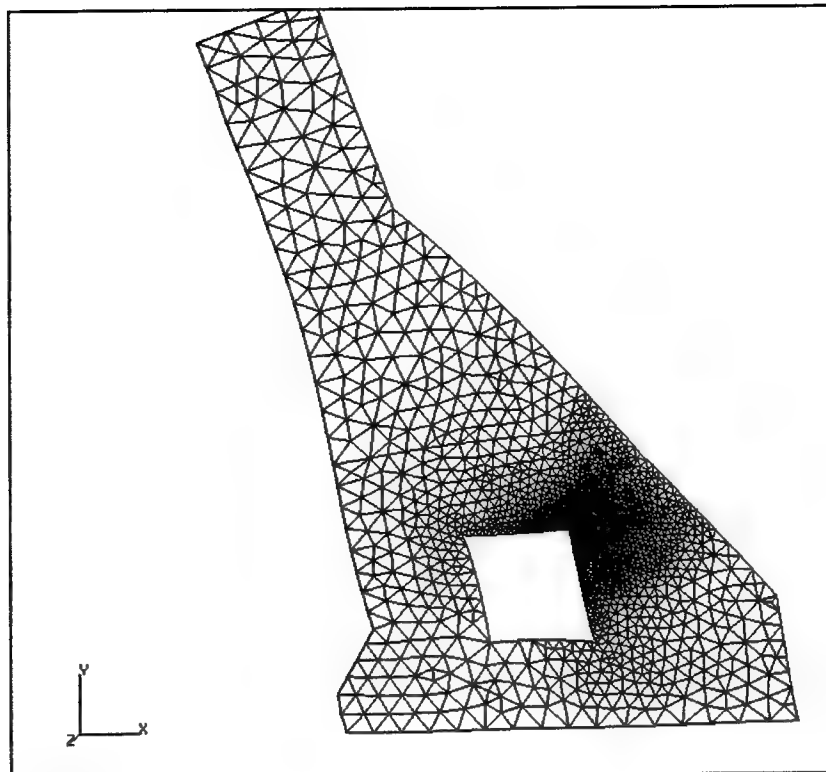
a. Monolith N-56
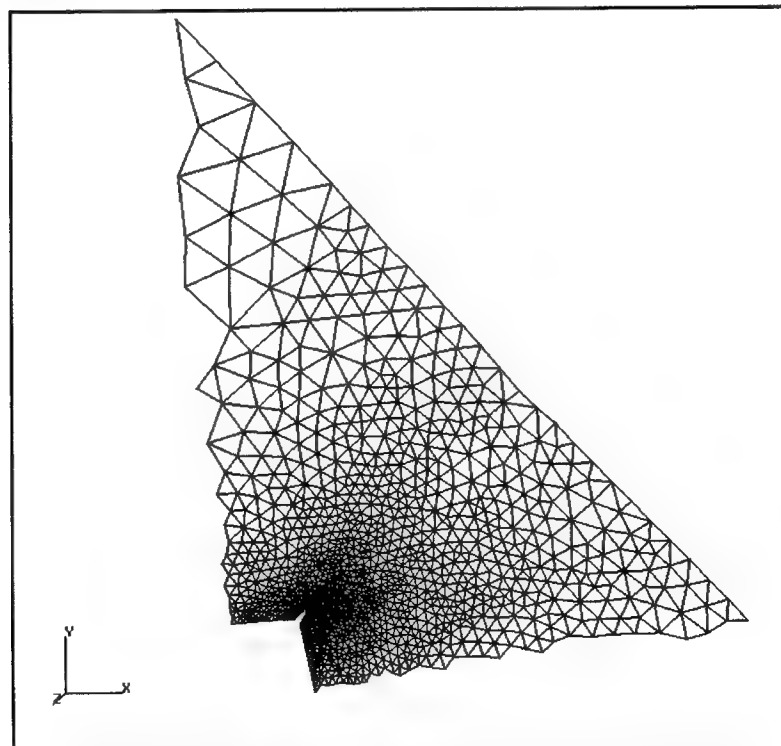
b. Region between the landward-ceiling corner of the filling and
   emptying culvert and the external backfill-face of the lock wall

Figure 4-5. Displaced FE mesh of Monolith N-56, a/L = 0.05 (Continued)
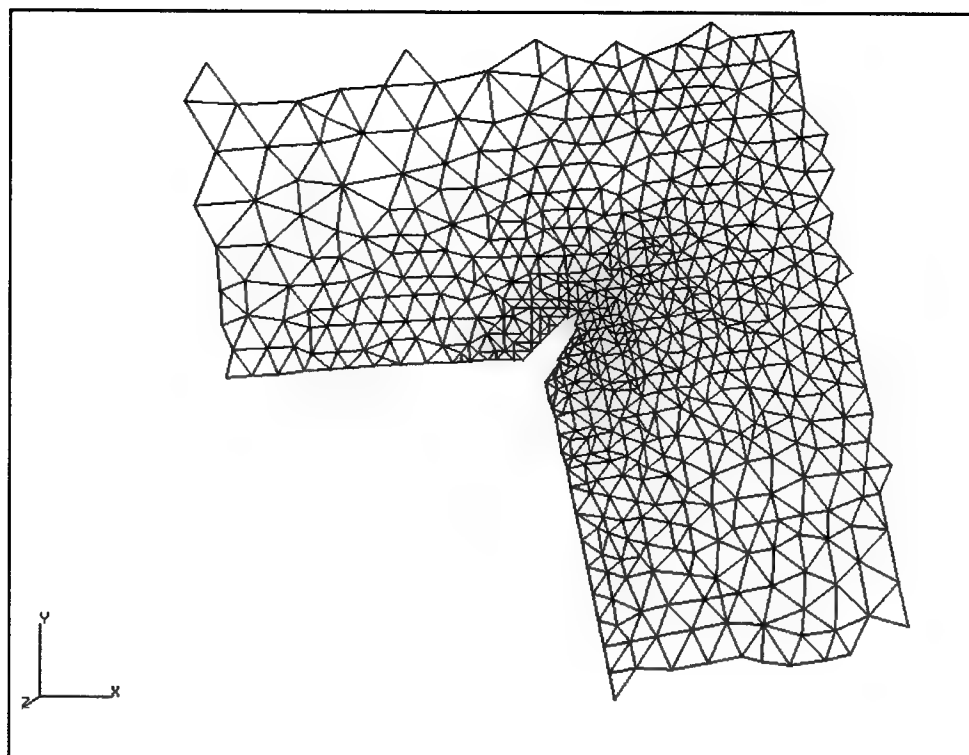
c. Region adjacent to the landward-ceiling corner of the filling and emptying culvert

Figure 4-5. (Concluded)

$\frac{a}{L}$	K_I psi$\sqrt{in}$	K_{II} psi$\sqrt{in}$	K_{eq} psi$\sqrt{in}$	$\sqrt{(K_I)^2 + (K_{II})^2}$ psi$\sqrt{in}$	θ degrees
0.05	969.6	−3.08	969.62	969.61	44.45
0.2	1019	11.91	1019.26	1019.10	45.84
0.35	1054	12.48	1054.28	1054.10	44.56
0.5	1172	16.05	1172.41	1172.11	43.83
0.7	1448	16.69	1448.36	1448.10	42.47

$$\theta_{Avg} = 44.20°$$

$$K_{eq} = K_I \cos^3 \frac{\theta}{2} - \frac{3}{2} K_{II} \cos \frac{\theta}{2} \sin\theta$$

Figure 4-6. Stress intensity factors and crack orientation, end of construction
(1 kN/m$^{3/2}$ = 0.91 psi$\sqrt{in.}$)

A contour path radius equal to 4 in. (0.102 m) is specified in the MERLIN analysis of the Figure 4-5 mesh with a crack of length a/L equal to 0.05 (normalized). The contour path radius is measured from the crack tip. In these MERLIN analyses the S-integral option using the contour integral method of Stern (Stern, Becker, and Dunham 1976; Hong and Stern 1978) is used to compute the stress intensity factors for LEFM analysis directly. The contour path radius defines the location of the integration contour in the analysis. MERLIN locates the integration contour along the edges of the finite elements that are in close proximity to the contour path radius. Specifically, the contour path integral uses the displacement and traction vector information computed along the integration contour to compute the stress intensity factors. Independent numerical evaluations made by Ebeling[1] using MERLIN have shown the values computed for K_I and K_{II} by the contour integral method can be both mesh dependent and path dependent. Coarse meshes can result in inaccurate values being computed for the stress intensity factors. For this analysis the contour path radius is set equal to approximately half of the length of the discrete crack so that the numerical evaluations made by the contour integral is at an optimum location relative to the crack tip and the landward-ceiling corner of the culvert. (Sharp corners introduce large stress/strain gradients.) Mesh refinement to the degree shown in Figure 4-5c is needed to ensure accuracy for the computed K_I and K_{II} values. Changing the value assigned to the contour path radius enables the accuracy of the results computed by MERLIN to be checked. A 25 percent change in contour path radius (both inward and outward) did not significantly alter the values computed for the stress intensity factors. Thus, it is concluded that a sufficiently fine mesh is being used in this analysis.

The displacement at the top of the lock is directed into the chamber and is computed to be 0.1603 in. (4 mm) for the mesh with a crack of length a/L equal to 0.05 (normalized). The increase in wall displacements with the introduction of the discrete crack is negligible (see the first two data entries in Figure 4-7).

4.4.3 LEFM analysis with a/L = 0.2

The initial LEFM mesh (Figure 4-5) is then altered for the second LEFM analysis by extending the discrete crack to a total length of 34.4 in. (0.874 m). The 25.8-in. (0.655-m) extension is oriented at 45.84 deg from horizontal using the preprocessor of MERLIN. A crack length of 34.4 in. (0.874 m) corresponds to 20 percent of the closest distance from the landward-ceiling corner of the filling and emptying culvert through the mass concrete to the exterior backfilled face of the lock wall ($a/L = 0.2$). Figure 4-8 shows the lock wall portion of the resulting FE mesh used for this second LEFM analysis of Monolith N-56. This figure shows the displaced mesh before and after loading is applied. These nodal point displacements have been multiplied by a factor equal to 2,000 to allow viewing of the discrete crack in these figures. This FE mesh comprises 5,951 elements and 12,204 nodal points. The values assigned to variable IMESH are the same as those given in Figure 4-4 with the exception that IMESH is set

---

[1] Personal Communication, 1999, R. M. Ebeling, U.S. Army Engineer Research and Development Center, Vicksburg, MS.

a/L	U_x Deflection (in)	$\frac{U_x}{\text{Height}}$
0.00	0.1601	.00013210
0.05	0.1603	.00013226
0.20	0.1611	.00013292
0.35	0.1616	.00013333
0.50	0.1632	.00013465
0.70	0.1669	.00013771

Height = 101 ft.

ELASTIC ROCK FOUNDATION
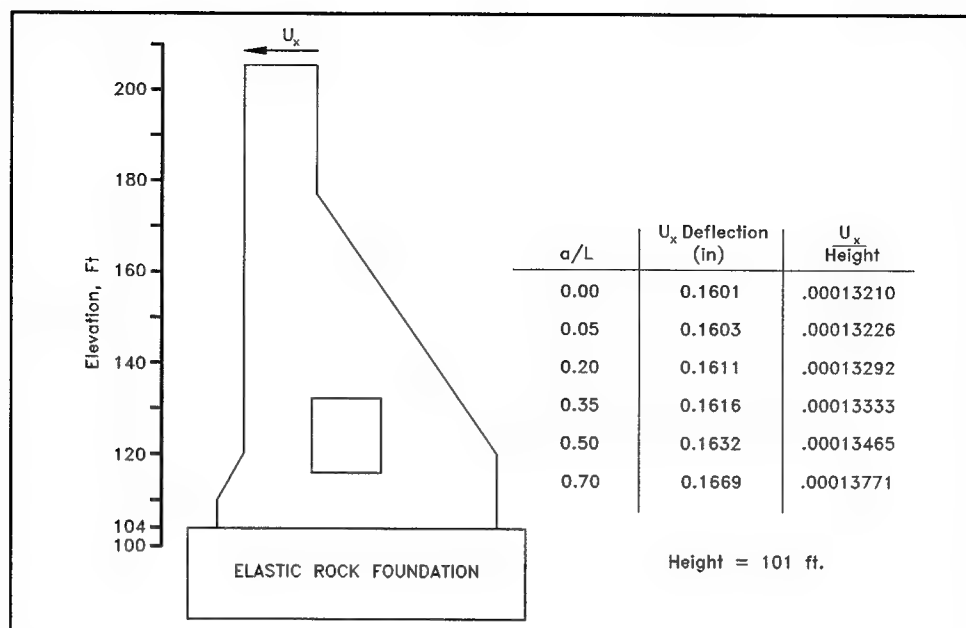
Figure 4-7. Horizontal deflection at top of lock wall, end-of-construction loading (1 in. = 25.4 mm, 1 ft = 0.305 m)

equal to 1.5 in. (38.1 mm) at the crack tip. (Recall from this figure that IMESH equals 1.5 in. (38.1 mm) at the landward-ceiling corner of the uncracked culvert.) This results in a sufficiently fine mesh within the lock region located between the landward-ceiling corner of the filling and emptying culvert and the exterior backfilled face of the lock wall.

With a/L equal to 0.2, Figure 4-6 lists the computed values of stress intensity factors K_I and K_{II} as equal to 1,019 $psi\sqrt{in}$. (1,119.7 KN/m$^{3/2}$) and to 11.91 $psi\sqrt{in}$. (13.1 KN/m$^{3/2}$), respectively. The value for K_{II} is quite small relative to the value for K_I, and Mode I opening mode continues to dominate the behavior at the crack tip. The demand has increased with the extension of the crack. (Recall that K_I is 969.6 $psi\sqrt{in}$. (1,065.4 KN/m$^{3/2}$) for the shorter crack with a/L equal to 0.05.) Assuming that the K_I value computed for the shorter crack is sufficient to overcome the fracture toughness of the concrete, the higher demand computed for this extended crack indicates that the crack will continue to advance.

A contour path radius equal to 15 in. (0.38 m) (as measured from the crack tip) is specified in the MERLIN analysis of the Figure 4-8 mesh with a crack of length a/L equal to 0.2 (normalized). Again, the contour path radius is set equal to approximately half of the length of the discrete crack. A 25 percent change in contour path radius (both inward and outward) did not significantly alter the values computed for the stress intensity factors. Thus, it is concluded that a sufficiently fine mesh is being used in this analysis.
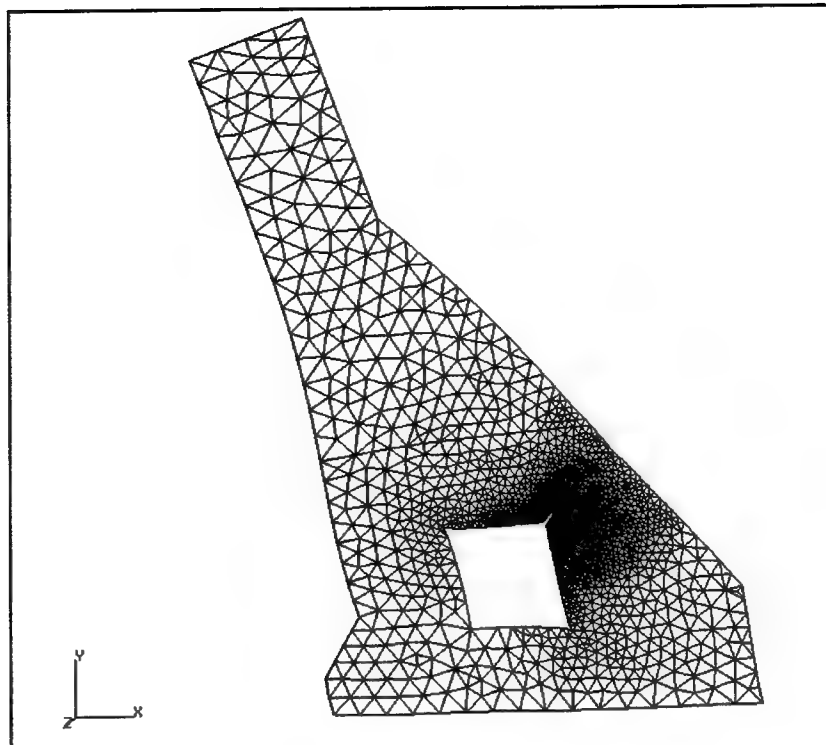
a. Monolith N-56
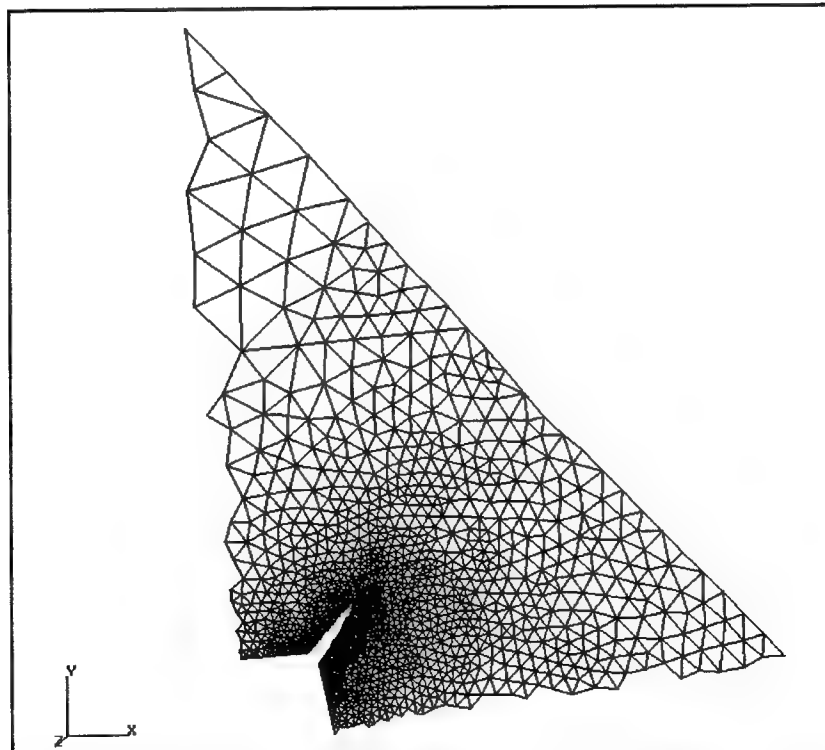
b. Region between the landward-ceiling corner of the filling and emptying culvert and the external backfill face of the lock wall

Figure 4-8. Displaced FE mesh of Monolith N-56, *a/L* = 0.2 (Continued)
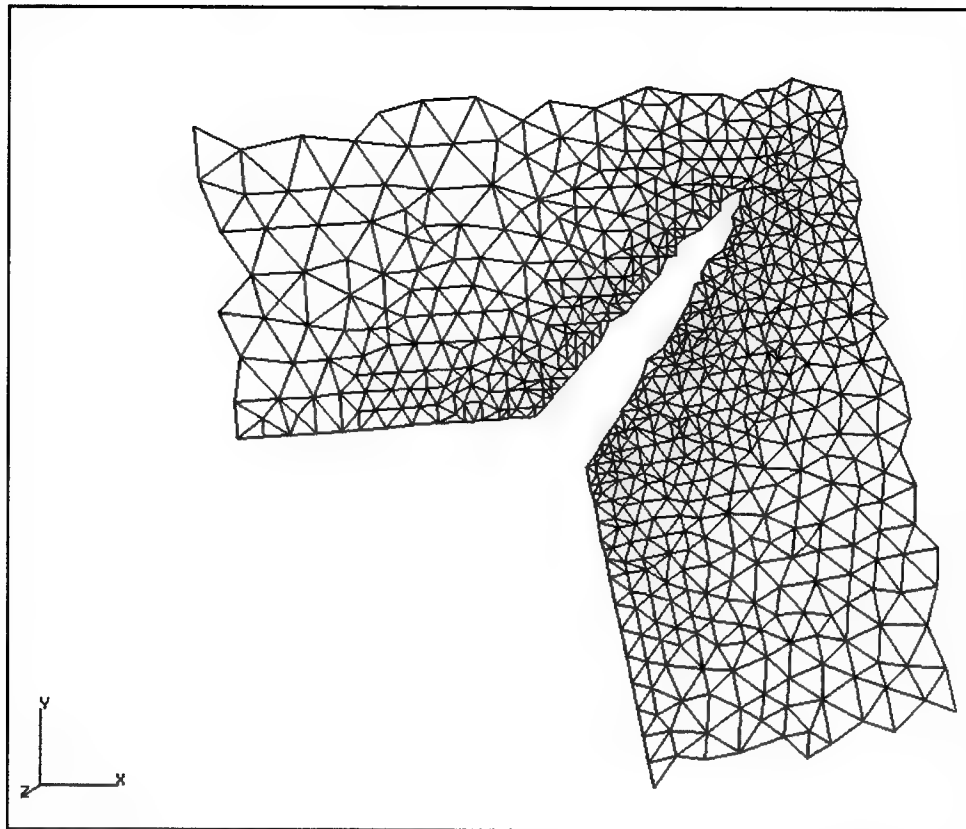
c. Region adjacent to the landward-ceiling corner of the filling and emptying culvert
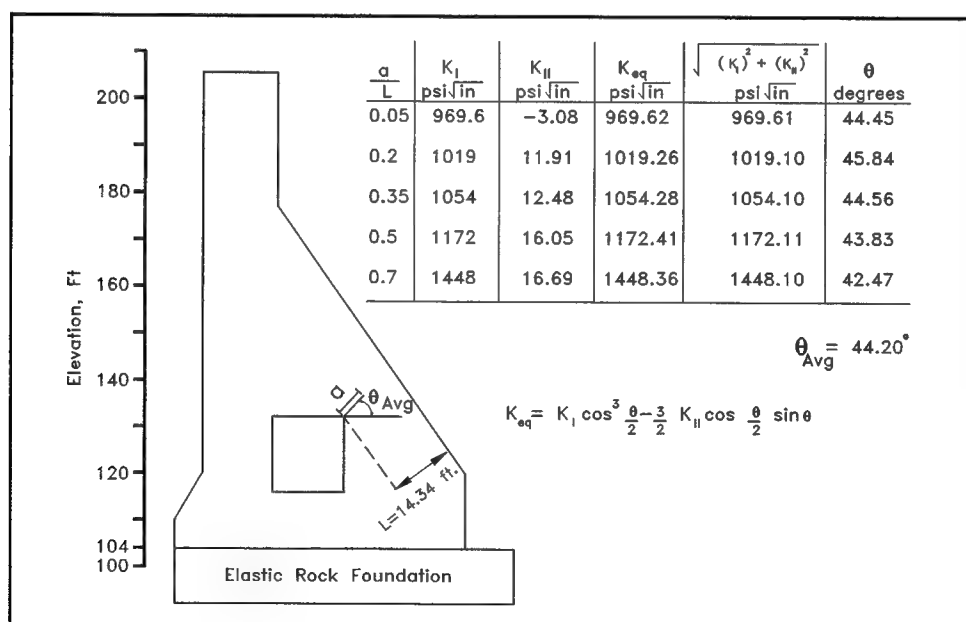
Figure 4-8. (Concluded)

4.4.4 LEFM analysis with a/L = 0.35

The Figure 4-8 LEFM mesh is altered for the third LEFM analyses by extending the discrete crack to a total length of 60.2 in. (1.53 m). The 25.8-in. (0.655-m) extension is oriented at 44.56 deg from horizontal using the preprocessor of MERLIN. A crack length of 60.2 in. (1.53 m) corresponds to 35 percent of the closest distance from the landward-ceiling corner of the filling and emptying culvert through the mass concrete to the exterior backfilled face of the lock wall ($a/L = 0.35$). The resulting FE mesh (not shown) comprises 5,205 elements and 10,696 nodal points. The values assigned to variable IMESH are the same as those given in Figure 4-4 with the exception that IMESH is set equal to 1.5 in. (38.1 mm) at the crack tip and 4 in. (101.6 mm) at the landward-ceiling corner of the culvert.

With a/L equal to 0.35, Figure 4.6 lists the computed values of stress intensity factors K_I and K_{II} as equal to 1,054 psi$\sqrt{\text{in}}$. (1,158.1 KN/m$^{3/2}$) and to 12.5 psi$\sqrt{\text{in}}$. (13.7 KN/m$^{3/2}$), respectively. The value for K_{II} is quite small relative to the value for K_I, and Mode I opening mode continues to dominate the behavior at the crack tip. The demand increases with the extension of the crack. (Recall that K_I is 1,019 psi$\sqrt{\text{in}}$. (1,119.7 KN/m$^{3/2}$) for the shorter crack with a/L

equal to 0.2.) Assuming that the K_I value computed for the shorter crack is sufficient to overcome the fracture toughness of the concrete, the higher demand computed for this extended crack indicates that the crack will continue to advance.

A contour path radius equal to 20 in. (0.51 m) is specified in the MERLIN analysis of the FE mesh with a crack of length a/L equal to 0.35 (normalized). A 25 percent change in contour path radius (both inward and outward) did not significantly alter the values computed for the stress intensity factors. Thus, it is concluded that a sufficiently fine mesh is being used in this analysis.

4.4.5 LEFM analysis with $a/L = 0.5$

The LEFM mesh is altered for the fourth LEFM analyses by extending the discrete crack to a total length of 86 in. (2.18 m). The 25.8-in. (0.655-m) extension is oriented at 43.83 deg from horizontal using the preprocessor of MERLIN. The resulting FE element mesh (not shown) comprises 5,383 elements and 11,072 nodal points. The values assigned to variable IMESH are the same as those given in Figure 4-4 with the exception that IMESH is set equal to 1.5 in. (38.1 mm) at the crack tip and 4 in. (101.6 mm) at the landward-ceiling corner of the culvert.

With a/L equal to 0.5, Figure 4-6 lists the computed values of stress intensity factors K_I and K_{II} as equal to 1,172 $\text{psi}\sqrt{\text{in.}}$ (1,287.8 KN/m$^{3/2}$) and to 16 $\text{psi}\sqrt{\text{in.}}$ (17.6 KN/m$^{3/2}$), respectively. The value for K_{II} is quite small relative to the value for K_I, and Mode I opening mode continues to dominate the behavior at the crack tip. The demand increases with the extension of the crack. (Recall that K_I is 1,054 $\text{psi}\sqrt{\text{in.}}$ (1,158.1 KN/m$^{3/2}$) for the shorter crack with a/L equal to 0.35.) Assuming that the K_I value computed for the shorter crack is sufficient to overcome the fracture toughness of the concrete, the higher demand computed for this extended crack indicates that the crack will continue to advance.

A contour path radius equal to 20 in. (0.51 m) is specified in the MERLIN analysis of the FE mesh with a crack of length a/L equal to 0.5 (normalized). A 25 percent change in contour path radius (both inward and outward) did not significantly alter the values computed for the stress intensity factors. Thus, it is concluded that a sufficiently fine mesh is being used in this analysis.

4.4.6 LEFM analysis with $a/L = 0.7$

The LEFM mesh is altered for the fifth LEFM analyses by extending the discrete crack to a total length of 120.5 in. (3.06 m). The 34.5-in. (0.876-m) extension is oriented at 42.27 deg from horizontal using the preprocessor of MERLIN. Figure 4-9 shows the lock wall portion of the resulting FE mesh used for the fifth LEFM analysis of Monolith N-56. This figure shows the
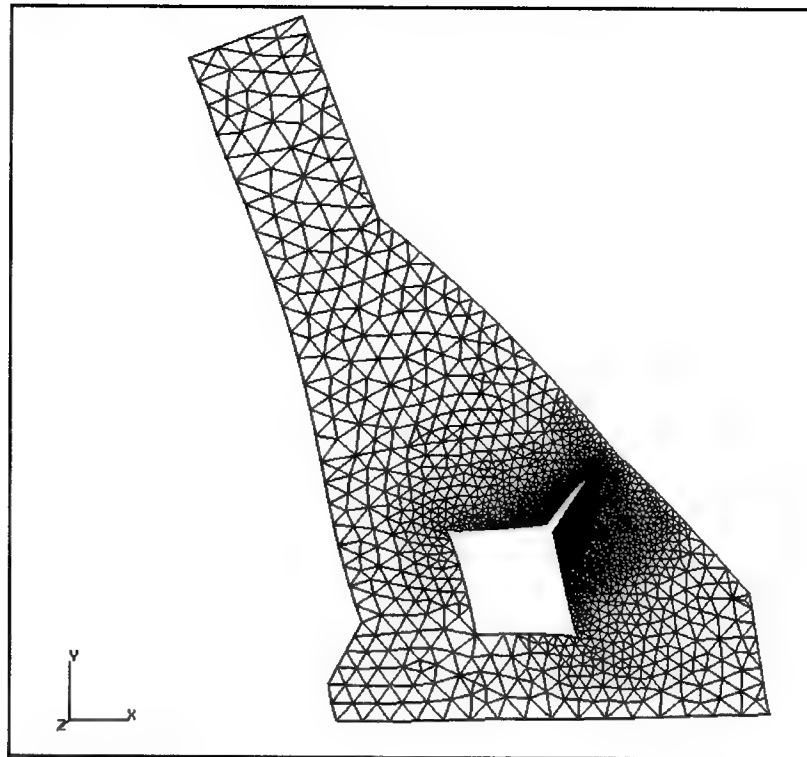
a. Monolith N-56
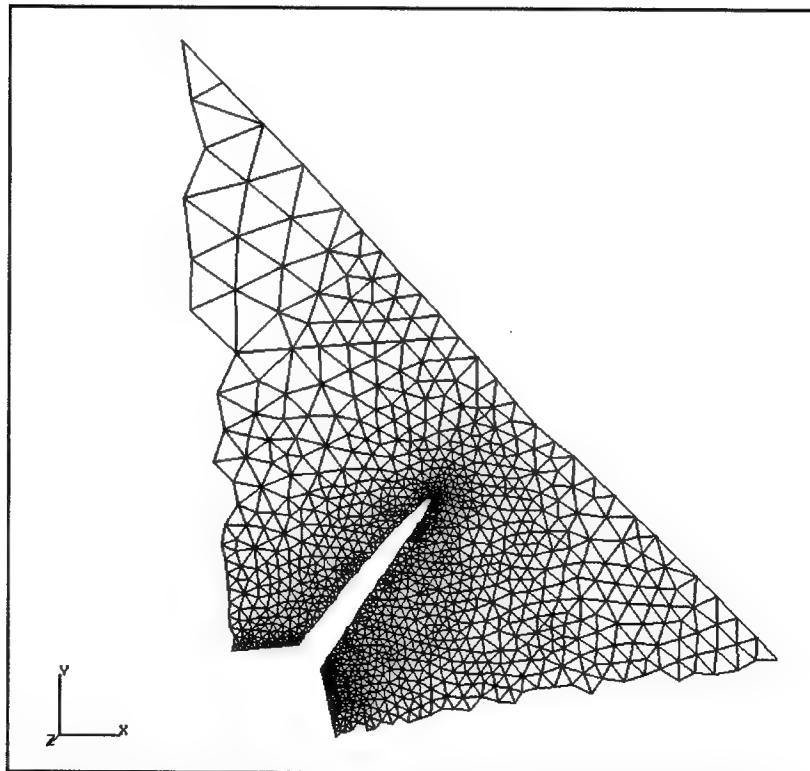
b. Region between the landward-ceiling corner of the filling and
   emptying culvert and the external backfill face of the lock wall

Figure 4-9. Displaced FE mesh of Monolith N-56, a/L = 0.7 (Continued)
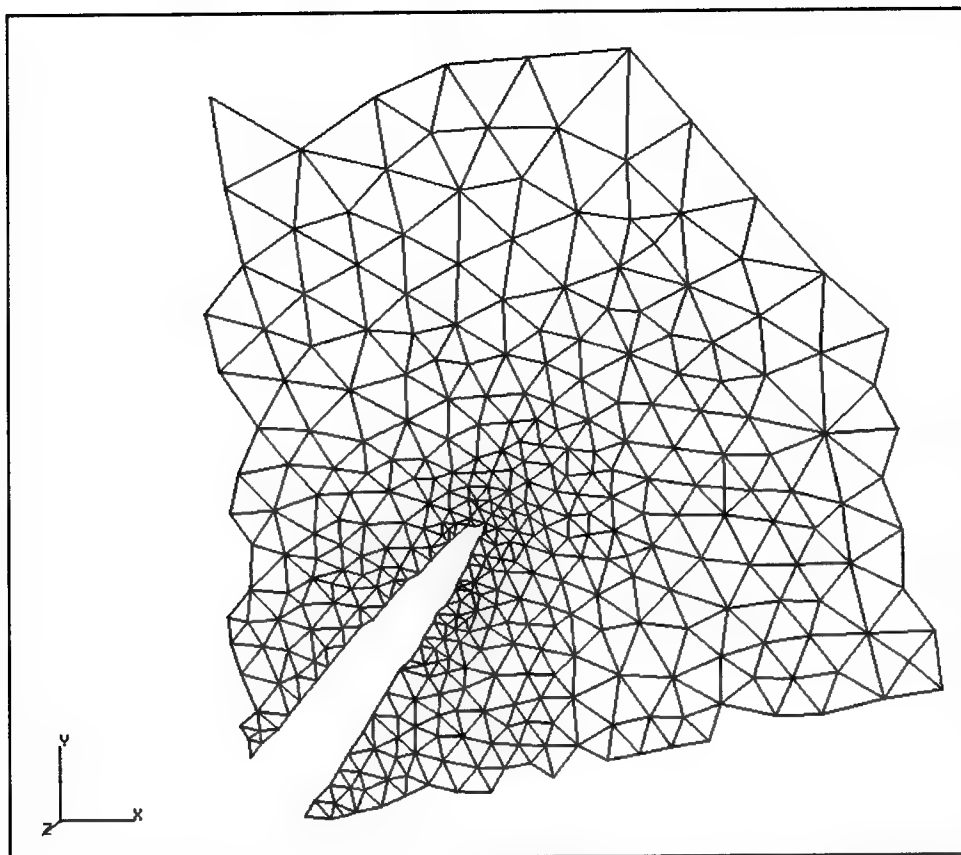
c. Region adjacent to the landward-ceiling corner of the filling and emptying culvert

Figure 4-9. (Concluded)

displaced mesh before and after loading is applied. These nodal point displacements have been multiplied by a factor equal to 2,000 to allow viewing of the discrete crack in these figures. The FE mesh comprises 5,219 elements and 10,766 nodal points. The values assigned to variable IMESH are the same as those given in Figure 4-4 with the exception that IMESH is set equal to 1.5 in. (38.1 mm) at the crack tip and 4 in. (101.6 mm) at the landward-ceiling corner of the culvert.

With a/L equal to 0.7, Figure 4-6 lists the computed values of stress intensity factors K_I and K_{II} as equal to 1,448 $psi\sqrt{in.}$ (1,591 $KN/m^{3/2}$) and 16.7 $psi\sqrt{in.}$ (18.3 $KN/m^{3/2}$), respectively. The value for K_{II} is quite small relative to the value for K_I, and Mode I opening mode continues to dominate the behavior at the crack tip. There is a significant increase in demand with this extension of the crack. (Recall that K_I is 1,172 $psi\sqrt{in.}$ (1,287.8 $KN/m^{3/2}$) for the shorter crack with a/L equal to 0.5.) Assuming that the K_I value computed for the shorter crack is sufficient to overcome the fracture toughness of the concrete, the higher demand computed for this extended crack indicates that the crack will continue to advance.

A contour path radius equal to 25 in. (0.64 m) (as measured from the crack tip) is specified in the MERLIN analysis of the FE mesh with a crack of length a/L equal to 0.7 (normalized). For this analysis the contour path radius is set equal to approximately half the distance between the tip of the discrete crack and the backfill face of the lock so that the numerical evaluations made by the contour integral are at an optimum location (relative to the crack tip and the backfilled face of the lock). A 25 percent change in contour path radius (both inward and outward) did not significantly alter the values computed for the stress intensity factors. Thus, it is concluded that a sufficiently fine mesh is being used in this analysis.

The displacement at the top of the lock is directed into the chamber and is computed to be 0.1669 in. (4 mm) for the mesh with a crack of length a/L equal to 0.7 (normalized). The increase in wall displacements over that computed for the lock without a discrete crack is negligible (see tabulated results in Figure 4-7).

The values computed for K_I and given in Figure 4-6 show that as the crack lengthens, the demand increases. Therefore, the discrete crack was not extended beyond a/L equal to 0.7.

4.5 LEFM Analysis of Snell Lock, Long-term Loading

The second crack extent evaluation of Snell Lock Monolith N-56 was made for the long-term earth and water loading. This load case occurred in the 1960's. Figure 4-10 shows the load cases modeled through end of construction in the LEFM analyses. Elevations of the water table in the backfill and the perched water table are based on field investigations as discussed in Chapter 2. The model of the concrete monolith was first subjected to gravity loading followed by earth and water loading.

4.5.1 Initial finite element analysis (no cracks)

The Figure 4-2 outline of the FE boundaries used for the previous series of end-of-construction analyses is also applicable to the long-term analyses described in this section. Appendix A outlines the calculations used to define the tractions acting parallel and normal to the backfill-to-lock interface. These surface tractions now include water loading due to the water table in the backfill and the perched water table. Beyond the lock, total overburden pressure is applied to the top of rock below the backfill in the model. A dewatered lock is assumed in these series of analyses.

Other than the change in earth loading from end of construction to long-term earth loading and the introduction of water in the backfill, all FE and LEFM analyses are the same as described previously. There was no change in the material parameters for the concrete and the rock. Values assigned to MERLIN's
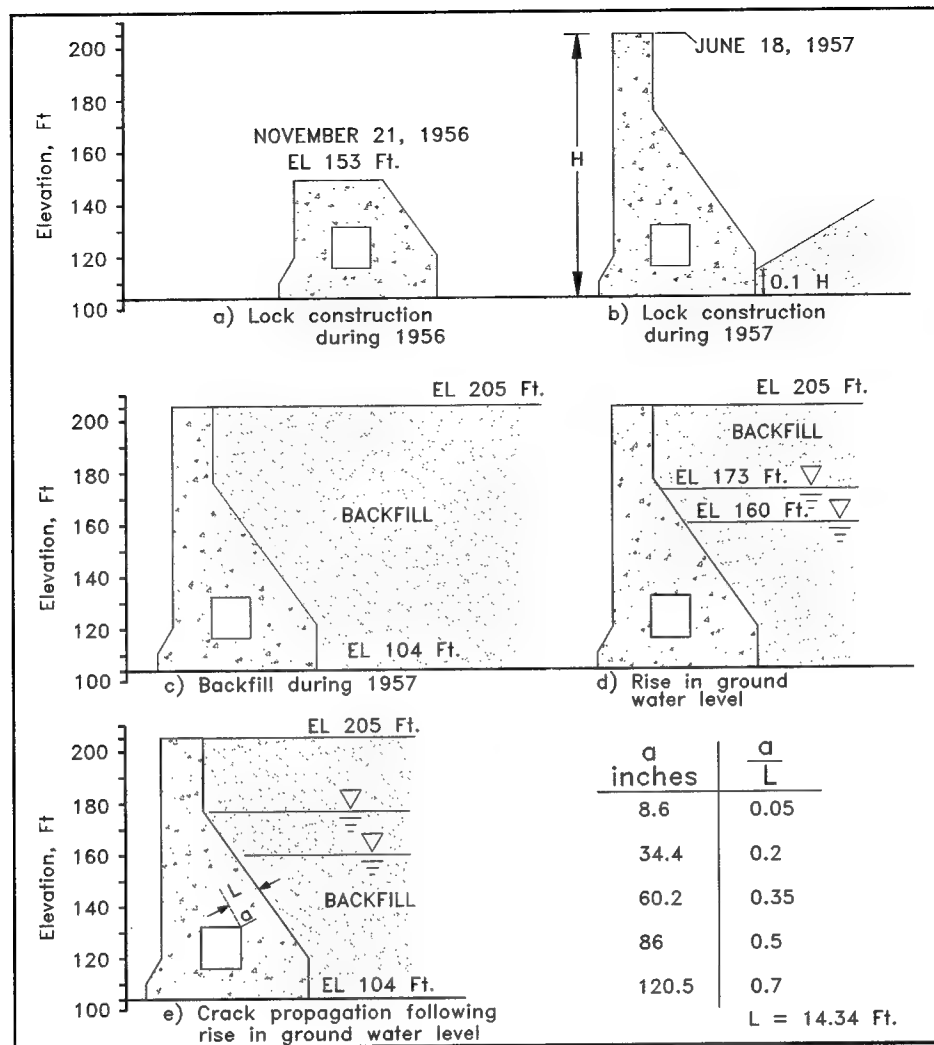
Figure 4-10.   Load cases modeled in the FE analyses through long-term loading
(1 ft = 0.305 m)

IMESH parameters and contour path radius are also the same as described in all
previous analyses.

An initial uncracked mesh similar to that shown in Figure 4-3 was subjected
first to gravity loads and then to the earth and water loading. In this FE analysis
of Monolith N-56 (with no discrete crack), tensile stresses were computed within
the region adjacent to the landward-ceiling corner of the filling and emptying
culvert. The largest principal (tensile) stress was computed by MERLIN to be
equal to 756.26 psi (5,214 KPa) at this culvert corner and normal to the plane
oriented at 44.73 degrees from horizontal. (This is nearly the same tensile stress
value as computed at the culvert corner in the end of construction analysis,
769.43 psi (5,305 KPa).) However, this value of tensile stress is no longer
15 percent of the unconfined compressive strength of concrete because of the
strength gain with time (see data in Appendix C). Thus, it is concluded that
although the tensile stress is significant, it is not as severe a situation as at the end
of construction when the concrete strength is lower.

4.5.2 LEFM analysis with a/L = 0.05

The initial FE mesh was then altered for the first LEFM analysis by introducing a discrete crack within the tensile stress region located at the landward-ceiling corner of the culvert. A discrete crack 8.6 in. (0.218 m) long and oriented at 44.73 deg from horizontal was introduced into the original (uncracked) mesh using the preprocessor of MERLIN. A crack length a of 8.6 in. (0.218 m) corresponds to 5 percent of the closest distance L from the landward-ceiling corner of the filling and emptying culvert through the mass concrete to the exterior backfilled face of the lock wall. The resulting mesh was similar to that shown in Figure 4-5. With a/L equal to 0.05, Figure 4-11 lists the computed values of stress intensity factors K_I and K_{II} as equal to 1,035 psi$\sqrt{\text{in}}$.

(1,137.2 KN/m$^{3/2}$) and to 16.44 psi$\sqrt{\text{in}}$. (18.1 KN/m$^{3/2}$), respectively. The value for K_{II} is quite small relative to the value for K_I. This implies that the Mode I opening mode dominates the behavior at this crack tip. (Recall that values of fracture toughness K_{Ic} from select laboratory and in situ tests on competent concrete typically range in value from approximately 850 psi$\sqrt{\text{in}}$. (934 KN/m$^{3/2}$) to 1,400 psi$\sqrt{\text{in}}$. (1,538 KN/m$^{3/2}$) (Appendix B).) With the computed value for K_I being within the range of likely values for K_{Ic}, crack advance is deemed likely in this numerical analysis. Additionally, the value of K_I computed for the long-term load case is nearly 7 percent larger than the value computed in the comparable end-of-construction load case.

$\frac{a}{L}$	K_I psi $\sqrt{\text{in}}$	K_{II} psi $\sqrt{\text{in}}$	K_{eq} psi$\sqrt{\text{in}}$	$\sqrt{(K_I)^2 + (K_{II})^2}$ psi$\sqrt{\text{in}}$	θ degrees
0.05	1035	16.44	1035.49	1035.13	44.73
0.2	1086	10.72	1086.20	1086.05	43.13
0.35	1176	10.12	1176.16	1176.04	42.0
0.5	1334	4.63	1334.03	1334.01	41.02
0.7	1700	20.67	1700.47	1700.13	40.61

$\theta_{Avg} = 42.3°$

$$K_{eq} = K_I \cos^3 \frac{\theta}{2} - \frac{3}{2} K_{II} \cos \frac{\theta}{2} \sin\theta$$
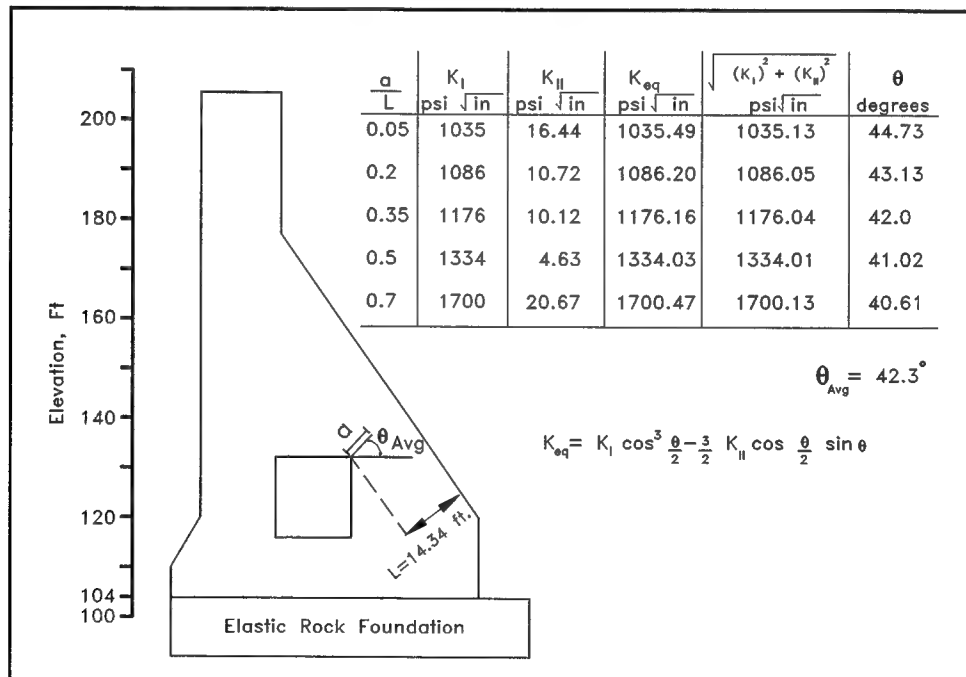
Figure 4-11. Stress intensity factors and crack orientation, long-term loading (1 kN/m$^{3/2}$ = psi$\sqrt{\text{in}}$.)

The displacement at the top of the lock was directed into the chamber and is computed to be 0.1345 in. (3.4 mm) for the mesh with a crack of length a/L equal to 0.05 (normalized). The increase in wall displacements with the introduction of the discrete crack was negligible (see the first two data entries in Figure 4-12).

a/L	U_x Deflection (in)	$\frac{U_x}{\text{Height}}$
0.00	.1343	.00011081
0.05	.1345	.00011097
0.20	.1353	.00011163
0.35	.1363	.00011246
0.50	.1382	.00011403
0.70	.1424	.00011749

Height = 101 ft.
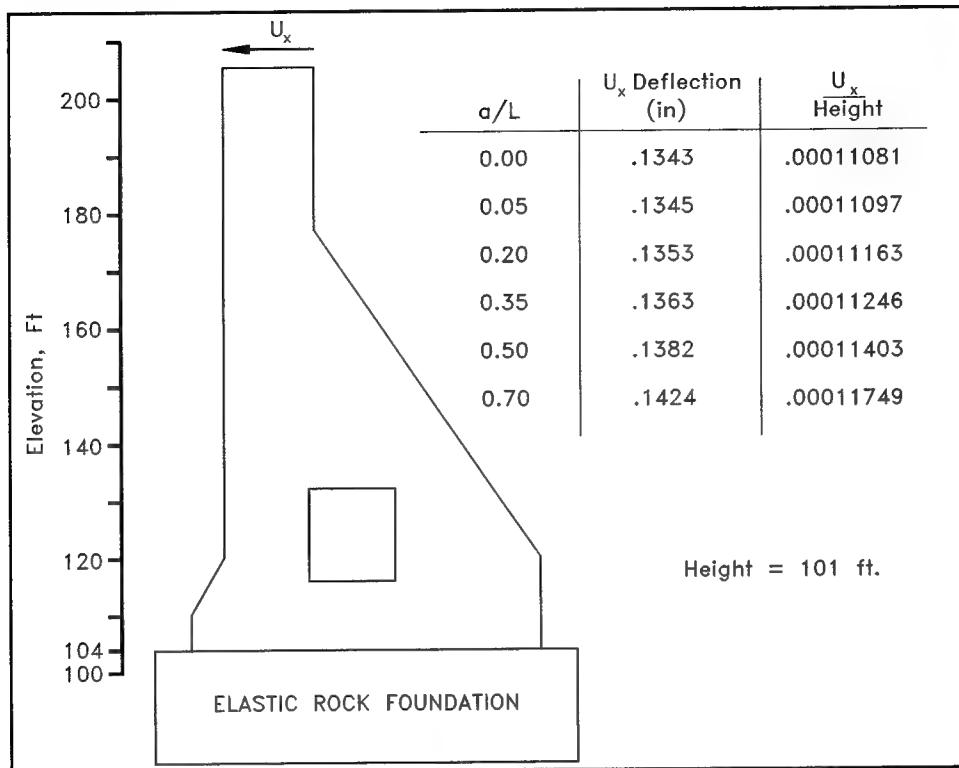
Figure 4-12.   Horizontal deflection at top of lock wall, long-term loading
(1 in. = 25.4 mm, 1 ft = 0.305 m)

4.5.3 LEFM analysis with $a/L = 0.2$

The initial LEFM mesh was then altered for the second LEFM analyses by extending the discrete crack to a total length of 34.4 in. (0.874 m). The 25.8-in. (0.655-m) extension was oriented at 43.13 deg from horizontal using the preprocessor of MERLIN. A crack length of 34.4 in. (0.874 m) corresponds to 20 percent of the closest distance from the landward-ceiling corner of the filling and emptying culvert through the mass concrete to the exterior backfilled face of the lock wall ($a/L = 0.2$). The resulting FE mesh is similar to that shown in Figure 4-8. With a/L equal to 0.2, Figure 4-11 lists the computed values of stress intensity factors K_I and K_{II} as equal to 1,086 $\mathrm{psi}\sqrt{\mathrm{in.}}$ (1,193.3 $\mathrm{KN/m^{3/2}}$) and to 10.7 $\mathrm{psi}\sqrt{\mathrm{in.}}$ (11.8 $\mathrm{KN/m^{3/2}}$), respectively. The value for K_{II} is quite small relative to the value for K_I, and Mode I opening mode continues to dominate the behavior at the crack tip. The demand increased with the extension of the crack. Assuming that the K_I value computed for the shorter crack is sufficient to overcome the fracture toughness of the concrete, the higher demand computed for this extended crack indicates that the crack will continue to advance.

4.5.4 LEFM analysis with *a/L* = 0.35

The LEFM mesh used in the second LEFM was altered for the third LEFM analysis by extending the discrete crack to a total length of 60.2 in. (1.53 m). The 25.8-in. (0.655-m) extension was oriented at 42.0 deg from horizontal using the preprocessor of MERLIN. A crack length of 60.2 in. (1.53 m) corresponds to 35 percent of the closest distance from the landward-ceiling corner of the filling and emptying culvert through the mass concrete to the exterior backfilled face of the lock wall (*a/L* = 0.35). With *a/L* equal to 0.35, Figure 4-11 lists the computed values of stress intensity factors K_I and K_{II} as equal to 1,176 psi$\sqrt{\text{in.}}$ (1,292.2 KN/m$^{3/2}$) and to 10.1 psi$\sqrt{\text{in.}}$ (11.1 KN/m$^{3/2}$), respectively. The value for K_{II} is quite small relative to the value for K_I, and Mode I opening mode continues to dominate the behavior at the crack tip. The demand continues to increase with the extension of the crack. Assuming that the K_I value computed for the shorter crack is sufficient to overcome the fracture toughness of the concrete, the higher demand computed for this extended crack indicates that the crack will continue to advance.

4.5.5 LEFM analysis with *a/L* = 0.5

The third LEFM mesh was altered for the fourth LEFM analysis by extending the discrete crack to a total length of 86 in. (2.18 m). The 25.8-in. (0.655-m) extension was oriented at 41.02 deg from horizontal using the preprocessor of MERLIN. With *a/L* equal to 0.5, Figure 4-11 lists the computed values of stress intensity factors K_I and K_{II} as equal to 1,334 psi$\sqrt{\text{in.}}$ (1,465.8 KN/m$^{3/2}$) and to 4.6 psi$\sqrt{\text{in.}}$ (5.1 KN/m$^{3/2}$), respectively. The value for K_{II} is quite small relative to the value for K_I, and Mode I opening mode continues to dominate the behavior at the crack tip. The demand increases with the extension of the crack. Assuming that the K_I value computed for the shorter crack is sufficient to overcome the fracture toughness of the concrete, the higher demand computed for this extended crack indicates that the crack will continue to advance.

4.5.6 LEFM analysis with *a/L* = 0.7

The fourth LEFM mesh was altered for the fifth LEFM analysis by extending the discrete crack to a total length of 120.5 in. (3.06 m). The 34.5-in. (0.876-m) extension was oriented at 40.61 deg from horizontal using the preprocessor of MERLIN. The resulting mesh is similar to that shown in Figure 4-9 used in the analysis of the end-of-construction load case. With *a/L* equal to 0.7, Figure 4-11 lists the computed values of stress intensity factors K_I and K_{II} as equal to 1,700 psi$\sqrt{\text{in.}}$ (1,867.9 KN/m$^{3/2}$) and 20.7 psi$\sqrt{\text{in.}}$ (22.7 KN/m$^{3/2}$), respectively. The value for K_{II} is quite small relative to the value for K_I, and Mode I opening mode continues to dominate the behavior at the crack tip. There is a significant increase in demand with this extension of the crack. Assuming that the K_I value computed for the shorter crack is sufficient to overcome the fracture toughness of

the concrete, the higher demand computed for this extended crack indicates that the crack will continue to advance.

The displacement at the top of the lock is directed into the chamber and is computed to be 0.1424 in. (3.6 mm) for the mesh with a crack of length a/L equal to 0.7 (normalized). The increase in wall displacements over that computed for the lock without a discrete crack is negligible (see tabulated results in Figure 4-12).

The values computed for K_I and given in Figure 4-11 show that as the crack lengthens, the demand increases. Therefore, the discrete crack was not extended beyond a value of a/L of 0.7.

4.6 LEFM Analysis of Snell Lock with the Top-of-Culvert Geometry in the Shape of a Half-Circle, Long-term Loading

The linear FE analyses of Snell Lock (with no discrete cracks) show that large tensile stresses are computed within the region adjacent to the landward-ceiling corner of the filling and emptying culvert, as shown in Figure 4-13. Peak tensile stress σ_p equals 756.25 psi (5,214 KPa) at this corner (Figure 4-14a). Note that the shape of the culvert of Snell Lock is rectangular (Figure 4-13a or Figure 4-14a). Sharp corners are known to introduce large stress/strain gradients. Therefore, an additional analysis was conducted to see if a change in culvert geometry would reduce crack potential and/or crack propagation. The top of the culvert was altered from a horizontal surface to a half-circle, as shown in Figure 4-14b. The center for this half-circle was located midway along the existing culvert ceiling. The closest distance L from the altered landward-ceiling geometry of the filling and emptying culvert through the mass concrete to the exterior backfilled face of the lock wall was maintained at the Snell Lock value of 14.34 ft (4.37 m). The base of the modified culvert was raised to maintain the same volume as that of the unaltered rectangular culvert. A linear elastic FE analysis of this altered lock geometry was conducted for long-term loading using MERLIN. The results for the hypothetical lock wall with the altered culvert geometry are summarized in Figures 4-14b and 4-14c and in Figure 4-15. The results of the original analyses of the rectangular culvert are included in Figure 4-14a for comparison. The linear FE analysis (with no crack) shows the culvert geometry to have a significant influence on crack initiation. Eliminating the sharp corner for the landward-ceiling corner of the culvert reduces the principal tensile stress from 756.26 psi (5,214 KPa) for the rectangular culvert in Figure 4-14a to 245.95 psi (1,696 KPa) for the half-circle top of the culvert in Figure 4-14c. This corresponds to a one-third reduction in principal tensile stress. Additionally, the principal stress contours are spaced further apart for the half-circle top of culvert (Figure 4-15b) than the contours for the rectangular culvert (Figure 4-13b). Note that the magnitude of the largest value of principal tensile stress for the half-circle top of culvert is well below the capacity of competent concrete. Thus, alteration of culvert geometry can be used to reduce the likelihood of <u>crack initiation.</u>
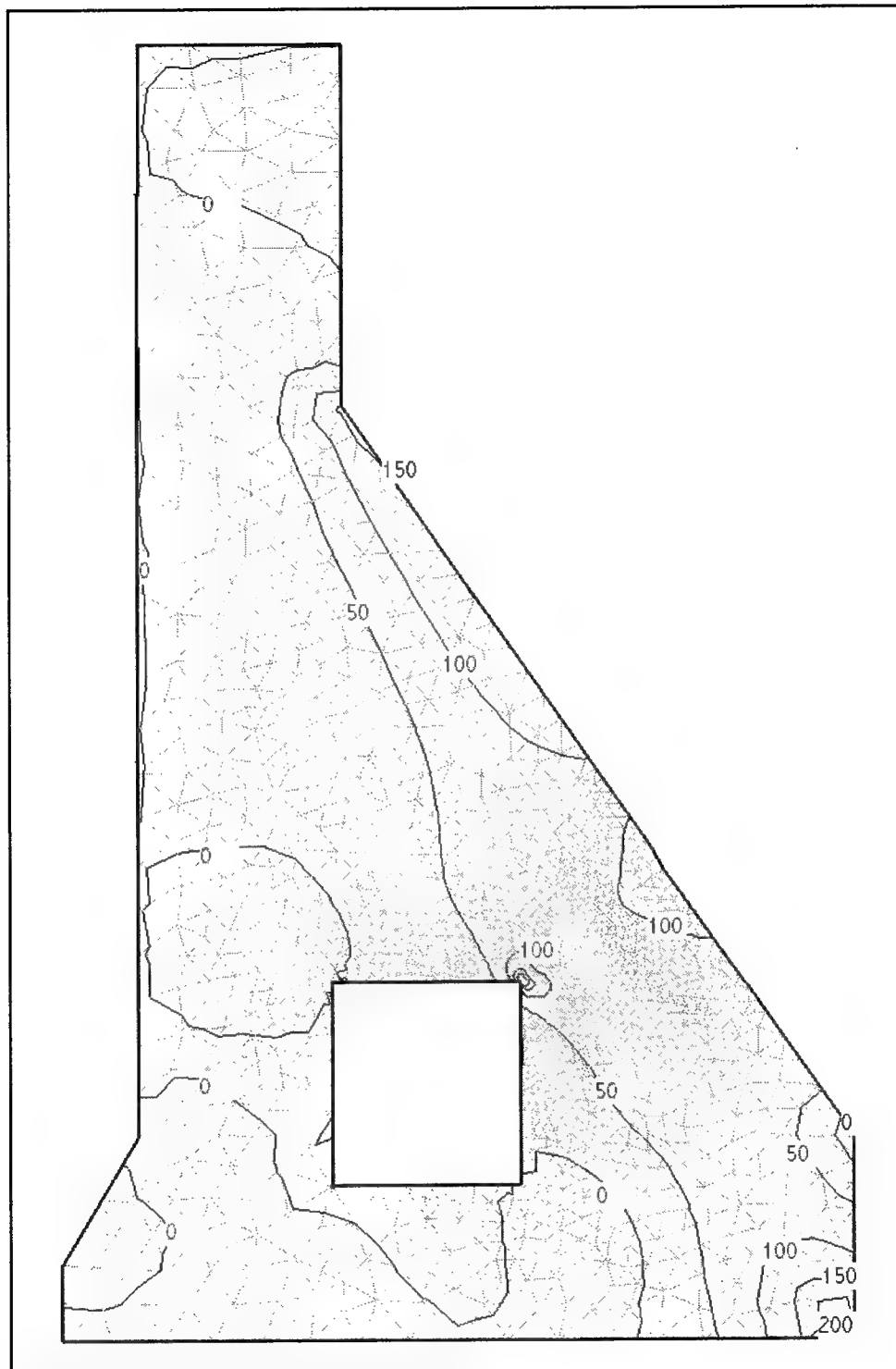
a. Rectangular filling and emptying culvert

Figure 4-13. Contours of principal tensile stress, psi, rectangular filling and emptying culvert (Continued)
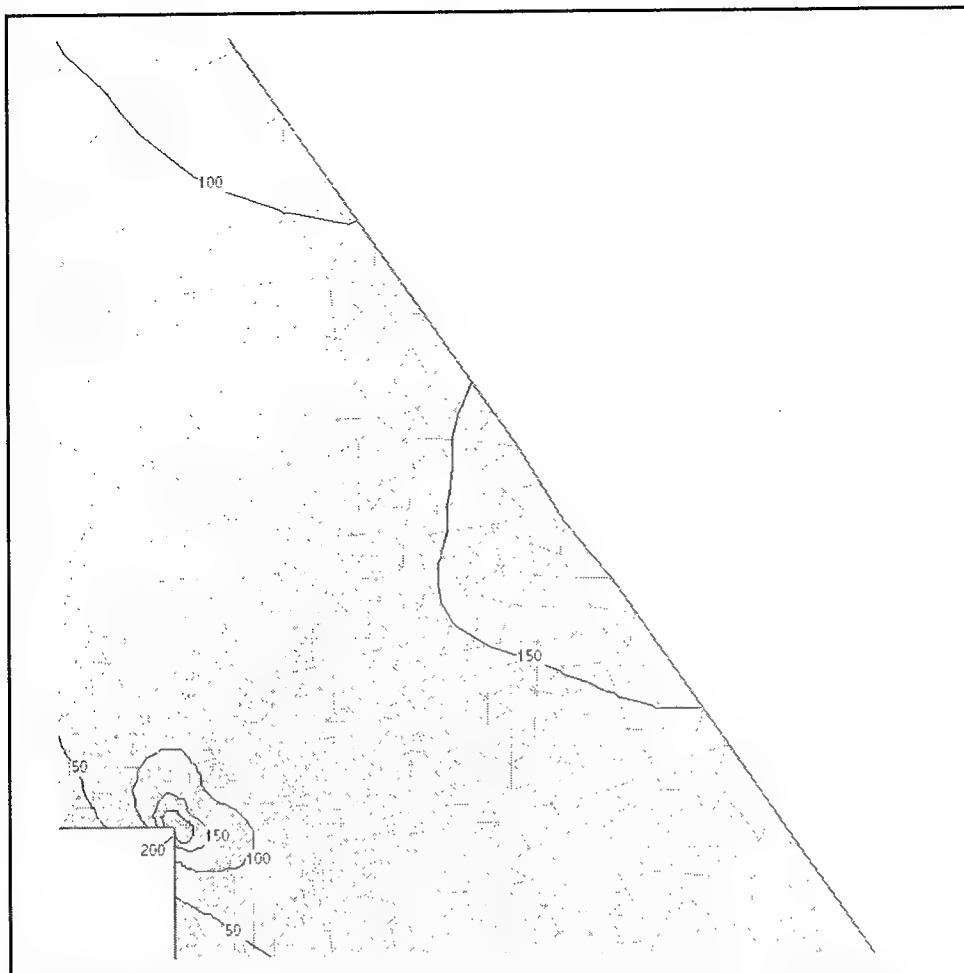
b. Region between the landward-ceiling corner of the filling and emptying culvert and the external backfill face of the lock wall

Figure 4-13. (Concluded)

The results for the LEFM analysis of a discrete crack corresponding to the normalized crack length a/L of 0.05 are reported in Figures 4-14b and 4-14c. These results show that the critical location shifts from the former culvert corner, designated as Point A in Figure 4-14b, to Point B in Figure 4-14c. Point B is at the 45-deg point along the 180-deg half-circle. The stress intensity factor is computed to be equal to 1,014 $psi\sqrt{in}$. (1,114.1 $KN/m^{3/2}$). Note that the stress intensity factor at Point A for the rectangular culvert, with the same crack length ($a/L = 0.05$), has nearly the same value for the stress intensity factor, 1,035 $psi\sqrt{in}$. (1,137.2 $KN/m^{3/2}$) (Figure 4-14a). This implies that once a discrete crack (with a normalized length of a/L equal to 0.05) has formed, the advantage of culvert geometry is nullified. For the given lock wall geometry and culvert location, the culvert geometry has virtually no impact on the magnitude of the stress intensity factor. Recall that the stress intensity factor characterizes the demand in a crack propagation evaluation of the lock wall.

Point A

a/L	σ_p psi	K_{eq} psi $\sqrt{in}$
0.00	756.3	——
0.05	——	1035

a) Rectangular Culvert

Point A

a/L	σ_p psi	K_{eq} psi $\sqrt{in}$
0.00	26.73	——
0.05	——	190

b) Half–Circle Culvert Ceiling

Point B

a/L	σ_p psi	K_{eq} psi $\sqrt{in}$
0.00	245.95	——
0.05	——	1014

c) Half–Circle Culvert Ceiling
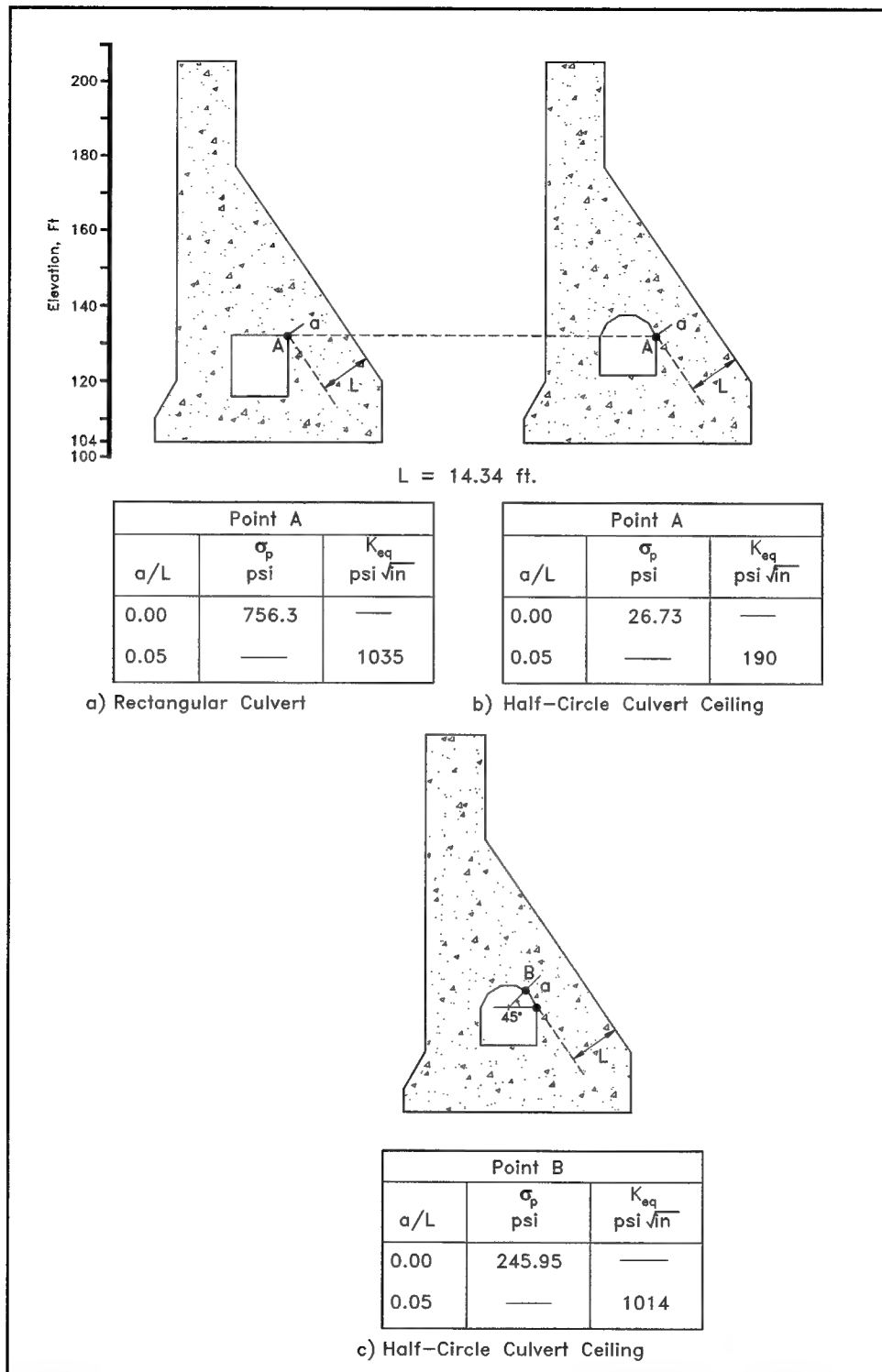
Figure 4-14. Influence of culvert geometry on tensile stresses and stress intensity factors for long-term loading (1 MPa = 145.04 psi, 1 kN/m$^{3/2}$ = 0.91 psi$\sqrt{in}$.)
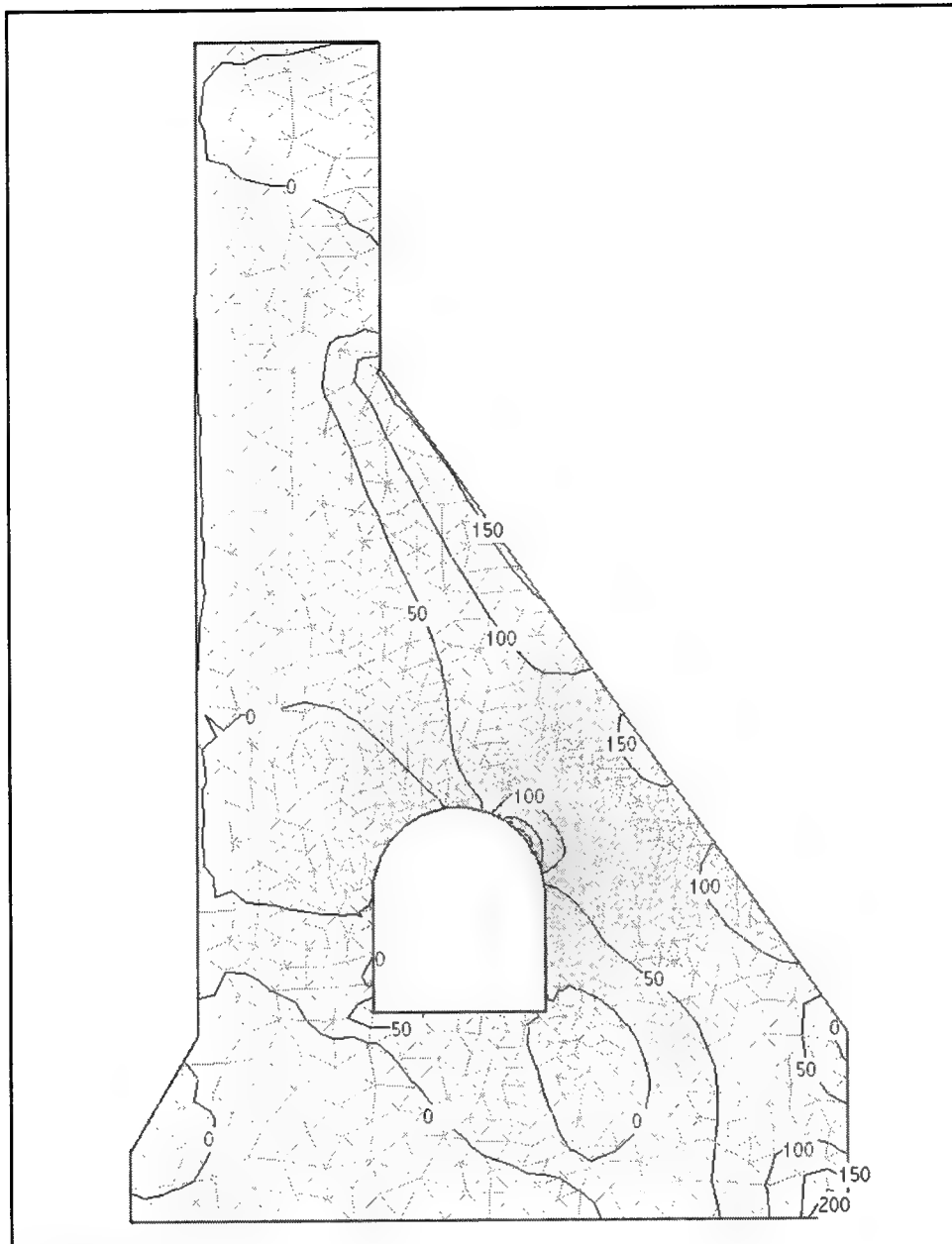
a. Half-circle top of culvert

Figure 4-15.   Contours of principal tensile stress, psi, half-circle top of culvert
(Continued)

b. Region between the top of the curved filling and emptying culvert and the
   external backfilled face of the lock wall

Figure 4-15. (Concluded)

In summary, the alteration of culvert geometry can be used to reduce the
likelihood of crack initiation so long as no thermally induced cracks or
construction defects (i.e., cracks or cold joints) are present. However, once a
crack has formed or is introduced at the half-circle top of culvert, the demand for
crack propagation for this altered monolith geometry is nearly the same as for the
rectangular culvert. This research did not explore the effects of altering culvert
location nor altering the thickness of the lock wall.

4.7 Conclusions

The conclusions of the studies described in this chapter are as follows:

a. A crack formed within the lock region located between the landward-
    ceiling corner of the filling and emptying culvert and the exterior
    backfilled face of the lock wall. The crack intersected the culvert at the

landward-ceiling corner. The precise trajectory of the crack through the monolith was not mapped when the crack was discovered in the field.

b. Significant tensile stresses were computed within the landward-ceiling corner culvert region of Snell Lock for both short-term, end-of-construction earth loading and long-term earth and water loading by linear FE analysis.

   (1) Short-term, end-of-construction analysis. The value of tensile stress computed within the landward-ceiling corner of the culvert was 769.43 psi (5,305 KPa). The computed tensile stress was equal to approximately 15 percent of the unconfined compressive strength of 1-year-old concrete specimens cast in 1956. These specimens are considered representative of the concrete placed within the landward-ceiling corner of the culvert.

   (2) Long-term analysis. The largest computed principal (tensile) stress was 756.26 psi (5,214 KPa) at the landward-ceiling culvert corner. This value is nearly the same tensile stress value as computed at the culvert corner in the end of construction analysis. However, this value of tensile stress is less than 15 percent of the unconfined compressive strength of concrete because of the strength gain with time (Chapter 3 and Appendix C).

   (3) Thus, it is concluded that although the tensile stress is significant for long-term loading, it is not as severe a situation as at the end of construction when the concrete strength is lower.

c. With no significant tensile stresses computed along the backfilled face of the lock wall, the linear FE analyses indicate that cracking is likely to have initiated at the landward-ceiling corner culvert region.

d. For the boundary condition of a crack initiating at the landward-ceiling corner of the filling and emptying culvert, both series of LEFM analyses show the demand (i.e., the stress intensity factor) increases with crack extension. This implies that if the demand is sufficient to overcome the capacity of the concrete (i.e., the fracture toughness) at the early stages of cracking, the crack will propagate to the backfilled face of the wall (assuming a uniform capacity for the concrete within this region).

e. The values computed for the stress intensity factors for the long-term loading analyses are larger than the values computed for the end-of-construction analyses (e.g., by 6.7 percent for the two analyses with a/L equal to 0.05 and by 17.4 percent for the two analyses with a/L equal to 0.7). In general, as the crack length increased, the difference in the values computed for the stress intensity factors for the two load cases increased.

f. The closest distance from the landward-ceiling corner of the filling and emptying culvert through the mass concrete to the exterior backfilled face of the lock wall is 14.34 ft (4.37 m) and is oriented at 35.2 deg from

horizontal. The short-term, end-of-construction LEFM analyses indicate the crack trajectory to average 44.2 degrees from horizontal (Figure 4-6). The long-term LEFM analyses indicate the crack trajectory to average 42.3 deg from horizontal (Figure 4-11). A factor that may contribute to the computed cracking trajectory not being the same as the closest distance is the presence of shearing stresses within this region of the lock monolith.

g. Linear elastic FE analyses and LEFM analyses show that the presence of the sharp corner for the culvert contributes to the development of significant tensile stresses within this region of the culvert.

h. Changing the geometry of the culvert to one that reduces stress concentrations by improving stress flow around the culvert may significantly reduce cracking potential. Analyses show that changing the geometry of the culvert ceiling from flat to a half-circle reduces the principal tensile stress a factor of one-third. These results also show that the critical location shifts from the former culvert corner to the 45-degree point along the 180-degree half-circle.

i. Once a discrete crack (with a/L equal to 0.05) has formed, the advantage of the half-circle top-of-culvert geometry is nullified. That is, once a crack has formed due to thermal loading or is introduced during construction, the demand for crack propagation within this monolith geometry is nearly the same demand as for the rectangular culvert.

5 Summary and Conclusions

5.1 Introduction

This report discusses the results of a crack initiation and propagation evaluation of Snell Lock, one of the locks on the St. Lawrence Seaway. The rock-founded, unreinforced concrete gravity lock walls of Snell Lock experienced cracking as a result of earth loading in excess of those anticipated during structural design. The objective of this study was to appraise two analytical procedures used to evaluate the potential for and/or the extent of cracking within massive concrete structures. Snell Lock was chosen because it is one of the lock case histories in Ebeling, Patev, and Mosher (1996) for which the earth and water loadings and the engineering properties for the mass, unreinforced concrete are well defined. A few years after the lock was put in service, a crack was found to extend from the landward-ceiling corner of the filling and emptying culvert through the mass concrete to the exterior backfilled face of the lock wall.

The two analytical procedures available for use in analyzing hydraulic structures that may exhibit cracking during loading are formulated based on either the smeared crack theory or the discrete crack theory (American Concrete Institute 1997 (ACI 446.3R-97)). The procedure based on the smeared crack theory has been implemented in the computer program ANACAP (ANATECH Corporation 1997). The second procedure uses the discrete crack theory and has been implemented in the computer program MERLIN (Reich, Cervenka, and Saouma 1995).

Cracking potential and crack extent for Snell Lock are assessed for both short-term, end-of-construction earth loading and long-term earth and water loading. The Snell Lock monolith selected for analysis is Monolith N-56, located approximately midway along the 860-ft- (262.13-m-) long lock chamber (Figure 2-9). The geometry of this monolith is representative of those defining the lock chamber at Snell.

5.2 Earth and Water Pressure Loading

The earth and water pressure forces applied to the back of Snell Lock Monolith N-56 in the finite element (FE) analyses are based on field instrumentation data, described in Chapter 2. Appendix A summarizes the results of equilibrium

calculations used to transform the earth and water loading from those acting along a plane extending vertically from the heel of the lock wall up through the backfill, shown in Figure 2-9, to those forces acting along the backfill-to-lock interface. Both horizontal and vertical shear resultant forces are included in these transformations. The horizontal earth pressures and downdrag, shear stresses acting along this vertical plane, are established using horizontal and vertical earth pressure coefficients. The water pressures acting normal to this vertical plane are established based on a steady-state water table at el 160 and a perched water table at el 173 within the backfill.

Appendix A delineates the continuous effective earth pressure σ'_h distribution with elevation as three discrete distributions, from el 104 to el 120, from el 120 to el 176.75, and from el 176.75 to el 205. The corresponding resultant horizontal effective forces F_{h1}, F_{h2}, and F_{h3} and points of action computed for each of the three pressure segments are identified in Figure A-2 and given in Table A-1. Values of the resultant water pressure forces shown in Figure A-2 are also given in Table A-1.

The applied loads are specified in the FE analyses in terms of surface tractions along the three lock-wall-to-soil-backfill interface regions. These surface tractions consist of both shear stresses τ and total stresses applied normal to the interface σ_n. Tables A-4, A-5, and A-6 list the values of the two surface tractions, σ_n and τ, specified in the FE analyses.

5.3 Two Analytical Procedures to Analyze Hydraulic Structures Exhibiting Cracking

One analytical procedure available for use in analyzing hydraulic structures that may exhibit cracking during loading is formulated based on the smeared crack theory. This analytical procedure has been implemented in the computer program ANACAP (ANATECH Corporation 1997).

The smeared crack theory uses a strength-of-materials approach to evaluate crack initiation potential and/or crack propagation in a material. According to the theory, cracks may develop on planes on which tensile strain and tensile stress act. The largest tensile strain(s) and stress(es) will develop on principal planes. In ANACAP, the potential for cracking is evaluated on the three principal planes at each integration point within every element composing the mesh for each stage of loading. ANACAP uses the strains acting on an infinitesimal cube at an integration point to determine the orientation of the three principal planes. If the material is isotropic and there is no pre-existing crack, then the three principal planes of strain and stress are coincident and can be determined from the stresses acting on the faces of an infinitesimal cube at the integration point. The principal values for tensile strain and tensile stress on each of the three principal planes are then compared to the smeared crack criterion specified for the material. Figure 3-1 shows an example of the criterion used in ANACAP. The diagonal line distinguishes crack initiation potential in Figure 3-1 and is defined by the two concrete material properties, the tensile fracture strain ε_s and Youngs modulus

$E(t)$. If any of these three pairs of principal strains and stresses is tensile (i.e., tensile fracture strains and tensile fracture stresses) and exceeds the diagonal solid line in Figure 3-1, a crack develops on that plane. Otherwise, no cracking occurs on that plane. Note that crack *initiation* is an explicit aspect of smeared crack theory. Chapter 3 summarizes the smeared crack analysis of Snell Lock using ANACAP.

Another analytical procedure available for use in analyzing hydraulic structures that may exhibit cracking during loading is formulated based on linear elastic fracture mechanics theory (LEFM). LEFM discrete crack analysis is used to assess if a crack will propagate or arrest for a given increment of loading. This analytical procedure has been implemented in the computer program MERLIN (Reich, Cervenka, and Saouma 1995). This fracture mechanics method can be used in structures for which the area surrounding the crack tip is relatively large compared to the fracture process zone (American Concrete Institute 1997 (ACI 446.3R-97)). For normal size building members (such as beams or columns), a nonlinear fracture mechanics is normally required.

The LEFM procedure is an FE method-based procedure to model the propagation of a discrete crack. Generally, LEFM relates the stress magnitude and distribution at the crack tip to the nominal stress applied to the structure; to the size, shape, and orientation of the crack or discontinuity; and to the material properties. The "demand" due to loading(s) applied to the retaining structure, and specifically to the region of cracking, is represented by stress intensity factors K_I, K_{II}, and K_{III} for the three cracking modes. Cracking Mode I is an opening mode, Mode II is a shearing mode, and Mode III is a tearing mode. Conceptually, the stress intensity factors indicate the rate at which the stress approaches infinity ahead of the crack tip for each of the three displacement modes. The stress intensity factors characterize the magnitude of the crack tip stress field for the potential cracking modes. The "capacity" of the material is characterized by the fracture toughness K_{Ic}. (Values of K_{Ic} from select laboratory and in situ tests on concrete are discussed in Appendix B.) Crack advance is monitored in an LEFM analysis by comparing the demand to capacity (e.g., K_I to K_{Ic}). When the value for K_I is greater than the value for K_{Ic}, the crack advances. Otherwise, the crack will not advance.

A limitation of LEFM as implemented in MERLIN is that there is no crack *initiation* aspect of the methodology (unlike the smeared crack theory). To circumvent this limitation, a strength-of-materials approach is first used *to assess the likely regions of potential cracking* within the monolith. Chapter 4 discusses the use of LEFM as implemented in MERLIN to analyze Snell Lock.

5.4 Smeared Crack Analyses of Snell Lock

The FE thermal analysis performed on Snell Lock Monolith N-56 gives the strong indication that the potential for a cracking in the upper right corner of the lower monolith did exist after the backfilling was complete in 1957 (referred to as end-of-construction earth loading in this report). These results also indicate that microcracks in the mass concrete in the culvert area were created during the

winter of 1956-1957. Upon an increase in stress intensity due to the backfilling and overcompaction of the glacial till, these cracks created an expansion of a crack to the inclined surface of the lock wall.

5.5 Discrete Crack Analyses of Snell Lock

The conclusions of the discrete crack analyses are as follows:

a. A crack formed within the lock region located between the landward-ceiling corner of the filling and emptying culvert and the exterior backfilled face of the lock wall. The crack intersected the culvert at the landward-ceiling corner. The precise trajectory of the crack through the monolith was not mapped when the crack was discovered in the field.

b. Significant tensile stresses were computed within the landward-ceiling corner culvert region of Snell Lock for both short-term, end-of-construction earth loading and long-term earth and water loading by linear FE analysis.

    (1) Short-term, end-of-construction analysis. The value of tensile stress computed within the landward-ceiling corner of the culvert was 769.43 psi (5,305 KPa). The computed tensile stress was equal to approximately 15 percent of the unconfined compressive strength of 1-year-old concrete specimens cast in 1956. These specimens are considered representative of the concrete placed within the landward-ceiling corner of the culvert.

    (2) Long-term analysis. The largest computed principal (tensile) stress was equal to 756.26 psi (5,214 KPa) at the landward-ceiling culvert corner. This value is nearly the same tensile stress value as computed at the culvert corner in the end-of-construction analysis. However, this value of tensile stress is less than 15 percent of the unconfined compressive strength of concrete because of strength gain with time (Chapter 3 and Appendix C).

    (3) Thus, it is concluded that although the tensile stress is significant for long-term loading, it is not as severe a situation as at the end of construction when the concrete strength is lower.

c. With no significant tensile stresses computed along the backfilled face of the lock wall, the linear FE analyses indicate that cracking is likely to have initiated at the landward-ceiling corner culvert region.

d. For the boundary condition of a crack initiating at the landward-ceiling corner of the filling and emptying culvert, both series of LEFM analyses show the demand (i.e., the stress intensity factor) increases with crack extension. This implies that if the demand is sufficient to overcome the capacity of the concrete (i.e., the fracture toughness) at the early stages of

cracking, the crack will propagate to the backfilled face of the wall (assuming a uniform capacity for the concrete within this region).

e. The values computed for the stress intensity factors for the long-term loading analyses are larger than the values computed for the end-of-construction analyses (e.g., by 6.7 percent for the two analyses with a/L equal to 0.05 and by 17.4 percent for the two analyses with a/l equal to 0.7). In general, as the crack length increased, the difference in the values computed for the stress intensity factors for the two load cases increased.

f. The closest distance from the landward-ceiling corner of the filling and emptying culvert through the mass concrete to the exterior backfilled face of the lock wall is 14.34 ft (4.37 m) and is oriented at 35.2 deg from horizontal. The short-term, end-of-construction LEFM analyses indicate the crack trajectory to average 44.2 deg from horizontal (Figure 4-6). The long-term LEFM analyses indicate the crack trajectory to average 42.3 deg from horizontal (Figure 4-11). A factor that may contribute to the computed cracking trajectory not being the same as the closest distance is the presence of shearing stresses within this region of the lock monolith.

g. Linear elastic FE analyses and LEFM analyses show that the presence of the sharp corner for the culvert contributes to the development of significant tensile stresses within this region of the culvert.

h. Changing the geometry of the culvert to one that reduces stress concentrations by improving stress flow around the culvert may significantly reduce the potential for crack initiation in an unreinforced concrete monolith. Analyses described in Section 4.6 of Chapter 4 show that by changing the geometry of the culvert ceiling from flat to a half-circle, the tensile stresses computed at the former location of the landward-ceiling corner become insignificant. However, the analyses also show that once a crack has formed (due to thermal loading or introduced during construction) the demand for crack propagation (expressed in terms of the stress intensity factor K_I in a LEFM analysis) for a monolith with a curved ceiling culvert is nearly the same demand as for a rectangular culvert.

References

American Concrete Institute. (1997). "Finite element analysis of fracture in concrete structures: State-of-the-art," Report No. ACI 446.3R-97, ACI Committee 446, Farmington Hills, MI. 33 pp.

ANATECH Corporation. (1997). "ANACAP, ANATECH Concrete Analysis Program user's manual, Version 2.5," San Diego, CA.

Buck, A. D., Mather, B., and Thorton, H. T. (1967). "Investigation of concrete in Eisenhower and Snell Locks, St. Lawrence Seaway," Technical Report No. 6-784, U.S. Army Engineer Waterways Experiment Station, Vicksburg, MS.

Diviney, J. G. (1990). "Performance of large gravity walls at Eisenhower and Snell Locks." *Design and performance of earth retaining structures, Proceedings of a Conference,* Cornell University, Ithaca, NY, June 18-20, 1990. Geotechnical Special Publication No. 25, Phillip C. Lambe and Lawrence A. Hansen, ed., ASCE, New York, 278-291.

Duncan, J. M., and Seed, R. B. (1986). "Compaction-induced earth pressures under K_o conditions," *Journal of the Geotechnical Engineering Division,* ASCE, 112(1), 1-22.

Ebeling, R. M., Pace, M. E., and Morrison, E. E. (1997). "Evaluating the stability of existing massive concrete gravity structures founded on rock," Technical Report No. REMR-CS-54, U.S. Army Engineer Waterways Experiment Station, Vicksburg, MS.

Ebeling, R. M., Patev, R. C., and Mosher, R. L. (1996). "Case histories of earth pressure-induced cracking of locks," Technical Report No. ITL-96-9, U.S. Army Engineer Waterways Experiment Station, Vicksburg, MS.

Empire Soils Investigation, Inc. (1985). "Geotechnical parameters, glacial till backfill, Eisenhower and Snell Locks/St. Lawrence Seaway," Groton, NY.

Filz, G. M., and Duncan, J. M. (1992). "An experimental and analytic study of earth loads on rigid retaining walls," Virginia Polytechnic Institute and State University, Geotechnical Engineering Division, Department of Civil Engineering, Blacksburg, VA.

Filz, G. M., and Duncan, J. M. (1996). "Earth pressures due to compaction: Comparison of theory with laboratory and field conditions," Paper No. 960139, Session on Practical Applications of Numerical Methods in Design, Transportation Research Board 75th Annual Meeting, Washington, DC.

Gannett Fleming Geotechinical Engineering, Inc. (1986). "Data collection and evaluation for engineering study of lock stability – Eisenhower and Snell Locks, Massena, New York," Volume I-V, Harrisburg, PA.

Goldberg-Zoino and Associates, Inc. (1986). "Eisenhower/Snell Locks, Contract DTSL55-86-C-C0368, In-Situ Testing - Final Report," Newton Upper Falls, MA.

Harza Engineering Company. (1981). "Survey report - Eisenhower and Snell Locks," Chicago, IL.

Hong, C-C., and Stern, M. (1978). "The computation of stress intensity factors in dis-similar materials," *Journal of Elasticity* 8(1), 21-34.

Mather, B. (1967). "Deterioration of concrete in Eisenhower Lock, St. Lawrence Seaway," Miscellaneous Paper No. 6-929, U.S. Army Engineer Waterways Experiment Station, Vicksburg, MS.

Mosher, R. L., Bevins, T. L., and Neeley, B. D. (1991). "Structural evaluation of Eisenhower and Snell Locks, Saint Lawrence Seaway, Massena, New York," Technical Report ITL-91-4, U.S. Army Engineer Waterways Experiment Station, Vicksburg, MS.

Refai, T. M. E., and Swartz, S. E. (1988). "Mode I fracture-energy methods for concrete," *Experimental Mechanics* 28, 395-401.

Reich, R., Cervenka, J., and Saouma, V. (1995). "MERLIN, a three-dimensional finite element program based on a mixed-iterative solution strategy for problems in elasticity, plasticity, and linear and nonlinear fracture mechanics," Technical Report to Electric Power Research Institute, Palo Alto, CA.

Saouma, V. E., Broz, J. J., and Boggs, H. L. (1991). "In situ field testing for fracture properties of dam concrete," *Journal of Materials in Civil Engineering*, ASCE, 3(3), 219-234.

Saouma, V. E., Broz, J. J., Bruhwiler, E., and Boggs, H. L. (1991). "Effect of aggregate and specimen size on fracture properties of dam concrete," *Journal of Materials in Civil Engineering*, ASCE, 3(3), 204-218.

Schmertmannn, J. H. (1986). "Final report: Horizontal pressures on Eisenhower & Snell Lock Walls," Schmertmann & Crapps, Inc., Gainesville, FL.

Slowik, V., Plizzari, G. A., and Saouma, V. E. (1996). "Fracture of concrete under variable amplitude fatigue loading," *ACI Materials Journal* 93(3), 272-283.

Stern, M., Becker, E. B., and Dunham, R. S. (1976). "A contour integral computation of mixed-mode stress intensity factors," *International Journal of Fracture* 12(3), 359-368.

U.S. Army Corps of Engineers. (1942). "Robinson Bay Lock/Analysis of Design, final report," Massena, NY.

U.S. Army Engineer District, Buffalo. (1957a). "Saint Lawrence Seaway – Dwight D. Eisenhowe Lock – Foundation Report," Massena, NY.

U.S. Army Engineer District, Buffalo. (1955). "St. Lawrence Seaway, International Rapids Section, works solely for Navigation and Thousand Islands Sections; Thermal studies," Design Memorandum No. 7, Buffalo, NY.

Appendix A
Earth and Water Forces

This appendix presents the results of equilibrium calculations used to transform the earth and water loadings from those acting along a plane extending vertically from the heel of the lock wall up through the backfill to those forces acting along the backfill-to-lock interface. Both horizontal and vertical shear resultant forces are included in these transformations. The Snell Lock monolith selected for analysis is Monolith N-56, located approximately midway along the 860-ft- (262.13-m-) long lock chamber. The geometry of this monolith is representative of those defining the lock chamber at Snell.

Figure A-1 shows a cross section of this monolith. Monolith N-56 is 101 ft (30.78 m) high and has a base width of 62 ft (18.9 m), corresponding to a base-to-height ratio of 0.61. The top of backfill is level with the top of the lock, el 205.[1] The base of Monolith N-56 is at el 104. The backfill-to-monolith interface extends vertically from the heel of the monolith to el 120. Above this elevation the thickness of the monolith decreases with elevation. Starting at el 120 the monolith-to-backfill interface is inclined at an angle of 35.18 deg from vertical to el 176.75. Between el 176.75 and the top of backfill, el 205, the monolith-to-backfill interface is vertical and the thickness of the monolith is constant.

A.1 Applied Forces

This section describes the computations made to determine the earth and water pressure forces used in the finite element (FE) analyses of Snell Lock. The earth and water pressures are defined using field instrumentation data in this problem along a plane extending vertically from the heel of the lock wall up through the backfill, as discussed in Chapter 2. The horizontal earth pressures and downdrag, shear stresses acting along this vertical plane, are established using horizontal and vertical earth pressure coefficients. The long-term water pressures acting normal to this vertical plane, are established based on a steady-state water table at el 160 and a perched water table at el 173 within the backfill.

---

[1] Elevations (el) cited in this appendix are in feet referred to the National Geodetic Vertical Datum (NGVD). To convert to meters, multiply by 0.305.

The horizontal effective earth pressure σ_h' at any given elevation is given by

$$\sigma_h' = K_h \bullet \sigma_v' \tag{A-1}$$

where

K_h = horizontal earth pressure coefficient

σ_v' = effective overburden pressure at the specified elevation

The effective overburden pressure σ_v' is computed as

$$\sigma_v' = \sigma_v - u \tag{A-2}$$

where

σ_v = total overburden pressure at the specified elevation

u = pore-water pressure

The total overburden pressure is computed using a total unit weight equal to 148 lb/ft^3 (2,370.7 kg/m^3) for the soil backfill. The results from in situ testing (pressure meter testing and hydrofracture testing) at Snell Lock show K_h to range from 0.75 to 1.75, depending upon elevation within the backfill (Figure 2-8). Below el 145 a K_h value equal to 0.75 is assumed. These high lateral earth pressures resulted from overcompaction of the backfill. In this study, the Figure 2-8 best estimate for K_h as reported by Diviney (1990 after Schmertman 1986)[1] is used in both the smeared crack and the discrete crack analyses of Snell Lock. Using the Figure 2-8 best estimate relationship for K_h, a horizontal effective earth pressure σ_h' distribution with elevation was computed along a plane extending vertically from the heel of the lock wall up through the backfill. The resulting distribution is nearly the same as the distribution labeled σ_h' mean estimate in Figure 2-7.

The continuous effective earth pressure σ_h' distribution with elevation is then delineated as three discrete distributions, from el 104 to el 120, from el 120 to el 176.75, and from el 176.75 to el 205. The corresponding resultant horizontal effective forces F_{h1}, F_{h2}, and F_{h3} and points of action computed for each of the three pressure segments are identified in Figure A-2 and given in Table A-1. Values of the resultant water pressure forces shown in Figure A-2 are also given in Table A-1.

Table A-1 and all subsequent tables list the resultant earth and water forces for two limiting cases. The first load case listed, referred to as long-term loading, corresponds to the conditions in the field at the time of the pressure meter and hydrofracture testing and the measurement of pore-water pressures within the

---

[1] References cited in this appendix are included in the References section at the end of the main text.

backfill. These field investigations occurred nearly 30 years after lock construction. The second case listed is referred to as the end-of-construction load case. It corresponds to loading immediately after lock construction and prior to flooding of the lock site.

The vertical shear stress τ or, equivalently, the downdrag, at any given elevation is given by

$$\tau = K_v \bullet \sigma_v' \tag{A-3}$$

where K_v is the vertical earth pressure coefficient.

Downdrag is mobilized in the backfill and along the back face of a concrete wall due either to the movement of the wall as the backfill is placed, or due to the settlement of the backfill. Both wall movement and backfill settlement introduce shear strains in the backfill material, which produce the vertical downdrag stresses and resultant shear forces. For Snell Lock and other massive concrete gravity lock walls founded on rock, the major factor in the development of downdrag is the differential settlement of the backfill adjacent to a roughened concrete lock wall face during placement and compaction of the soil backfill. No field tests were made at Snell Lock to determine the level of downdrag developing within the backfill. The results from the Ebeling, Pace, and Morrison (1997) complete soil-structure interaction analysis of a lock of comparable wall geometry resulted in the vertical earth pressure coefficients K_v shown in Figure A-3. These values for K_v are used to compute the distributions of shear stress τ and the resulting downdrag forces F_v acting along each of the imaginary sections shown in this diagram of Snell Lock. Values of the Figure A-2 resultant shear forces F_v are listed in Table A-1.

Figure A-4 shows the free-body force diagrams for soil block 1 and soil block 2. Table A-2 gives the values of the forces shown in this figure for soil block 1. Table A-3 gives the values of the forces for soil block 2.

Figure A-5 shows the free-body force diagram for soil block 1 as well as the three equilibrium equations used to compute the three unknowns, T_{1-2}, N_{1-2}, and X_{N1-2}. The values of all forces acting on soil block 1 are listed in Table A-2.

Figure A-6 shows the distribution of water pressures acting on the two faces of soil block 2 for the hydrostatic water table below el 160 and perched water table below el 173 (applicable to the long-term load case only). The magnitude of water pressure varies linearly with depth. Values for key water pressures u_{n1} and u_{n2} defining the four boundary water pressure distributions are given in this figure. A unit weight of water equal to 62.4 pcf (999.55 kg/m^3) is used in these analyses. The resultant forces for each of these distributions are also shown in the figure. Values of these resultant water pressure forces are listed in Table A-3.

Figure A-7 shows the free-body force diagram for soil block 2 as well as the general transformation matrix used to resolve forces defined in the global x-, y-coordinate system to their force components in the local x'-,y'- coordinate system. This local coordinate system corresponds to planes parallel and normal to the lock wall-to-soil block 2 interface. Two unknown forces are shown in this figure, T_2, N_2', as well as the unknown point of effective force N_2' application, L_{N2}. The Figure A-7 water pressure force U_2 is the resultant of the Figure A-6 water pressure forces U_{2-top} and $U_{2-bottom}$ and its point of application is L_{U2}. Using the components of forces resolved into the x'-, y'-axes, the three equations of equilibrium are used to compute the values of T_2, N_2', and L_{N2}. The resulting equations are

$$\sum F_{x'} = 0 \tag{A-4}$$

$$N_2' = (U_{X2-top} + U_{X2-bottom})\cos\alpha + F_{h2}\cos\alpha + F_{v2}\sin\alpha + W_2\sin\alpha$$
$$+ T_{1-2}\cos\alpha + N_{1-2}\sin\alpha - U_2 \tag{A-5}$$

$$\sum F_{y'} = 0 \tag{A-6}$$

$$T_2 = -(U_{X2-top} + U_{X2-bottom})\sin\alpha - F_{h2}\sin\alpha + F_{v2}\cos\alpha$$
$$+ W_2\cos\alpha - T_{1-2}\sin\alpha + N_{1-2}\cos\alpha \tag{A-7}$$

$$\sum M_{pt.o} = 0 \tag{A-8}$$

$$L_{N'2} = \frac{1}{N_2'}[U_{X2-top}Y_{UX2-t} + U_{X2-bottom}Y_{UX2-b} + F_{h2}Y_{Fh2} +$$
$$W_2 X_{W2} + T_{1-2}Y_{B2} + N_{1-2}(40\,ft - X_{N1-2}) - U_2 L_{U2}] \tag{A-9}$$

The values of $T2$, N_2', and L_{N2} and all other forces acting on soil block 2 are listed in Table A-3.

A.2 Surface Tractions Applied in the FE Analyses

The applied loads are specified in the FE analyses in terms of surface tractions along the three lock wall-to-soil backfill interface regions. These surface tractions consist of both shear stresses and total stresses applied normal to the interface. This section describes the computation of these two surface tractions.

Figure A-8 shows the distribution of total normal stress σ_n along the lock wall-to-soil block 2 interface. A linear variation in total stress normal to the

interface is assumed. The total normal force N_2 is equal to the sum of N_2' plus U_2 of Figure A-7. Figure A-8 also lists the equations used to compute the total stresses at both ends of the linear normal stress distribution using values of total force N_2 and its eccentricity from center line of the interface e. The values of N_2 and its eccentricity e are given in Table A-4. Values of the total normal stresses $\sigma_{n-176.75}$ and σ_{n-120}, located at either end of the 69.43-ft (21.16-m) long interface, are also given in Table A-4.

The distribution of shear stress along the lock wall-to-soil block 2 interface (Figure A-7) is based on the assumption that the effective angle of friction mobilized along the interface δ'_{mob} is a constant value. The value of δ'_{mob} is computed using the relationship

$$\tan(\delta'_{mob}) = \frac{T}{N_2'} \qquad (A-10)$$

The previously computed values of T and N_2' are listed in Table A-4 for both long-term loading and the end of construction. The values of δ'_{mob} are computed to be 10.96 deg for long-term loading and 11.29 deg at the end of construction. To compute the distribution of shear stress τ along the interface, the distribution of normal effective stress σ_n' along the interface is first determined. The distribution of σ_n' is equal to the Figure A-8 linear total stress distribution σ_n minus the Figure A-6 water pressure distribution for the long-term load case. (For the end-of-construction load case, no water pressures are present in the backfill. Thus the distribution of σ_n' is equal to the linear distribution of σ_n at the end of construction.) The distribution of shear stress τ along the interface is proportional to the distribution of normal effective stress σ_n' by the relationship

$$\tau = \sigma_n' \bullet \tan(\delta'_{mob}) \qquad (A-11)$$

Values of τ at key elevations along the lock wall-to-soil block 2 interface are given in Table A-4. A linear distribution in shear stress is assumed between these key points. On the free body diagram of the lock wall, both the resultant shear force T_2 and its corresponding shear stress τ distribution are directed downward along the interface.

In summary, Table A-4 lists the values of the two surface tractions, σ_n and τ, specified in the FE analyses. The distributions of stresses are assumed to be linear between the values given at key elevations along the lock wall-to-soil block 2 interface.

Table A-5 lists the values of the two surface tractions, σ_n and τ, applied at key elevations along the upper, vertical lock wall-to-soil block 1 interface in the FE analyses. The distributions of stresses are assumed to be linear between these key values. The values of the resultant normal and shear forces for these stress distributions, F_{hl-w} and F_{vl-w}, respectively, are given in Table A-2 (refer to Figure A-4).

Table A-6 lists the values of the two surface tractions, σ_n and τ, applied at key elevations along the lower, vertical lock wall-to-soil block 3 interface in the FE analyses. The distributions of stresses are assumed to be linear between these key values. The value of the resultant shear force for the shear stress distribution, F_{v3}, is given in Table A-1 (refer to Figure A-4). The value of the resultant total normal force, corresponding to the total normal stress distribution along interface 3, is equal to the sum of the effective horizontal earth pressure force F_{h3} plus the water pressure force U_{x3} (values given in Table A-1).
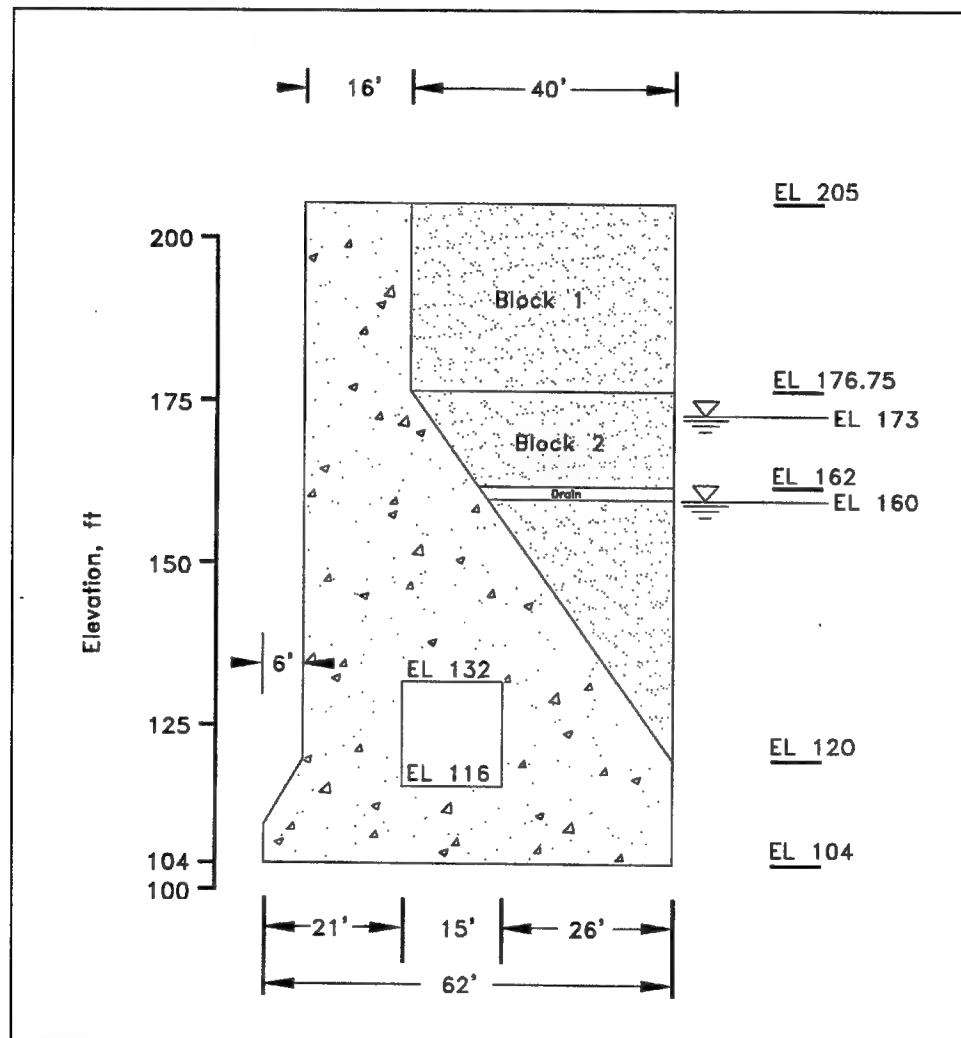
Figure A-1. Two blocks comprising the soil wedge behind Monolith N-56 at Snell Lock (1 ft = 0.305 m)
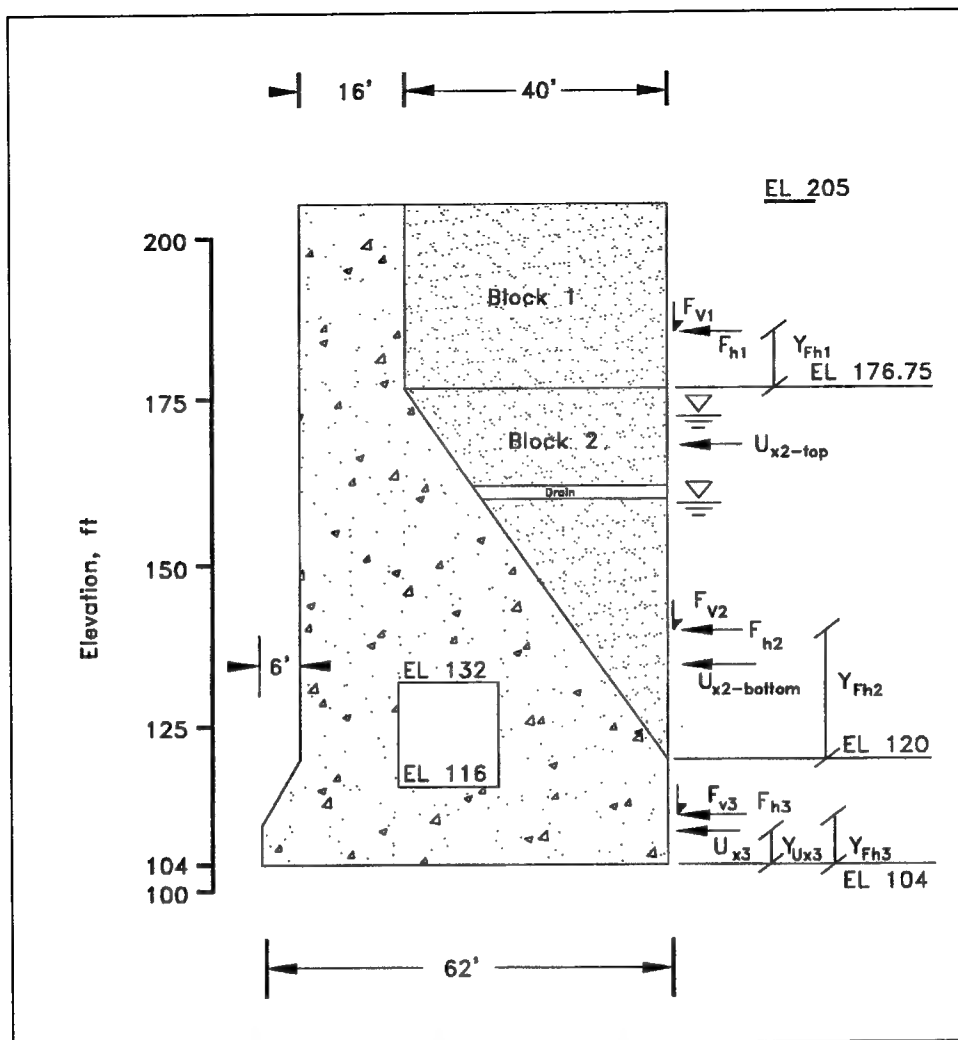
Figure A-2. Resultant horizontal and vertical earth pressure forces and water pressure forces acting on soil wedge (1 ft = 0.305 m)

Figure A-3.   Vertical earth pressure coefficients within backfill
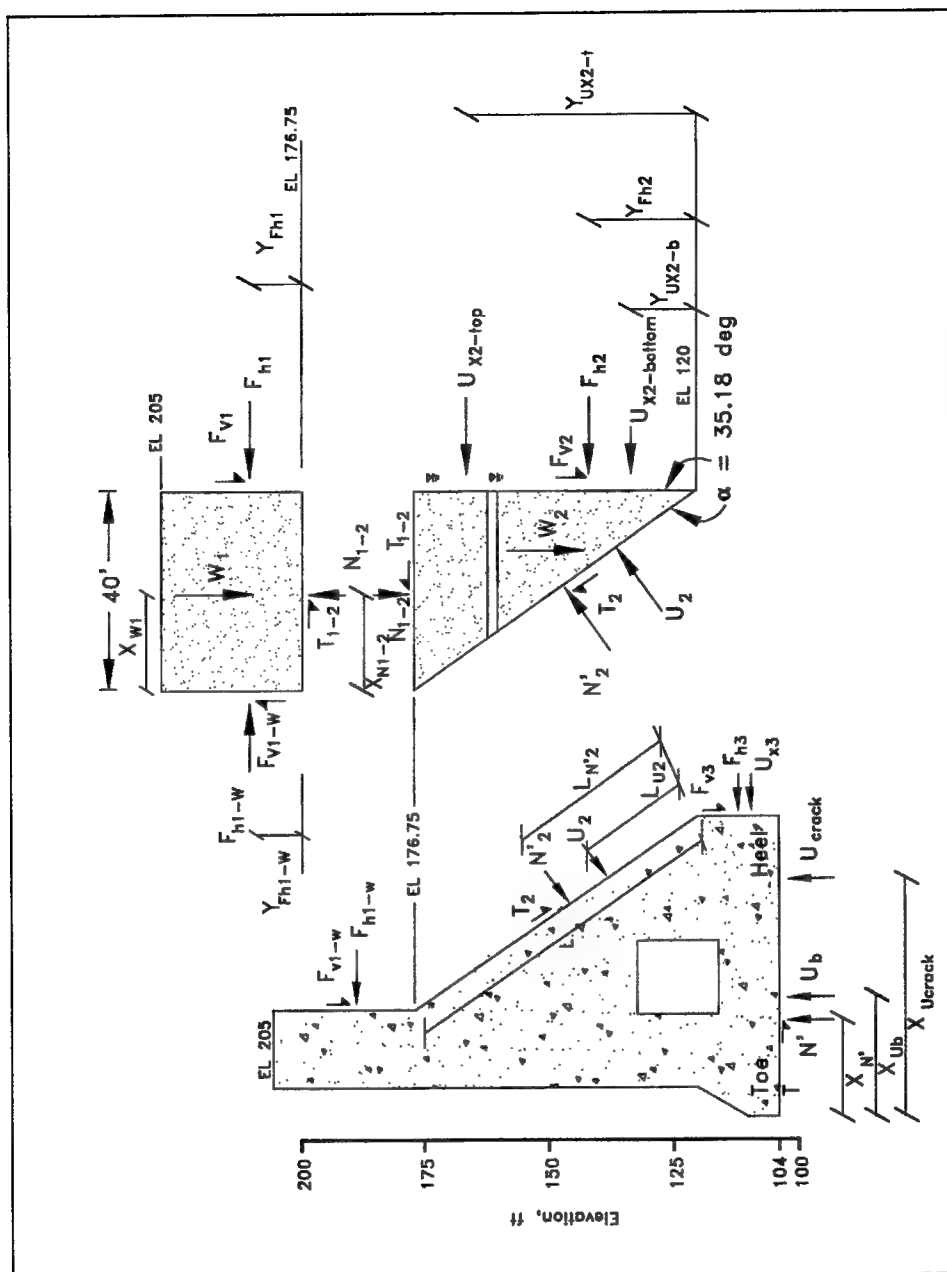
Figure A-4. Resultant forces acting on monolith and soil wedge (1 ft = 0.305 m)

$$\Sigma F_X = 0$$

$$T_{1-2} = F_{h1} - F_{h1-w}$$

$$\Sigma F_v = 0$$

$$N_{1-2} = W_1 + F_{v1} - F_{v1-w}$$

$$\Sigma M_{Pt.0} = 0$$

$$X_{N1-2} = \frac{1}{N_{1-2}} \bullet \left[W_1 \bullet X_{w1} + F_{v1} \bullet 40'\right.$$

$$\left. - F_{h1} \bullet Y_{Fh1} + F_{h1-w} \bullet Y_{Fh1-w} \right]$$

$$\tan \delta_{modified \ 1-2} = \frac{T}{N}$$
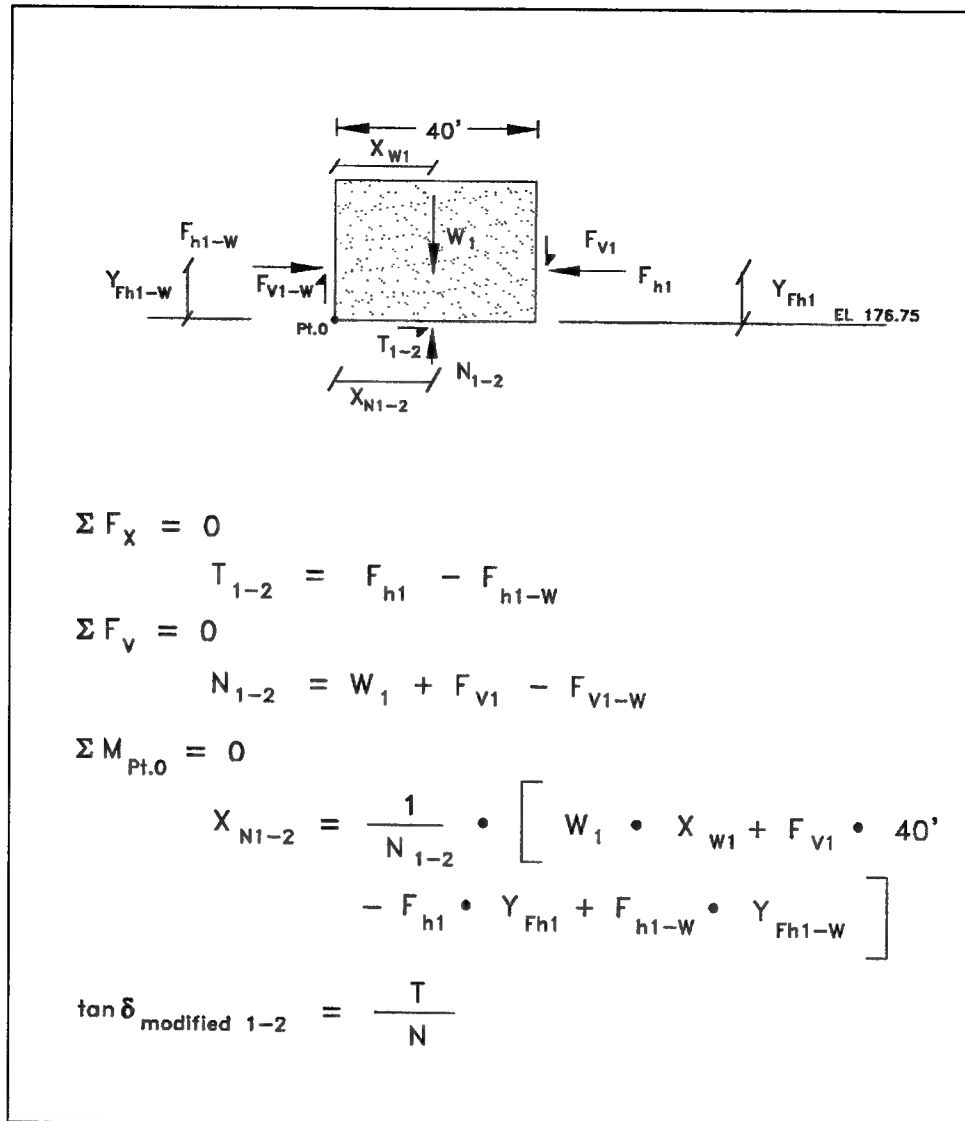
Figure A-5. Resultant forces acting on soil block 1 (1 ft = 0.305 m)
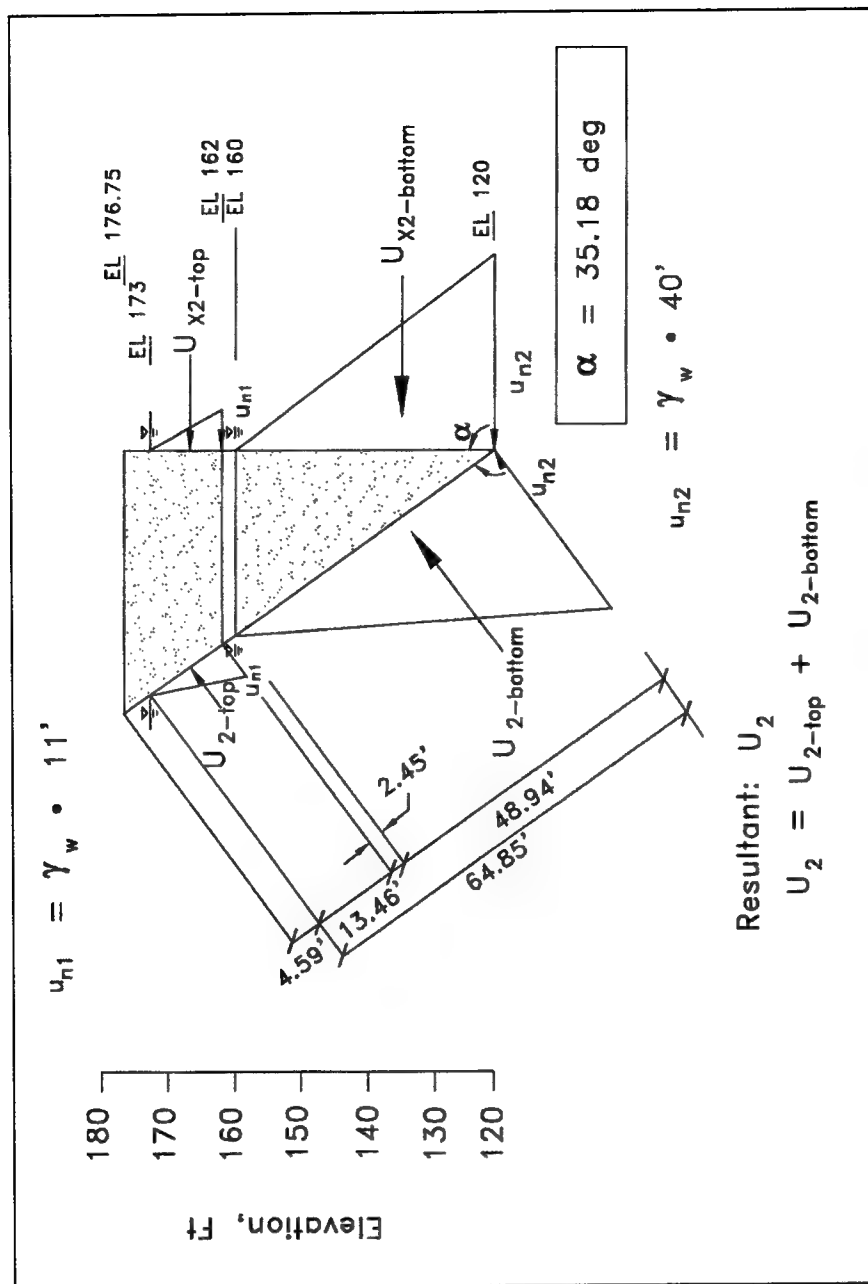
Figure A-6. Hydrostatic boundary water pressures and forces acting on soil block 2 (1 ft = 0.305 m)
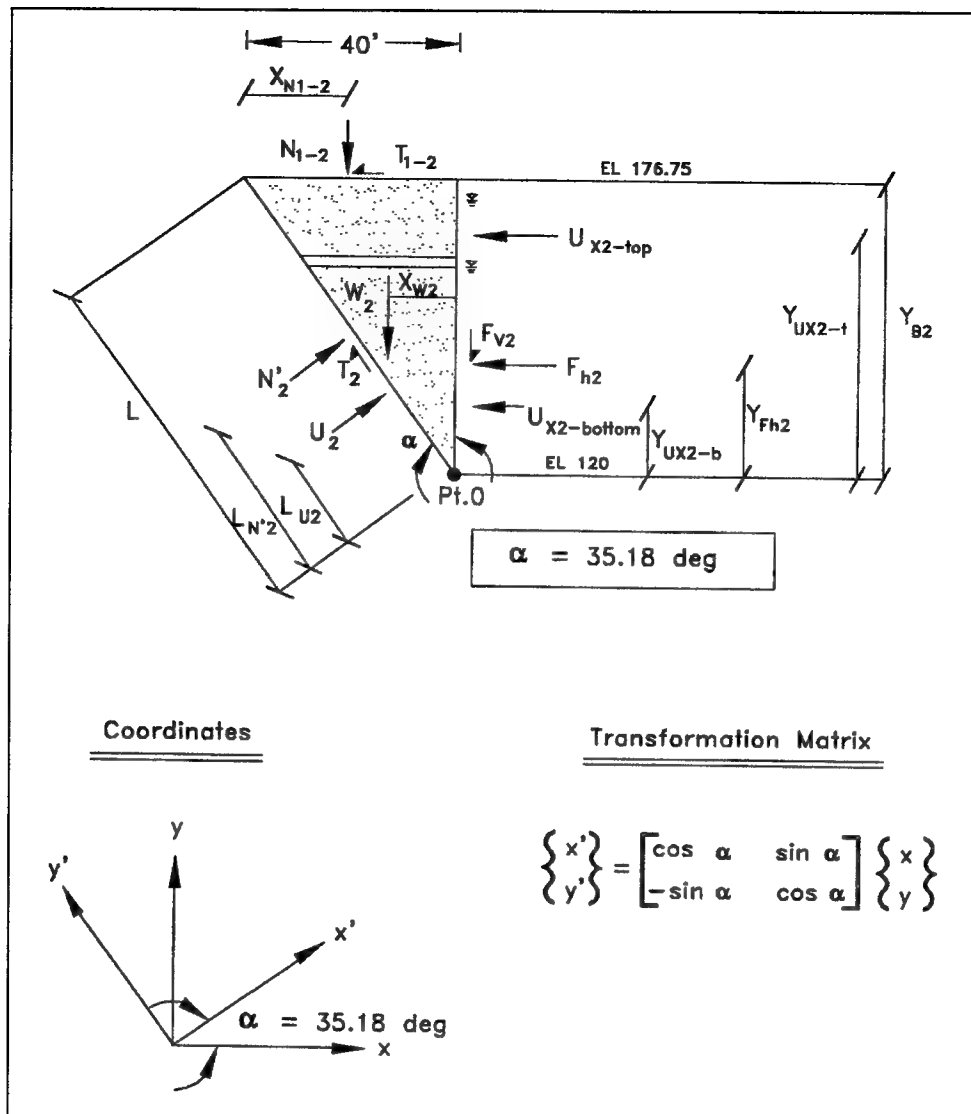
Figure A-7. Resultant forces acting on soil block 2 (1 ft = 0.305.m)

$$e = \frac{L}{2} - L_{N2}$$

$$\sigma_{n-176.75} = \frac{N_2}{L} \cdot \left(1 - \frac{6e}{L}\right)$$

$$\sigma_{n-120} = \frac{N_2}{L} \cdot \left(1 + \frac{6e}{L}\right)$$
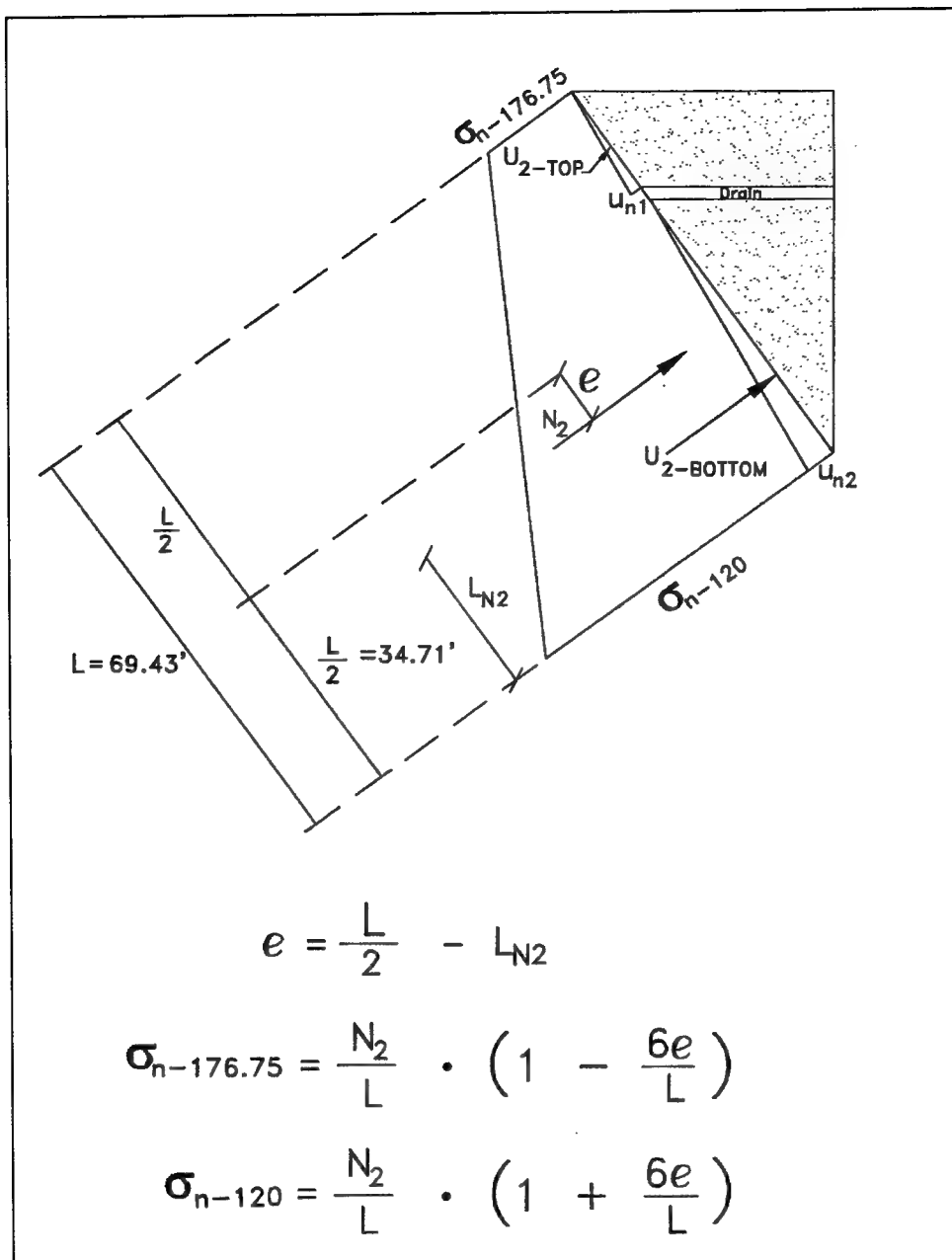
Figure A-8. Total normal stresses and boundary water pressures on monolith to soil block 2 interface (1 ft = 0.305)

Table A-1
Resultant Horizontal and Vertical Earth Pressure Forces and Water Pressure Forces Acting Along a Plane Extending Vertically from the Heel of the Lock Wall up Through the Backfill (1 ft = 0.305 m, 1 lb = 4.448 N)

a) Horizontal effective earth pressure forces

	F_{h1} lbs	Y_{Fh1} ft	F_{h2} lbs	Y_{Fh2} ft	F_{h3} lbs	Y_{Fh3} ft
Long-Term Loading	81,824.71	10.21	307,465.11	23.17	129,225.6	7.83
End of Construction	81,824.71	10.21	344,002.18	22.15	165,168	7.77

b) Vertical shear forces

	F_{v1} lbs	F_{v2} lbs	F_{v3} lbs
Long-Term Loading	590.57	33,751.65	27,568.16
End of Construction	590.57	38,047.47	35,235.84

c) Horizontal water pressure forces

	U_{x2-top} lbs	El of U_{x2-top}	$U_{x2-bottom}$ lbs	El of $U_{x2-bottom}$	U_{x3} lbs	El of U_{x3}
Long-Term Loading	3,775.2	165.67	49,920	133.33	47,923.2	111.56
End of Construction	0	-	0	-	0	-

Table A-2
Resultant Forces Acting on Soil Block 1 and Along the Lock Wall-to-Soil Block 1 Interface (1 ft = 0.305 m, 1 lb = 4.448 N)

a) Weight of soil block 1

	W_1 lbs	X_{W1} ft
Long-Term Loading	167,240	20
End of Construction	167,240	20

b) Forces acting along the soil block 1-soil block 2 interface

	N_{1-2} lbs	X_{N1-2} ft	T_{1-2} lbs
Long-Term Loading	156,019.2	21.59	0
End of Construction	156,019.2	21.59	0

c) Forces acting along the soil-to-soil free-body vertical section made through the backfill

	F_{v1} lbs	F_{h1} lbs	Y_{Fh1} ft
Long-Term Loading	11,811.33	81,824.71	10.21
End of Construction	11,811.33	81,824.71	10.21

d) Forces acting along the soil block 1-to-wall interface

	F_{v1-w} lbs	F_{h1-w} lbs	Y_{Fh1-w} ft
Long-Term Loading	11,811.33	81,824.71	10.21
End of Construction	11,811.33	81,824.71	10.21

Table A-3
Resultant Forces Acting on Soil Block 2 and Along the Lock Wall-to-Soil Block 2 Interface (1 ft = 0.305 m, 1 lb = 4.448 N)

a) Weight of soil block 2

	W_2 lbs	X_{W2} ft
Long-Term Loading	167,980	13.33
End of Construction	167,980	13.33

b) Forces acting along the soil block 1-soil block 2 interface

	N_{1-2} lbs	X_{N1-2} ft	T_{1-2} lbs
Long-Term Loading	156,019.2	21.59	0
End of Construction	156,019.2	21.59	0

c) Earth forces acting along the soil-soil free-body vertical section made through the backfill

	F_{v2} lbs	F_{h2} lbs	Y_{Fh2} ft
Long-Term Loading	33,751.65	307,465.11	23.17
End of Construction	38,047.47	344,002.18	22.15

d) Water pressure forces acting along the soil-soil free-body vertical section made through the backfill

	U_{x2-top} lbs	EL of U_{x2-top}	$U_{x2-bottom}$ lbs	EL of U_{x2-top}
Long-Term Loading	3,775.2	165.67	49,920	133.33
End of Construction	0	-	0	-

e) Earth forces acting along the soil block 2-wall interface

	T_2 lbs	N'_2 lbs	$L_{N'2}$ ft	L ft
Long-Term Loading	84,340	435,610	27.13	69.43
End of Construction	97,740	489,760	29.99	69.43

f) Water pressure forces acting along the soil block 2-wall interface

	U_2 lbs	L_{U2} ft
Long-Term Loading	65,696.59	19.09
End of Construction	0	-

Table A-4
Total and Effective Normal Pressures, Shear Stresses and Resultant Forces Along the Lock Wall-to-Soil Block 2 Interface (1 ft = 0.305 m, 1 lb = 4.448 N, 1 MPa = 20,885.5 lbf/ft^2)

a) Total normal stresses and resultant normal force

	N_2 lbs	e ft	$\sigma_{n\text{-}176.75}$ psf	$\sigma_{n\text{-}120}$ psf
Long-Term Loading	501,306.59	8.64	1,829.26	12,611.38
End of Construction	489,760	8.72	1,738.36	12,369.67

b) Shear force, normal effective force and the effective angle of friction mobilized along the interface

	T_2 lbs	N'_2 lbs	δ'_{mob} deg
Long-Term Loading	84,340	435,610	10.96
End of Construction	97,740	489,760	11.29

c) Stresses along the interface – long-term loading

El	σ_n psf	u psf	σ'_n psf	τ psf
176.75	1,827	0	1,827	354.4
173	2,543	0	2,543	492.3
162.01	4,632	686	3,946	764
161.99	4,632	0	4,632	896.9
160	5,012	0	5,012	970.4
120	12,610	2,496	10,115	1,958.3

d) Stresses along the interface – end of construction

El	σ_n psf	u psf	σ'_n psf	τ psf
176.75	1,737	0	1,737	346.6
173	2,440	0	2,440	486.9
162.01	4,500	0	4,500	898.2
161.99	4,500	0	4,500	898.2
160	4,876	0	4,876	973
120	12,371	0	12,371	2,468.8

Table A-5
Total and Effective Normal Pressures and Shear Stresses Along the Upper, Vertical Lock Wall-to-Soil Block 1 Interface (1 ft = 0.305 m, 1 MPa = 20,885.5 lbf/ft^2)

a) Stresses along the upper vertical interface – long-term loading

El	σ_n psf	u psf	σ'_n psf	τ psf
205	0	0	0	0
200	1,017.5	0	1,017.5	148
195	2590	0	2590	296
190	3496.5	0	3496.5	444
185	4144	0	4144	592
180	4440	0	4440	740
176.75	4473.67	0	4473.67	836.2

b) Stresses along the upper vertical interface – end of construction

El	σ_n psf	u psf	σ'_n psf	τ psf
205	0	0	0	0
200	1,017.5	0	1,017.5	148
195	2590	0	2590	296
190	3496.5	0	3496.5	444
185	4144	0	4144	592
180	4440	0	4440	740
176.75	4473.67	0	4473.67	836.2

Table A-6
Total and Effective Normal Pressures and Shear Stresses Along the Lower, Vertical Lock Wall-to-Soil Block 3 Interface (1 ft = 0.305 m, 1 MPa = 20,885.5 lbf/ft^2)

a) Stresses along the lower vertical interface – long-term loading

El	σ_n psf	u psf	σ'_n psf	τ psf
120	10,059	2,496	7,563	1,613.44
104	12,084.6	3,494.4	8,590.2	1,832.58

b) Stresses along the lower vertical interface – end of construction

El	σ_n psf	u psf	σ'_n psf	τ psf
120	9,435	0	9,435	2,012.8
104	11,211	0	11,211	2,391.68

Appendix B
Fracture Toughness of Concrete

This appendix discusses the results of laboratory and field tests made to determine the Mode I fracture toughness of concrete K_{Ic}. The value for the parameter K_{Ic} may be viewed as material property used to characterize the capacity of the concrete against crack propagation in a crack opening mode of failure. The results of laboratory tests are given in this appendix for large, unreinforced wedge-splitting concrete specimens tested to failure and for unreinforced concrete beams tested to failure in three-point bend beam testing. In addition, a set of results of in situ testing of concrete is also included.

B.1 Saouma, Broz, Bruhwiler, and Boggs (1991)[1] Wedge-Splitting Test Results

This section summarizes the fracture properties of concrete used in dams obtained from laboratory experiments of large wedge-splitting specimens with heights of 12 in. (0.31 m), 36 in. (0.91 m), and 60 in. (1.52 m). One of the unique aspects of this testing program is that concrete specimens with maximum size aggregate consistent with the size used in some dams and locks was included in the testing program. Various concrete mixes of 0.75 in. (19 mm), 1.5 in. (38 mm), and 3 in. (76 mm) maximum aggregate size were investigated. Two types of aggregates were used in the experimental program, rounded aggregates and subangular aggregates.

Table B-1 summarizes the results of the concrete material properties for the three concrete mixes and the mixture batched with quarried subangular aggregates. The compressive strength, f_c', the tensile splitting strength $f_{t,sp}'$, and Young's modulus E are based on tests made on cylinder specimens performed according to American Society for Testing and Materials (ASTM) standards. Tests on the wedge-splitting specimens were used to determine the

---

[1] References cited in this appendix are included in the References section at the end of the main text.

Mode I fracture toughness for the various specimens and the specific fracture energy G_f. The wedge-splitting specimen has a large fracture area compared with the concrete volume, approximately 4.6 times greater than commonly used three-point bend beam geometry of equal volume. The large fracture area, compared with the aggregate size and specimen volume, makes the wedge splitting geometry well-suited for the large maximum size aggregate and specimens under laboratory conditions, according to Saouma, Broz, Bruhwiler, and Boggs.

Saouma, Broz, Bruhwiler, and Boggs used the compliance method to compute the fracture toughness K_{Ic} for each specimen. The specific fracture energy G_f is defined as the total energy required to break a specimen into halves, normalized by the projected fracture area. G_f is ideally obtained from the area underneath the load deformation curve in a direct tension test. Alternatively, specific fracture energy can also be obtained directly from flexural-based specimen geometries, such as the wedge-splitting specimen.

Saouma, Broz, Bruhwiler, and Boggs found the fracture toughness K_{Ic} and specific fracture energy G_f to be aggregate and specimen-size independent only if certain minimum specimen dimensions are exceeded. For all specimens using the three mixes and containing rounded aggregates, the average values for K_{Ic} are within a narrow range of 929 to 957 $\mathrm{psi}\sqrt{\mathrm{in.}}$ (1.02 to 1.05 MN/m$^{3/2}$) and have a coefficient of variation between 14 and 18 percent. However, they appear to be dependent on the aggregate shape and type. For the two aggregates used in the experimental program, more energy was required to fracture the subangular aggregates than to debond the rounded ones. For the specimens made of Mixture 2 and containing subangular aggregates, the average value for K_{Ic} is 1,220 $\mathrm{psi}\sqrt{\mathrm{in.}}$ (1.34 MN/m$^{3/2}$), with a coefficient of variation of 10 percent. Aggregate debonding was prevalent in fracture surface of the rounded specimens; however, aggregate failures were more predominant in the subangular specimens.

B.2 Slowik, Plizzari, and Saouma (1996) Wedge-Splitting Test Results

This section summarizes the Mode I fracture properties of concrete obtained from laboratory experiments of large and small wedge-splitting specimens. The large concrete specimens possess a height of 36 in. (0.91m) and a width of 24 in. (0.61 m), while the smaller specimens possess a height of 12 in. (0.31 m) and a width of 12 in. (0.31 m). The maximum size aggregate used in the concrete mix is 1 in. (25.4 mm).

Table B-2 summarizes the results of the concrete material properties for the concrete mix. The compressive strength f_c' and Young's modulus E_c are based on tests made on cylinder specimens performed according to ASTM standards. Tests on the wedge-splitting specimens were used to determine the Mode I fracture toughness for the various specimens and the specific fracture energy G_f.

The average values for K_{Ic} are 1,350 psi$\sqrt{\text{in.}}$ (1.48 MN/m$^{3/2}$) for the large specimens and 860 psi$\sqrt{\text{in.}}$ (0.95 MN/m$^{3/2}$) for the smaller specimens.

B.3 Refai and Swartz (1988) Three-Point Beam Bending Test Results

This section summarizes the Mode I fracture properties of concrete beams of different sizes with constant width (3 in. (76.2 mm)) span-depth ratio (3.75) tested in three-point bending. One of the unique aspects of this testing program is that various energy methods are evaluated using the results for beams tested. In 1988, Refai and Swartz used load-deflection curves to introduce two methods to estimate the energy-release rate for Mode I fracture. One of the new methods identified as the energy-release method, which is based directly on the definition of energy-release rate, gives results which are size independent for precracked beams and also invariant with crack length.

Tables B-3 and B-4 summarize the results of the concrete material properties for the three-point beam bending tests on precracked beams and notched beams, respectively. A single concrete mix was used in this study. The concrete mix has a maximum size aggregate (crushed limestone) of 0.75 in. (19 mm). The compressive strength f_c' , the tensile splitting strength f_t' , and Young's modulus are based on tests made on cylinder specimens performed according to ASTM standards. Tests on the three-point beam bending test specimens were used to determine the energetic parameter J_{Ic} by the J-integral method, the specific fracture energy G_f, the energy release rate G_{Ic} calculated using three different methods, the fracture toughness in Mode I K_{Ic}, and the ratio $(K_{Ic})^2/E_c$. The average values reported in these tables for G_{Ic} computed by the direct energy method are for beams with a ratio of crack length divided by height of beam less than or equal to 0.65.

Refai and Swartz conclude from the results listed in Tables B-3 and B-4 that the general agreement of the values obtained for J_{Ic}, G_{Ic}, and G_f seems to imply the validity of the linear elastic fracture mechanics method. The average values of Mode I fracture toughness are for beam series B, K_{Ic} = 1,024 psi$\sqrt{\text{in.}}$ (1.13 MN/m$^{3/2}$) with a coefficient of variation of 5.5 percent for 19 beams tested; and for beam series C, K_{Ic} = 1,048 psi$\sqrt{\text{in.}}$ (1.15 MN/m$^{3/2}$) with a coefficient of variation of 3.5 percent for 19 beams tested. Corresponding values of $(K_{Ic})^2/E_c$ are 0.188 lb/in. and 0.192 lb/in. Refai and Swartz conclude that these values are reasonably size independent. They also conclude that the difference between G_{Ic} and $(K_{Ic})^2/E_c$ may be attributed to fracture process zone development, which is also seen to be approximately constant so long as the ratio of crack length divided by height of beam is less than or equal to 0.65.

Refai and Swartz observe that the energy release method gives consistent results that are independent of crack length and beam size, as mentioned

previously. The relatively constant value for G_{Ic} implies a uniform resistance to crack growth for varying crack lengths. Both the RIELM and direct energy results are shown to be affected by crack length and beam size even for precracked beams. The size effect is not observed for the J-integral, energy release method or the approximate method.

B.4 Saouma, Broz, and Boggs (1991) In Situ Test Results

This section summarizes the fracture properties of concrete used in dams obtained from laboratory experiments of in situ testing on large-scale cubical concrete specimens. Three concrete mixes of 0.75 in. (19 mm), 1.5 in. (38 mm), and 3 in. (76 mm) maximum aggregate size were investigated. Only rounded aggregates were used in the three concrete mixes. Concrete mixtures identical to those used in the Saouma, Broz, Bruhwiler, and Boggs (1991) study were used in this study. One of the unique aspects of this testing program is that concrete specimens with maximum size aggregate consistent with the size used in some dams and locks were included in the testing program.

Saouma, Broz, and Boggs developed a methodology involving both testing procedure and data interpretation for fracture testing of concrete specimens in the laboratory environment under simulated field conditions. The fracture-based testing procedure involved pressurizing a borehole and recording the diametrical changes in a large, uniaxially confined concrete cube. The 4.25-in.- (108-mm-) diameter borehole in the cubical specimen was pressurized using a borehole dilatometer probe. On the basis of experimental results, effective crack lengths and corresponding apparent fracture toughness K_{Ic}^{app} values were determined by application of the compliance method in conjunction with a finite element calibration. The authors caution that the apparent fracture toughness should not be confused with the material property, fracture toughness K_{Ic}. K_{Ic}^{app} is considered to be analogous to the effective stress σ' used in the von Mises and Tresca failure criteria for describing a complex state through a single value.

Table B-5 summarizes the results of the concrete material properties for the three concrete mixes and the mixtures batched with rounded aggregates. The tensile splitting strength $f_{t,sp}'$ is based on tests made on cylinder specimens performed according to ASTM standards. The experimental values $f_{t,exp}'$ for each mix are determined from the results of the borehole tests. The authors state that the higher values for the splitting tensile strengths obtained from the cubical specimens may result from the confining stresses (100 psi (0.69 MPa)) present in the cubical specimen. As evidenced by the experimental results, the simulated in situ conditions in the cube tests affected material response, resulting in measured tensile strengths that were higher than the splitting strengths obtained from unconfined specimens tested under laboratory conditions.

In their 1991 paper describing wedge-splitting tests, Saouma, Broz, Bruhwiler, and Boggs concluded that the fracture toughness K_{Ic} is aggregate- and specimen-size-independent for the three concrete mixtures tested. Saouma, Broz, and Boggs used the same three concrete mixtures to make the twelve large-scale cubical concrete specimens (36 by 36 by 45 in. (0.91 by 0.91 by 1.14 m). Therefore, it is considered appropriate to use the average value for the Mode I fracture toughness for all 36-in.- (0.91-m-) high wedge-splitting specimens to characterize all three groups of concrete mixtures used to make the cubical concrete specimens. For the 36-in.- (0.91 m-) high concrete specimens made using the three mixes and containing rounded aggregates, Saouma, Broz, Bruhwiler, and Boggs (1991) found the average value for K_{Ic} to be equal to 941 psi$\sqrt{\text{in.}}$ (1.03 MN/m$^{3/2}$), with a coefficient of variation of 16 percent. The average value of K_{Ic}^{app} for the twelve cubical specimens tested in this study is equal to 1,389 psi$\sqrt{\text{in.}}$ (1.52 MN/m$^{3/2}$), with a coefficient of variation of 24.5 percent. In summary, the value for the apparent fracture toughness of the cubes is approximately 50 percent higher than the K_{Ic} value determined from the wedge-splitting specimen tests.

Table B-1
Fracture Toughness Test Results from Wedge-Splitting Tests by Saouma, Broz, Bruhwiler, and Boggs (1991) (1 in. = 25.4 mm, 1 MPa = 145.04 psi, 1 MPa = 0.145 ksi, 1 kN/m$^{3/2}$ = 0.91 psi$\sqrt{\text{in.}}$, 1 lb/in. = 175.13 N/m)

Concrete Mixtures:

1. Water to Cement Ratio (W/C)   = 0.55
   Cement : Sand : Gravel   = 1 : 3.10 : 3.30 by weight
   Maximum gravel size (gravel 1, rounded river) = 0.75 in.

2. W/C   = 0.55
   Cement : Sand : Gravel 1 : Gravel 2   = 1 : 3.11 : 2.43 : 2.43
          by weight
   Maximum gravel size (Gravel 2, rounded river
   and quarried sub-angular)   = 1.50 in.
   Maximum gravel size (Gravel 1, rounded river) = 0.75 in.

3. W/C   = 0.55
   Cement : Sand : Gravel 1 : Gravel 2 : Gravel 3   = 1: 3.71 : 2.63 : 2.63 : 2.63
          by weight
   Maximum gravel size (Gravel 3, rounded river) = 3.00 in.
   Maximum gravel size (Gravel 2, rounded river) = 1.50 in.
   Maximum gravel size (Gravel 1, rounded river) = 0.75 in.

Concrete Mixture	Max. Aggregate size in.	f_c' psi	$f_{t, sp}'$ psi	E_c ksi	K_{Ic} psi$\sqrt{\text{in.}}$	G_f lbs/in.
Mixture 1	0.75	3,710	407	2,610	941	1.08
Mixture 2	1.5	3,600	388	2,460	929	1.37
Mixture 2 with subangular aggregates	1.5	5,317	574	3,360	1,220	1.58
Mixture 3	3.0	2,740	349	2,400	957	1.31

Table B-2
Fracture Toughness Test Results from Wedge-Splitting Tests by Slowic, Plizzari, and Saouma (1996) (1 in. = 25.4 mm, 1 lb/yd^3 = 0.593 kg/m^3, 1 MPa = 145.04 psi, 1 MPa = 0.145 ksi, 1 kN/m$^{3/2}$ = 0.91 psi$\sqrt{\text{in.}}$, 1 lb/in. = 175.13 N/m)

Concrete Mixture

1. Cement, Type I   = 590 lb/yd^3
    Water   = 308 lb/yd^3
    Gravel 1 (3/16 to 1/2 in.)   = 1,034 lb/yd^3
    Gravel 2 (1/2 to 1 in.)   = 906 lb/yd^3
    Sand (0 to 3/16 in.)   = 1,282 lb/yd^3

Specimen Size in.	Max. Aggregate size in.	f'_c psi	E_c ksi	K_{Ic} psi$\sqrt{\text{in.}}$	G_f lb/in.
36 by 24	1	4,351	2,466	1,350	1.17
12 by 12	1	4,351	2,320	860	0.9

Table B-3
Fracture Toughness Test Results from Three-Point Beam Bending Tests on Precracked Beams by Refai and Swartz (1988) (1 in. = 25.4 mm, 1 MPa = 145.04 psi, 1 MPa = 0.145 ksi, 1 lb/in. = 175.13 N/m, 1 kN/m$^{3/2}$ = 0.91 psi$\sqrt{\text{in.}}$, 1 lb/in. = 175.13 N/m)

Concrete Mixture

Cement type I	
W/C	= 0.50
Specific Gravity, Coarse	= 2.56
Specific Gravity, Fine	= 2.65
Specific Gravity, Cement	= 3.15
Sand-Fineness Modulus	= 2.91
Maximum gravel size (crushed limestone)	= 19.0 mm (0.75 in.)
Maximum sand grain size	= not available
Percent Coarse by Weight	= 47.46
Percent Fine by Weight	= 32.68
Percent Cement by Weight	= 13.24
Percent Water by Weight	= 6.62

Beam Series Designation	Span Between Supports in.	Height of Beam in.	Width of Beam in.	f_c' psi	f_t' psi	E_c At 0.45 f_c' ksi
B	30	8	3	7,700	580	5,570
C	45	12	3	7,890	546	5,710

Beam Series Designation	J-Integral Method J_{Ic} lb/in.	RILEM Method G_f With Roughness Factor of 1.15 lb/in.	Direct Energy Method G_{Ic} lb/in.	Energy Release Method G_{Ic} lb/in.	Approximate Method G_{Ic} lb/in.	K_{Ic} psi$\sqrt{\text{in.}}$	K_{Ic}^2/E_c lb/in.
B	0.577	0.748	0.454	0.605	0.868	1,024	0.188
C	0.544	0.588	0.362	0.702	0.942	1,048	0.192

Table B-4
Fracture Toughness Test Results from Three-Point Beam Bending Tests on Notched Beams by Refai and Swartz (1988) (1 in. = 25.4 mm, 1 MPa = 145.04 psi, 1 MPa = 0.145 ksi, 1 lb/in. = 175.13 N/m, 1kN/m$^{3/2}$ = 0.91 psi$\sqrt{\text{in.}}$, 1 lb/in. = 175.13 N/m)

Concrete Mixture

Cement type I	
W/C	= 0.50
Specific Gravity, Coarse	= 2.56
Specific Gravity, Fine	= 2.65
Specific Gravity, Cement	= 3.15
Sand-Fineness Modulus	= 2.91
Maximum Gravel Size (crushed limestone)	= 0.75 in.
Maximum Sand Grain Size	= not available
Percent Coarse by Weight	= 47.46
Percent Fine by Weight	= 32.68
Percent Cement by Weight	= 13.24
Percent Water by Weight	= 6.62

Beam Series Designation	Span Between Supports in.	Height of Beam in.	Width of Beam in.	f'_c psi	f'_t psi	E_c At 0.45 f'_c ksi
B	30	8	3	7,700	580	5,570
C	45	12	3	7,890	546	5,710

Beam Series Designation	J-Integral Method J_{Ic} lb/in.	RILEM Method G_f lb/in.	Direct Energy Method G_{Ic} lb/in.	Energy Release Method G_{Ic} lb/in.	Approximate Method G_{Ic} lb/in.	K_{Ic} psi$\sqrt{\text{in.}}$	K_{Ic}^2/E_c lb/in.
B	0.501	0.388	0.387	0.333	0.622	1,024	0.188
C	0.940	0.640	0.538	0.645	1.176	1,048	0.192

Table B5
Fracture Toughness Test Results from In Situ Testing for Fracture Properties by Saouma, Broz, and Boggs (1991) (1 in. = 25.4 mm, 1 MPa = 145.04 psi, 1 kN/m$^{3/2}$ = 0.91 psi$\sqrt{\text{in.}}$)

Concrete Mixtures:

1. Water to Cement Ratio (W/C)   = 0.55
   Cement : Sand : Gravel   = 1 : 3.10 : 3.30 by weight
   Maximum gravel size (gravel 1, rounded river)   = 0.75 in.

2. W/C   = 0.55
   Cement : Sand : Gravel 1 : Gravel 2   = 1 : 3.11 : 2.43 : 2.43
                                                                                     by weight
   Maximum gravel size (Gravel 2, rounded river) = 1.50 in.
   Maximum gravel size (Gravel 1, rounded river) = 0.75 in.

3. W/C   = 0.55
   Cement : Sand : Gravel 1 : Gravel 2 : Gravel 3   = 1: 3.71 : 2.63 : 2.63 : 2.63
                                                                                     by weight
   Maximum gravel size (Gravel 3, rounded river) = 3.00 in.
   Maximum gravel size (Gravel 2, rounded river) = 1.50 in.
   Maximum gravel size (Gravel 1, rounded river) = 0.75 in.

Concrete Mixture	Max. Aggregate size in.	$f'_{t,sp}$ psi	$f'_{t,exp}$ psi	K_{Ic} psi$\sqrt{\text{in.}}$	K_{Ic}^{app} psi$\sqrt{\text{in.}}$
Mixture 1	0.75	406	509	923	1,290
Mixture 2	1.5	413	505	909	1,480
Mixture 3	3.0	397	378	991	1,260

Appendix C
Time-Dependent Variation of Compressive Strength for Snell Lock Concrete

This appendix presents figures showing the variations of the compressive strength results with time using data reported by Buck, Mather, and Thorton (1967)[1] and by Mosher, Bevins, and Neeley (1991) for tests conducted on Snell Lock concrete specimens. Snell Lock was constructed during the 1956 and 1957 construction seasons. Each monolith comprises about 60 percent exterior concrete mixture and 40 percent interior grade concrete mixture.

Figures C-1 through C-4 show the time-dependent variation of compressive strength f_c' for the 1956 exterior and interior mixtures while Figures C-5 through C-8 show the variation for the 1957 exterior and interior mixtures. The f_c' results for both Snell and Eisenhower Locks are reported in these eight figures. (Eisenhower Lock data are included for reference only.)

Figure C-1 shows the variation in compressive strength over the first 12 months for the 1956 exterior mixture. Figure C-2 shows these same data combined with additional f_c' measurements obtained during both the Buck, Mather, and Thorton 1967 study and the Mosher, Bevins, and Neeley 1991 study.

The value of Young's modulus E_c is known to correlate with the compressive strength. A frequently used relationship to approximate the value for Young's modulus in psi is

$$E_c = 33(w_c^{1.5})\sqrt{f_c'} \tag{C-1}$$

---

[1] References cited in this appendix are included in the References section at the end of the main text.

where w_c is the weight of concrete in lb/ft³, equal to 158.3 pcf (2,535.7 kg/m³) for Snell Lock, and f_c' is the compressive strength in psi. Another frequently used relationship is

$$E_c = 57,000\sqrt{f_c'} \qquad\qquad\qquad (C\text{-}2)$$

Mosher, Bevins, and Neeley (1991) conducted laboratory tests to measure values for Young's modulus and compressive strength f_c' using Snell Lock concrete specimens they recovered from borings in several of the lock monoliths (Table C-1). The Young's modulus values measured on ten of the concrete specimens were found to be in excess of values computed by the authors of this report using Equation C-1 by an average value of 29 percent (ranging from a low of 11 percent to a high of 57 percent). These calculations were made using the f_c' values measured in the laboratory by Mosher, Bevins, and Neeley and are listed in Table C-1. A similar series of computations was made by the authors of this report using Equation C-2, and it was observed that the measured Young's modulus values exceed the Equation C-2 value by an average of 49 percent (ranging from a low of 27 percent to a high of 80 percent).

Equations C-1 and C-2 were used by the authors of this report to estimate values of Young's modulus using the Snell Lock compressive strengths reported in Figures C-1 and C-2 for the 1956 exterior concrete mix. When Equation C-1 was used, a factor of 1.29 was applied to the computed results to correct for the observations described in the previous paragraph. Similarly, a factor of 1.49 was applied to the results computed using Equation C-2. The results of these computations are shown in Figures C-1b and C-2b. This approach was used on all Young's modulus approximations shown in Figures C-1 through C-8 for the Snell Lock concrete.
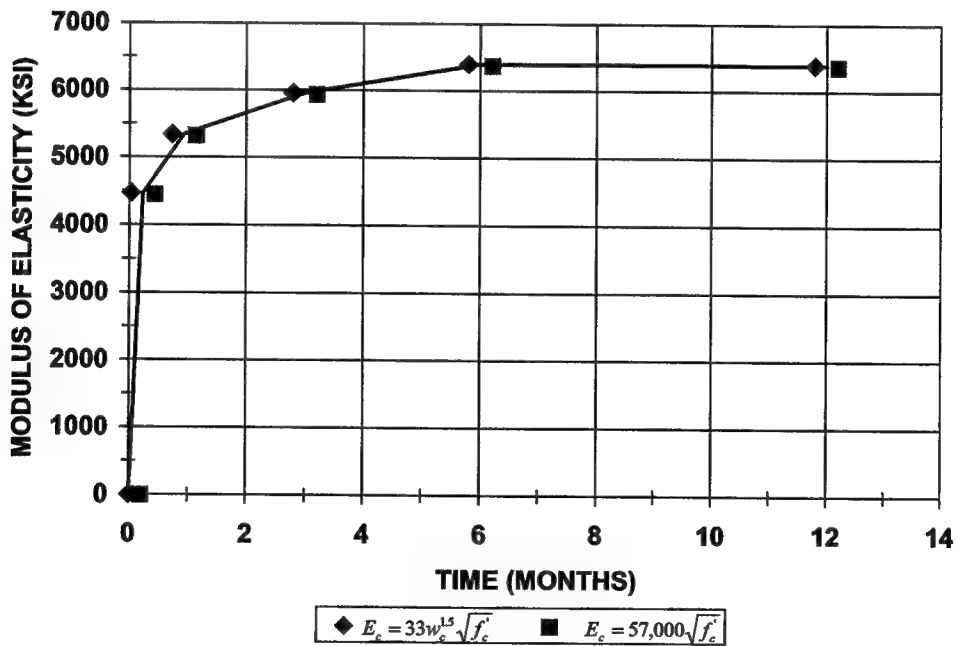
Figure C-3 shows the variation in compressive strength over the first 12 months for the 1956 interior mixture. Figure C-4 shows these same data combined with additional f_c' measurements obtained during both the Buck, Mather, and Thorton (1967) study and the Mosher, Bevins, and Neeley (1991) study. Also shown in these figures are values computed for the Young's modulus of Snell concrete using the two widely used relationships given in the figure multiplied by the previously described correction factors.

Figure C-5 shows the variation in compressive strength over the first 12 months for the 1957 exterior mixture. Figure C-6 shows these same data combined with additional f_c' measurements obtained during the Buck, Mather, and Thorton (1967) study and the Mosher, Bevins, and Neeley (1991) study. Also shown in these figures are values computed for the Young's modulus of Snell concrete using the two widely used relationships given in the figure multiplied by the previously described correction factors.

Figure C-7 shows the variation in compressive strength over the first 12 months for the 1957 interior mixture. Figure C-8 shows these same data combined with additional f_c' measurements obtained during the Buck, Mather, and Thorton (1967) study and the Mosher, Bevins, and Neeley (1991) study. Also shown in these figures are values computed for the Young's modulus of Snell concrete using the two widely used relationships given in the figure multiplied by the previously described correction factors.
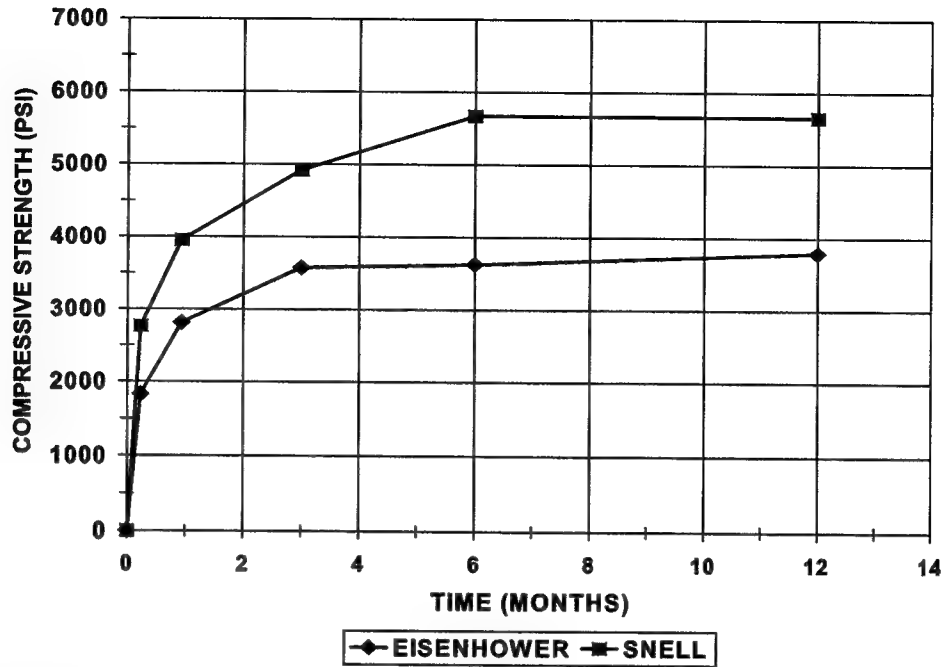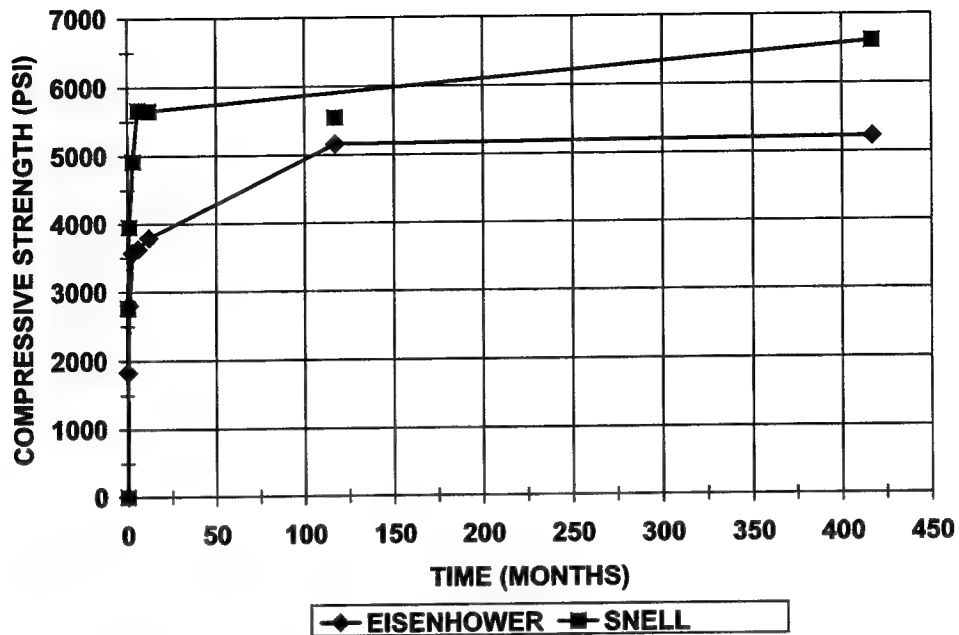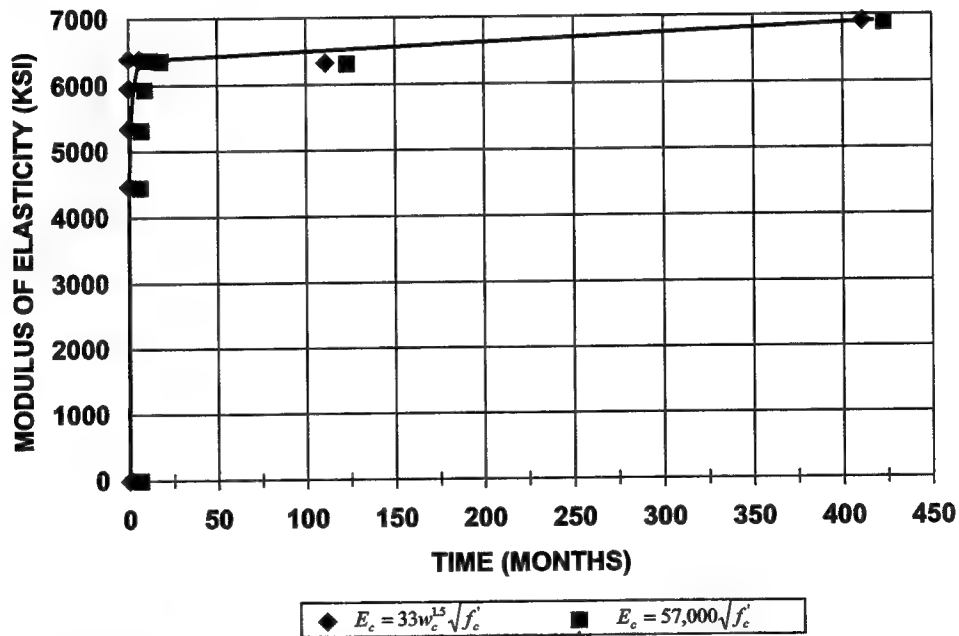
a. Measured compressive strength

b. Calculated modulus of elasticity

Figure C-1. Twelve-month variation in compresisve strength and modulus of elasticity with time for 1956 exterior mixture

COMPRESSIVE STRENGTH (PSI)

7000
6000
5000
4000
3000
2000
1000
0

0 50 100 150 200 250 300 350 400 450

TIME (MONTHS)

EISENHOWER SNELL

a. Measured compressive strength

MODULUS OF ELASTICITY (KSI)

7000
6000
5000
4000
3000
2000
1000
0

0 50 100 150 200 250 300 350 400 450

TIME (MONTHS)

$E_c = 33w_c^{1.5}\sqrt{f_c'}$ $E_c = 57,000\sqrt{f_c'}$

b. Calculated modulus of elasticity

Figure C-2. Multiyear variation in compressive strength and modulus of elasticity with time for 1956 exterior mixture with additional f_c' measurements from Buck, Mather, and Thorton (1967) and Mosher, Bevins, and Neeley (1991)

a. Measured compressive strength

b. Calculated modulus of elasticity

Figure C-3. Twelve-month variation of compressive strength and modulus of elasticity with time for 1956 interior mixture
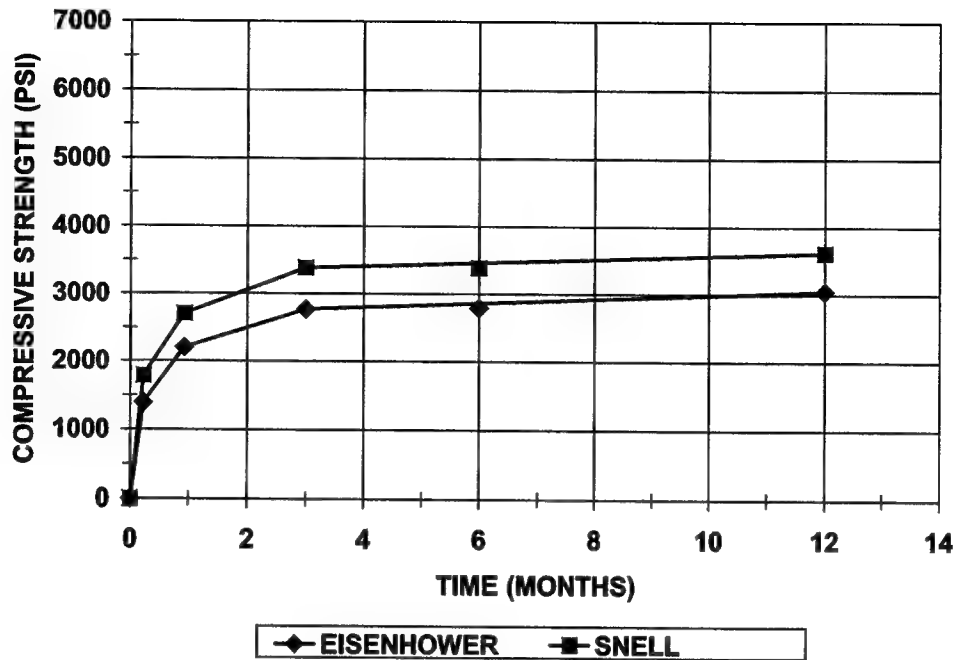
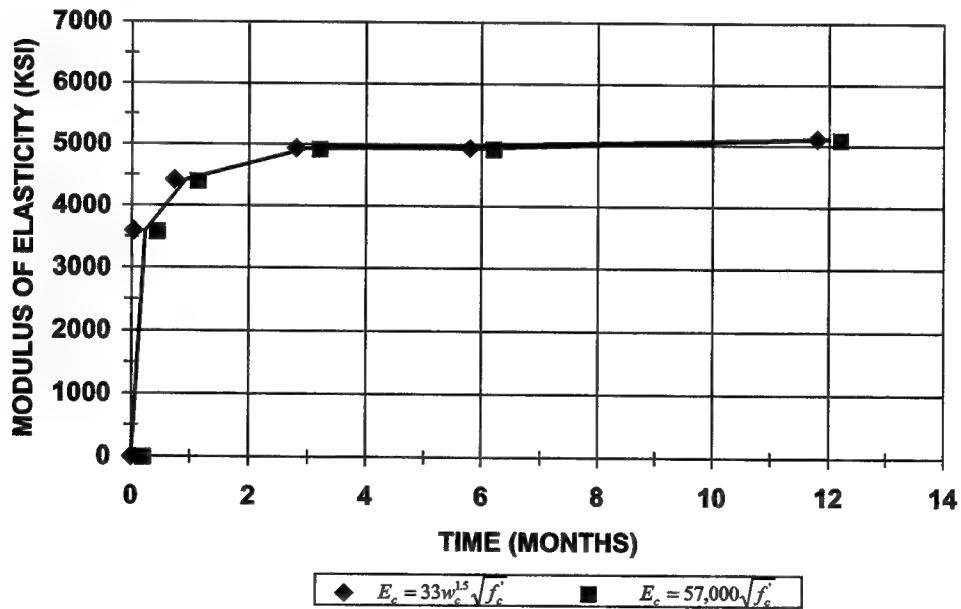a. Measured compressive strength

b. Caluclated modulus of elasticity

Figure C-4.   Multiyear variation in compressive strength and modulus of elasticity with time for 1956 interior mixture with additional f_c' measurements from Buck, Mather, and Thorton (1967) and Mosher, Bevins, and Neeley (1991)
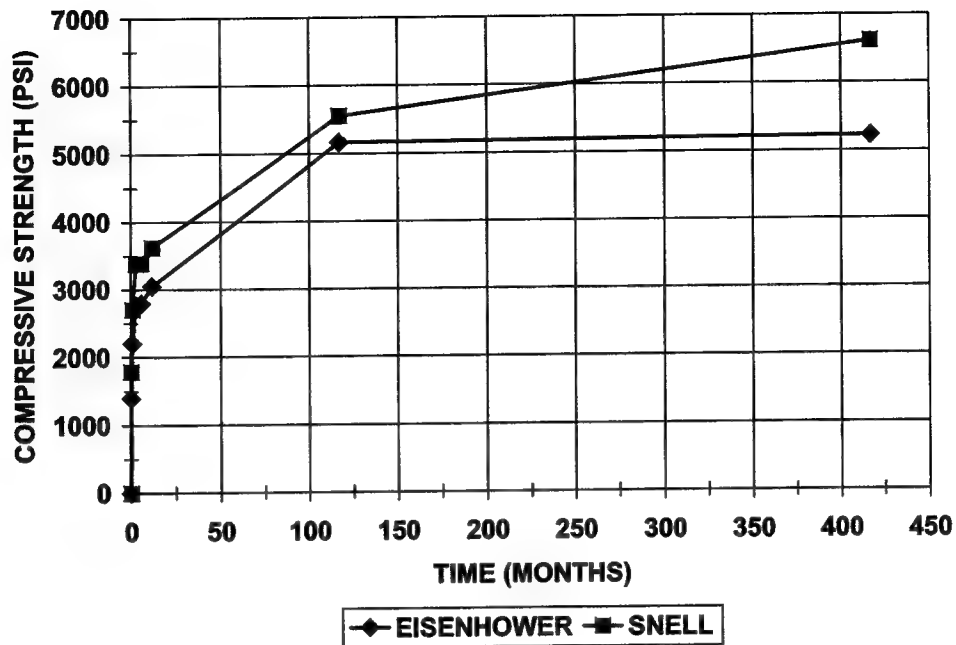
a. Measured compressive strength

b. Calculated modulus of elasticity

Figure C-5. Twelve-month variation in compressive strength and modulus of elasticity with time for 1957 exterior mixture

Appendix C   Time-Dependent Variation of Compressive Strength for Snell Lock Concrete
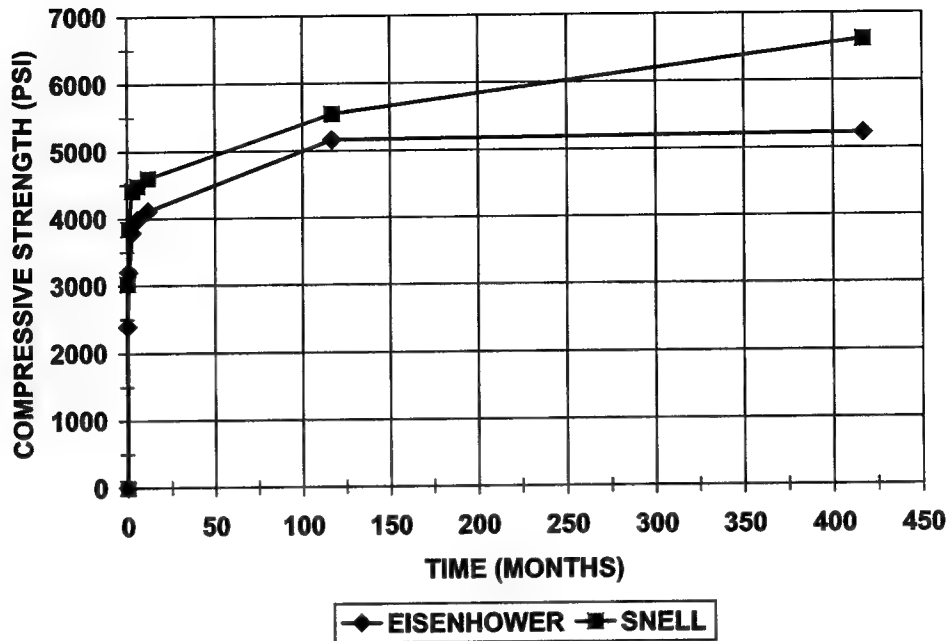
a. Measured compressive strength
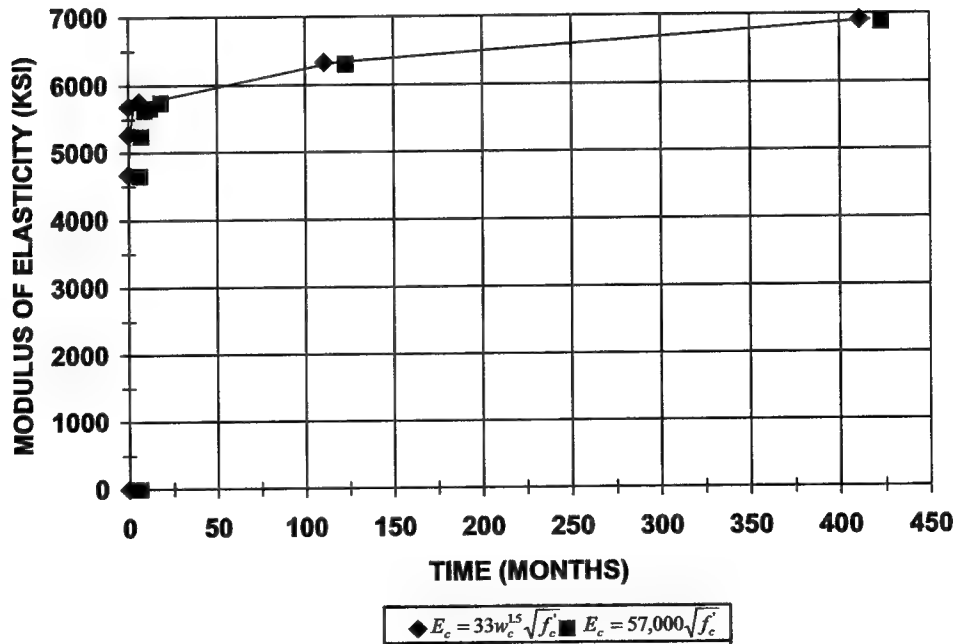
b. Calculated modulus of elasticity

Figure C-6. Multiyear variation in compressive strength and modulus of elasticity with time for 1957 exterior mixture with additional f_c' measurements from Buck, Mather, and Thorton (1967) and Mosher, Bevins, and Neeley (1991)
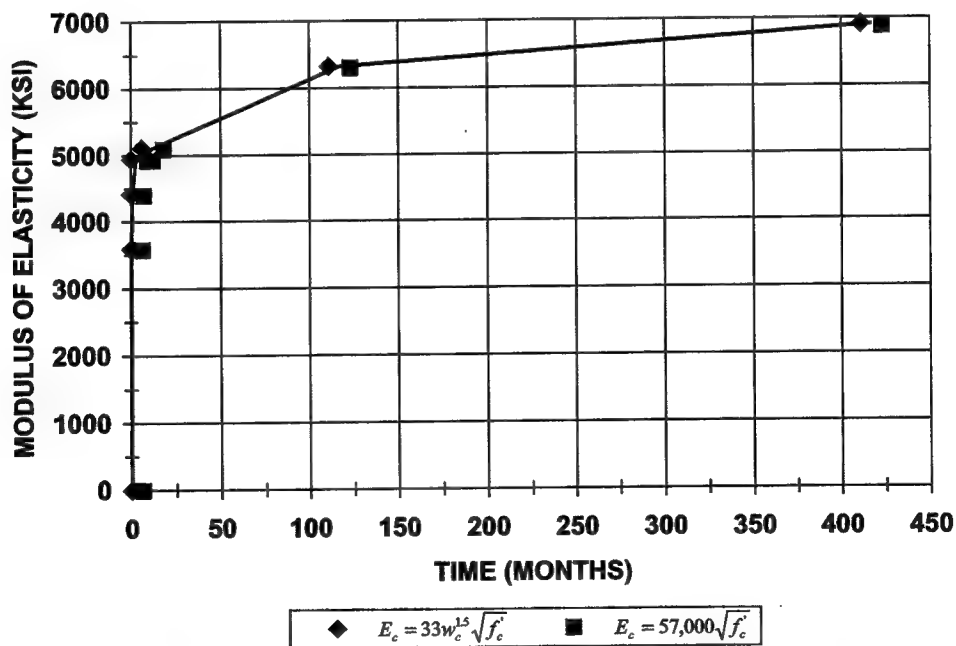
a. Measured compressive strength

b. Calculated modulus of elasticity

Figure C-7.   Twelve-month variation in compressive strength and modulus of
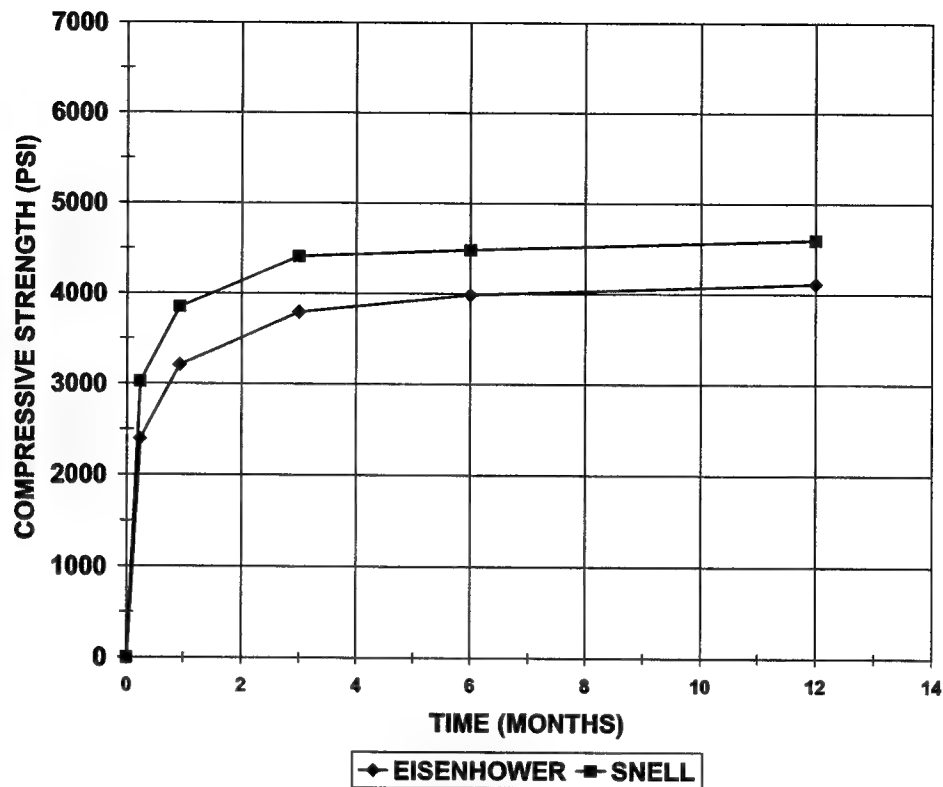elasticity with time for 1957 interior mixture
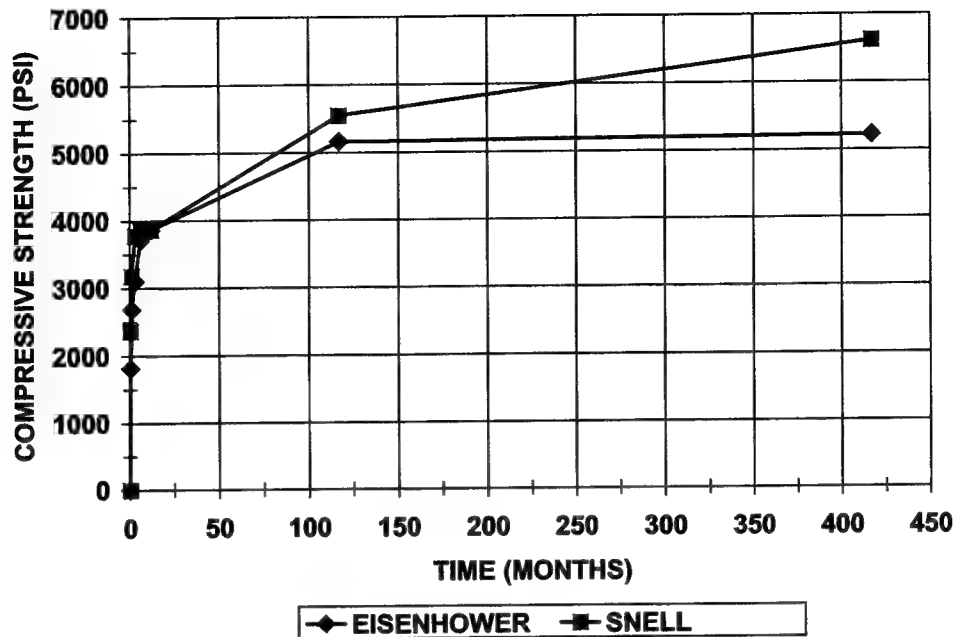
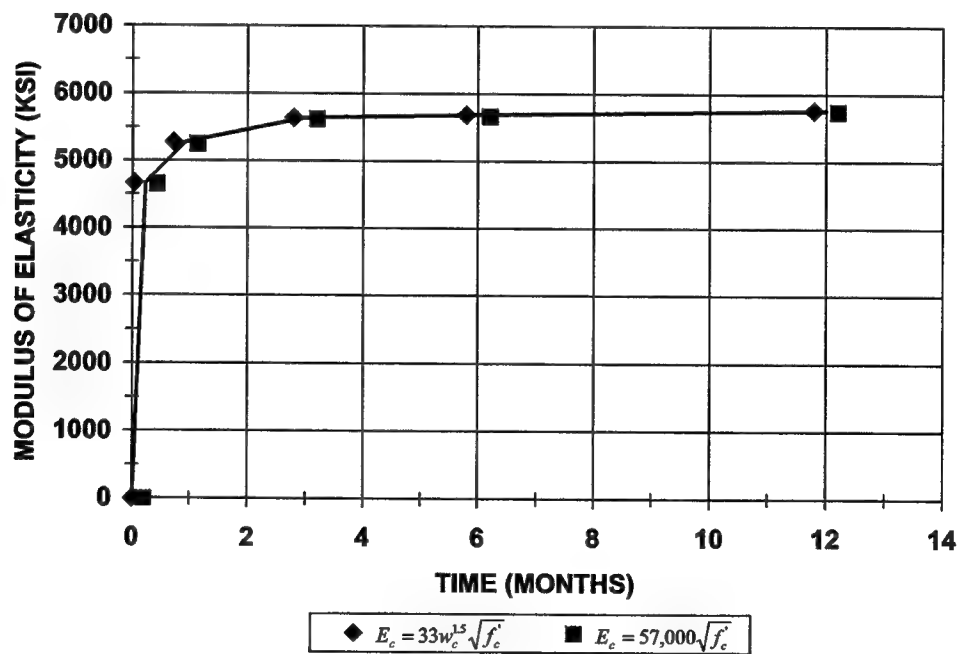a. Measured compressive strength
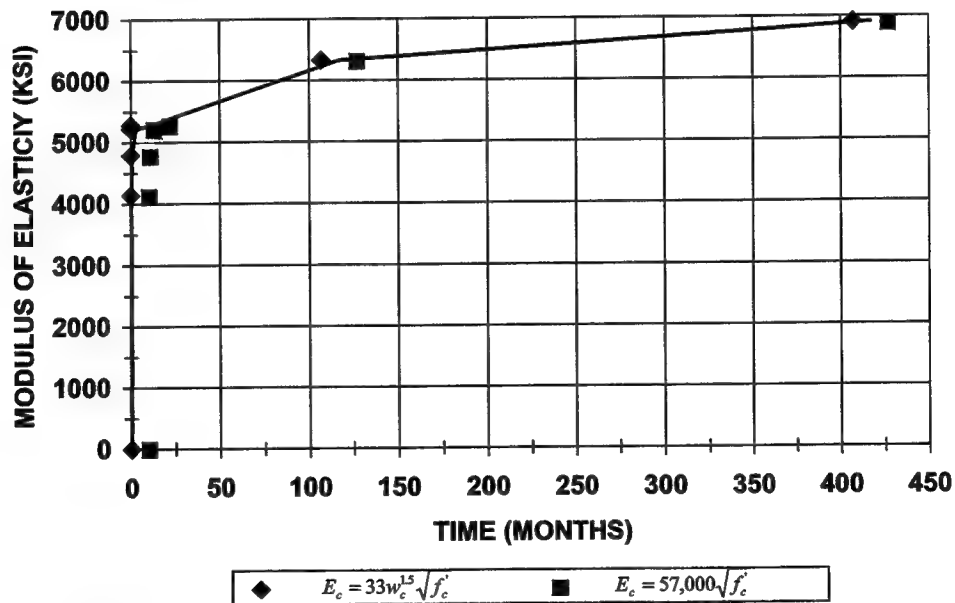
b. Calculated modulus of elasticity

Figure C-8. Multiyear variation in compressive strength and modulus of elasticity with time for 1957 interior mixture with additional f_c' measurements from Buck, Mather, and Thorton (1967) and Mosher, Bevins, and Neeley (1991)
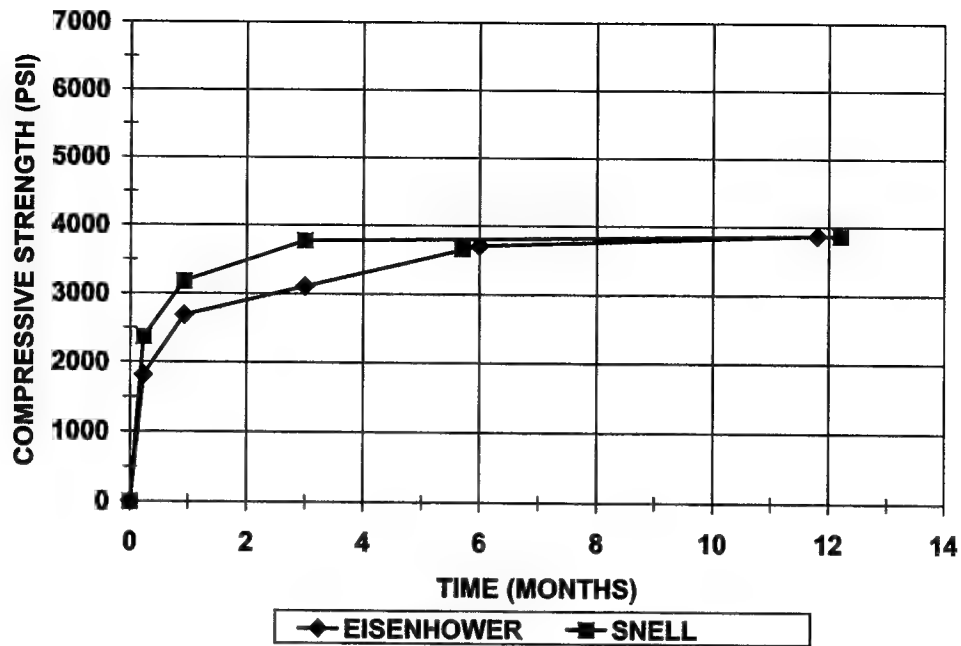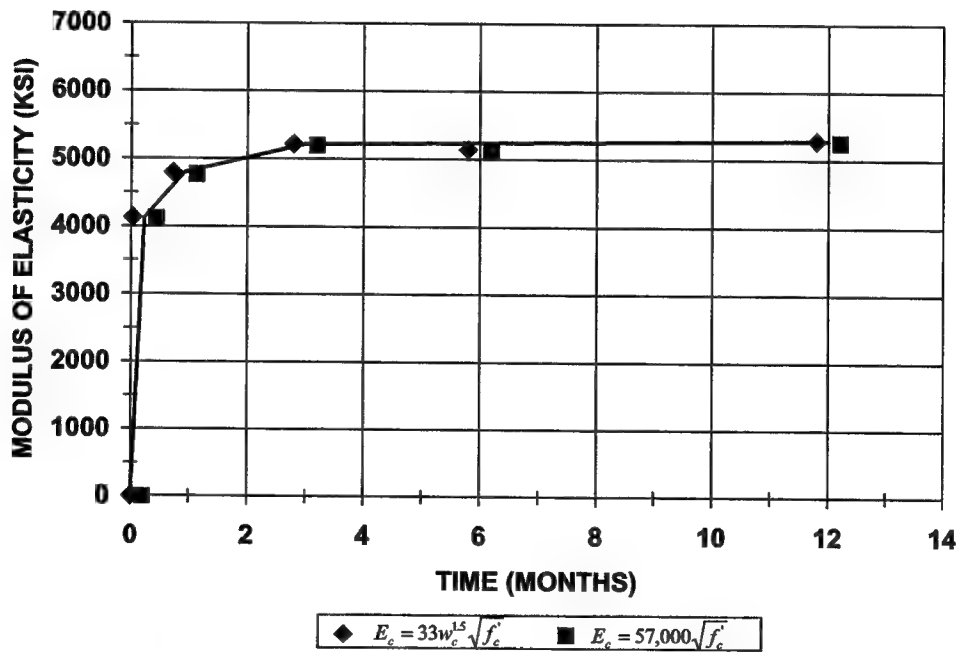
Table C-1
Evaluation of Scaling Factors for Two Empirical Young's Modulus Relationships Using Snell Lock Concrete Data (1 ft = 0.305 m, 1 pcf =16.018 kg/m^3, 1 MPa = 145.04 psi)

Snell Specimen No.	Average EI ft	Density pcf	f'_c psi	Measured E_c million psi	E		Scaling Factor	
					Eqn. C-1 million psi	Eqn. C-2 million psi	Eqn. C-1	Eqn. C-2
1-50	2.25	156.50	7420	6.60	5.57	4.91	1.19	1.34
6-52	25.95	159.10	5940	6.95	5.10	4.39	1.36	1.58
11-54	48.15	155.50	7460	7.70	5.53	4.92	1.39	1.56
19-56	82.5	157.40	7870	6.40	5.78	5.06	1.11	1.27
23-58	98.2	155.90	3730	4.60	3.92	3.48	1.17	1.32
3-63	10.8	162.90	8360	7.50	6.27	5.21	1.20	1.44
9-64	35.7	161.10	5980	6.45	5.22	4.41	1.24	1.46
12-67	47.9	158.70	8590	8.95	6.11	5.28	1.46	1.69
16-69	64.85	157.20	4540	6.90	4.38	3.84	1.57	1.80
17-70	69.35	155.30	6260	6.25	5.05	4.51	1.24	1.39

Average =   1.29   1.49

REPORT DOCUMENTATION PAGE		Form Approved OMB No. 0704-0188

1. REPORT DATE (DD-MM-YYYY) December 2001	2. REPORT TYPE Final report	3. DATES COVERED (From - To)

4. TITLE AND SUBTITLE
Smeared and Discrete Crack Evaluations of a Lock Exhibiting Earth Pressure-Induced Cracking

5a. CONTRACT NUMBER

5b. GRANT NUMBER

5c. PROGRAM ELEMENT NUMBER

6. AUTHOR(S)

Robert M. Ebeling, Robert C. Patev, Guillermo A. Riveros

5d. PROJECT NUMBER

5e. TASK NUMBER

5f. WORK UNIT NUMBER
31589

7. PERFORMING ORGANIZATION NAME(S) AND ADDRESS(ES)

U.S. Army Engineer Research and Development Center
Information Technology Laboratory
3909 Halls Ferry Road
Vicksburg, MS 39180-6199;
U.S. Army Engineer District, New England
969 Virginia Road
Concord, MA 01742-2751

8. PERFORMING ORGANIZATION REPORT NUMBER

ERDC/ITL TR-01-7

9. SPONSORING / MONITORING AGENCY NAME(S) AND ADDRESS(ES)

U.S. Army Corps of Engineers
Washington, DC 20314-1000

10. SPONSOR/MONITOR'S ACRONYM(S)

11. SPONSOR/MONITOR'S REPORT NUMBER(S)

12. DISTRIBUTION / AVAILABILITY STATEMENT

Approved for public release; distribution is unlimited.

13. SUPPLEMENTARY NOTES

14. ABSTRACT
    This report discusses the results of an evaluation of crack initiation and propagation at Snell Lock, one of the locks constructed on the St. Lawrence Seaway during 1956 and 1957. The rock-founded, unreinforced concrete gravity lock walls of Snell Lock experienced cracking as a result of earth loading in excess of those anticipated during structural design. The objective of this study is to appraise two analytical procedures used to evaluate the potential for and/or the extent of cracking within massive concrete structures.

    The two analytical procedures available for analyzing hydraulic structures that may exhibit cracking during loading are based on either the smeared crack theory or the discrete crack theory. The smeared crack theory uses a strength-of-materials approach to evaluate crack initiation potential and/or crack propagation in a material. A linear elastic fracture mechanics (LEFM) discrete crack analysis is used to assess if a discrete crack will propagate or arrest for a given increment of loading. Generally, LEFM relate the stress magnitude and distribution at the crack tip to the nominal stress applied to the structure; to the size, shape, and orientation of the crack or discontinuity; and to the material properties. The *demand* due to loading(s) applied to the retaining structure and specifically to the region of cracking is represented by stress intensity factors. The *capacity* of the material is characterized by the fracture toughness.

(Continued)

15. SUBJECT TERMS

Aging of concrete	Crack	Hydraulic concrete structure	NISA
At-rest earth pressures	Discrete crack	LEFM	Smeared crack
Compaction-induced earth pressures	Fracture mechanics	Massive concrete lock wall	Thermal stresses

16. SECURITY CLASSIFICATION OF:			17. LIMITATION OF ABSTRACT	18. NUMBER OF PAGES	19a. NAME OF RESPONSIBLE PERSON
a. REPORT UNCLASSIFIED	c. ABSTRACT UNCLASSIFIED	c. THIS PAGE UNCLASSIFIED		131	19b. TELEPHONE NUMBER (include area code)

14. (Concluded).

Cracking potential and crack extent for Snell Lock are assessed for both short-term, end-of-construction earth loading and long-term earth and water loading. A finite element thermal analysis (a nonlinear incremental structural analysis (NISA) based on smeared crack theory) performed on Snell Lock Monolith N-56 gives the strong indication that the potential for cracking in the upper right corner of the lower monolith did exist after the backfilling was complete in 1957 (referred to as end of construction earth loading in this report). These results also indicate that microcracks in the mass concrete in the culvert area were created during the winter of 1956/1957. Upon an increase in stress intensity due to the backfilling and overcompaction of the glacial till, these cracks extended to the inclined surface (i.e., the back face) of the lock wall. For the boundary condition of a crack initiating at the landward-ceiling corner of the filling and emptying culvert, both series of LEFM analyses show that the demand (i.e., the stress intensity factor) increases with crack extension. This implies that if the demand was sufficient to overcome the capacity of the concrete (i.e., the fracture toughness) at the early stages of cracking, the crack will propagate to the backfilled face of the wall.

REPORTS PUBLISHED UNDER THE COMPUTER-AIDED STRUCTURAL ENGINEERING (CASE) PROJECT

	Title	Date
Technical Report K-78-1	List of Computer Programs for Computer-Aided Structural Engineering	Feb 1978
Instruction Report 0-79-2	User's Guide: Computer Program with Interactive Graphics for Analysis of Plane Frame Structures (CFRAME)	Mar 1979
Technical Report K-80-1	Survey of Bridge-Oriented Design Software	Jan 1980
Technical Report K-80-2	Evaluation of Computer Programs for the Design/Analysis of Highway and Railway Bridges	Jan 1980
Instruction Report K-80-1	User's Guide: Computer Program for Design/Review of Curvi-linear Conduits/Culveris (CURCON)	Feb 1980
Instruction Report K-80-3	A Three-Dimensional Finite Element Data Edit Program	Mar 1980
Instruction Report K-80-4	A Three-Dimensional Stability Analysis/Design Program (3DSAD) Report 1: General Geometry Module Report 3: General Analysis Module (CGAM) Report 4: Special-Purpose Modules for Dams (CDAMS)	Jun 1980 Jun 1982 Aug 1983
Instruction Report K-80-6	Basic User's Guide: Computer Program for Design and Analysis of Inverted-T Retaining Walls and Floodwalls (TWDA)	Dec 1980
Instruction Report K-80-7	User's Reference Manual: Computer Program for Design and Analysis of Inverted-T Retaining Walls and Floodwalls (TWDA)	Dec 1980
Technical Report K-80-4	Documentation of Finite Element Analyses Report 1: Longview Outlet Works Conduit Report 2: Anchored Wall Monolith, Bay Springs Lock	Dec 1980 Dec 1980
Technical Report K-80-5	Basic Pile Group Behavior	Dec 1980
Instruction Report K-81-2	User's Guide: Computer Program for Design and Analysis of Sheet Pile Walls by Classical Methods (CSHTWAL) Report 1: Computational Processes Report 2: Interactive Graphics Options	Feb 1981 Mar 1981
Instruction Report K-81-3	Validation Report: Computer Program for Design and Analysis of Inverted-T Retaining Walls and Floodwalls (TWDA)	Feb 1981
Instruction Report K-81-4	User's Guide: Computer Program for Design and Analysis of Cast-in-Place Tunnel Linings (NEWTUN)	Mar 1981
Instruction Report K-81-6	User's Guide: Computer Program for Optimum Nonlinear Dynamic Design of Reinforced Concrete Slabs Under Blast Loading (CBARCS)	Mar 1981
Instruction Report K-81-7	User's Guide: Computer Program for Design or Investigation of Orthogonal Culverts (CORTCUL)	Mar 1981
Instruction Report K-81-9	User's Guide: Computer Program for Three-Dimensional Analysis of Building Systems (CTABS80)	Aug 1981
Technical Report K-81-2	Theoretical Basis for CTABS80: A Computer Program for Three-Dimensional Analysis of Building Systems	Sep 1981

(Continued)

REPORTS PUBLISHED UNDER THE COMPUTER-AIDED
STRUCTURAL ENGINEERING (CASE) PROJECT

	Title	Date
Instruction Report K-82-6	User's Guide: Computer Program for Analysis of Beam-Column Structures with Nonlinear Supports (CBEAMC)	Jun 1982
Instruction Report K-82-7	User's Guide: Computer Program for Bearing Capacity Analysis of Shallow Foundations (CBEAR)	Jun 1982
Instruction Report K-83-1	User's Guide: Computer Program with Interactive Graphics for Analysis of Plane Frame Structures (CFRAME)	Jan 1983
Instruction Report K-83-2	User's Guide: Computer Program for Generation of Engineering Geometry (SKETCH)	Jun 1983
Instruction Report K-83-5	User's Guide: Computer Program to Calculate Shear, Moment, and Thrust (CSMT) from Stress Results of a Two-Dimensional Finite Element Analysis	Jul 1983
Technical Report K-83-1	Basic Pile Group Behavior	Sep 1983
Technical Report K-83-3	Reference Manual: Computer Graphics Program for Generation of Engineering Geometry (SKETCH)	Sep 1983
Technical Report K-83-4	Case Study of Six Major General-Purpose Finite Element Programs	Oct 1983
Instruction Report K-84-2	User's Guide: Computer Program for Optimum Dynamic Design of Nonlinear Metal Plates Under Blast Loading (CSDOOR)	Jan 1984
Instruction Report K-84-7	User's Guide: Computer Program for Determining Induced Stresses and Consolidation Settlements (CSETT)	Aug 1984
Instruction Report K-84-8	Seepage Analysis of Confined Flow Problems by the Method of Fragments (CFRAG)	Sep 1984
Instruction Report K-84-11	User's Guide for Computer Program CGFAG, Concrete General Flexure Analysis with Graphics	Sep 1984
Technical Report K-84-3	Computer-Aided Drafting and Design for Corps Structural Engineers	Oct 1984
Technical Report ATC-86-5	Decision Logic Table Formulation of ACI 318-77, Building Code Requirements for Reinforced Concrete for Automated Constraint Processing, Volumes I and 11	Jun 1986
Technical Report ITL-87-2	A Case Committee Study of Finite Element Analysis of Concrete Flat Slabs	Jan 1987
Instruction Report ITL-87-2 (Revised)	User's Guide for Concrete Strength Investigation and Design (CASTR) in Accordance with ACI 318-89	Mar 1992
Instruction Report ITL-87-1	User's Guide: Computer Program for Two-Dimensional Analysis of U-Frame Structures (CUFRAM)	Apr 1987
Instruction Report ITL-87-2	User's Guide: For Concrete Strength Investigation and Design (CASTR) in Accordance with ACI 318-83	May 1987
Technical Report ITL-87-6	Finite-Element Method Package for Solving Steady-State Seepage Problems	May 1987

(Continued)

REPORTS PUBLISHED UNDER THE COMPUTER-AIDED STRUCTURAL ENGINEERING (CASE) PROJECT

	Title	Date
Instruction Report ITL-87-3	User's Guide: A Three-Dimensional Stability Analysis/Design Program (3DSAD) Module	Jun 1987
	Report 1: Revision 1: General Geometry	Jun 1987
	Report 2: General Loads Module	Sep 1989
	Report 6: Free-Body Module	Sep 1989
Instruction Report ITL-87-4	User's Guide: 2-D Frame Analysis Link Program (LINK2D)	Jun 1987
Technical Report ITL-87-4	Finite Element Studies of a Horizontally Framed Miter Gate	Aug 1987
	Report 1: Initial and Refined Finite Element Models (Phases A, B, and C), Volumes I and 11	
	Report 2: Simplified Frame Model (Phase D)	
	Report 3: Alternate Configuration Miter Gate Finite Element Studies-Open Section	
	Report 4: Alternate Configuration Miter Gate Finite Element Studies-Closed Sections	
	Report 5: Alternate Configuration Miter Gate Finite Element Studies-Additional Closed Sections	
	Report 6: Elastic Buckling of Girders in Horizontally Framed Miter Gates	
	Report 7: Application and Summary	
Instruction Report GL-87-1	User's Guide: UTEXAS2 Slope-Stability Package; Volume 1, User's Manual	Aug 1987
Instruction Report ITL-87-5	Sliding Stability of Concrete Structures (CSLIDE)	Oct 1987
Instruction Report ITL-87-6	Criteria Specifications for and Validation of a Computer Program for the Design or Investigation of Horizontally Framed Miter Gates (CMITER)	Dec 1987
Technical Report ITL-87-8	Procedure for Static Analysis of Gravity Dams Using the Finite Element Method - Phase la	Jan 1988
Instruction Report ITL-88-1	User's Guide: Computer Program for Analysis of Planar Grid Structures (CGRID)	Feb 1988
Technical Report ITL-88-1	Development of Design Formulas for Ribbed Mat Foundations on Expansive Soils	Apr 1988
Technical Report ITL-88-2	User's Guide: Pile Group Graphics Display (CPGG) Postprocessor to CPGA Program	Apr 1988
Instruction Report ITL-88-2	User's Guide for Design and Investigation of Horizontally Framed Miter Gates (CMITER)	Jun 1988
Instruction Report ITL-88-4	User's Guide for Revised Computer Program to Calculate Shear, Moment, and Thrust (CSMT)	Sep 1988
Instruction Report GL-87-1	User's Guide: UTEXAS2 Slope-Stability Package; Volume 11, Theory	Feb 1989
Technical Report ITL-89-3	User's Guide: Pile Group Analysis (CPGA) Computer Group	Jul 1989

(Continued)

3

REPORTS PUBLISHED UNDER THE COMPUTER-AIDED
STRUCTURAL ENGINEERING (CASE) PROJECT

	Title	Date
Technical Report ITL-89-4	CBASIN-Structural Design of Saint Anthony Falls Stilling Basins According to Corps of Engineers Criteria for Hydraulic Structures; Computer Program X0098	Aug 1989
Technical Report ITL-89-5	CCHAN-Structural Design of Rectangular Channels According to Corps of Engineers Criteria for Hydraulic Structures; Computer Program X0097	Aug 1989
Technical Report ITL-89-6	The Response-Spectrum Dynamic Analysis of Gravity Dams Using the Finite Element Method; Phase 11	Aug 1989
Contract Report ITL-89-1	State of the Art on Expert Systems Applications in Design, Construction, and Maintenance of Structures	Sep 1989
Instruction Report ITL-90-1	User's Guide: Computer Program for Design and Analysis of Sheet Pile Walls by Classical Methods (CWALSHT)	Feb 1990
Instruction Report ITL-90-2	User's Guide: Pile Group-Concrete Pile Analysis Program (CPGC) Preprocessor to CPGA Program	Jun 1990
Instruction Report ITL-90-3	Investigation and Design of U-Frame Structures Using Program CUFRBC	
	Volume A: Program Criteria and Documentation	May 1990
	Volume B: User's Guide for Basins	May 1990
	Volume C: User's Guide for Channels	May 1990
Instruction Report ITL-90-6	User's Guide: Computer Program for Two-Dimensional Analysis of U-Frame or W-Frame Structures (CWFRAM)	Sep 1990
Technical Report ITL-91-3	Application of Finite Element, Grid Generation, and Scientific Visualization Techniques to 2-D and 3-D Seepage and Groundwater Modeling	Sep 1990
Instruction Report ITL-91-1	User's Guide: Computer Program for Design and Analysis of Sheet-Pile Walls by Classical Methods (CWALSHT) Including Rowe's Moment Reduction	Oct 1991
Technical Report ITL-92-2	Finite Element Modeling of Welded Thick Plates for Bonneville Navigation Lock	May 1992
Technical Report ITL-92-4	Introduction to the Computation of Response Spectrum for Earthquake Loading	Jun 1992
Instruction Report ITL-92-3	Concept Design Example, Computer-Aided Structural Modeling (CASM)	
	Report 1: Scheme A	Jun 1992
	Report 2: Scheme B	Jun 1992
	Report 3: Scheme C	Jun 1992
Instruction Report ITL-92-4	User's Guide: Computer-Aided Structural Modeling (CASM) – Version 3.00	Apr 1992
Instruction Report ITL-92-5	Tutorial Guide: Computer-Aided Structural Modeling (CASM) - Version 3.00	Apr 1992

(Continued)

REPORTS PUBLISHED UNDER THE COMPUTER-AIDED STRUCTURAL ENGINEERING (CASE) PROJECT

	Title	Date
Contract Report ITL-92-1	Optimization of Steel Pile Foundations Using Optimality Criteria	Jun 1992
Technical Report ITL-92-7	Refined Stress Analysis of Melvin Price Locks and Dam	Sep 1992
Contract Report ITL-92-2	Knowledge-Based Expert System for Selection and Design of Retaining Structures	Sep 1992
Contract Report ITL-92-3	Evaluation of Thermal and Incremental Construction Effects for Monoliths AL-3 and AL-5 of the Melvin Price Locks and Dam	Sep 1992
Instruction Report GL-87-1	User's Guide: UTEXAS3 Slope-Stability Package; Volume IV, User's Manual	Nov 1992
Technical Report ITL-92-11	The Seismic Design of Waterfront Retaining Structures	Nov 1992
Technical Report ITL-92-12	Computer-Aided, Field-Verified Structural Evaluation	
	Report 1: Development of Computer Modeling Techniques for Miter Lock Gates	Nov 1992
	Report 2: Field Test and Analysis Correlation at John Hollis Bankhead Lock and Dam	Dec 1992
	Report 3: Field Test and Analysis Correlation of a Vertically Framed Miter Gate at Emsworth Lock and Dam	Dec 1993
Instruction Report GL-87-1	Users Guide: UTEXAS3 Slope-Stability Package; Volume III, Example Problems	Dec 1992
Technical Report ITL-93-1	Theoretical Manual for Analysis of Arch Dams	Jul 1993
Technical Report ITL-93-2	Steel Structures for Civil Works, General Considerations for Design and Rehabilitation	Aug 1993
Technical Report ITL-93-3	Soil-Structure Interaction Study of Red River Lock and Dam No. 1 Subjected to Sediment Loading	Sep 1993
Instruction Report ITL-93-3	User's Manual-ADAP, Graphics-Based Dam Analysis Program	Aug 1993
Instruction Report ITL-93-4	Load and Resistance Factor Design for Steel Miter Gates	Oct 1993
Technical Report ITL-94-2	User's Guide for the Incremental Construction, Soil-Structure Interaction Program SOILSTRUCT with Far-Field Boundary Elements	Mar 1994
Instruction Report ITL-94-1	Tutorial Guide: Computer-Aided Structural Modeling (CASM); Version 5.00	Apr 1994
Instruction Report ITL-94-2	User's Guide: Computer-Aided Structural Modeling (CASM); Version 5.00	Apr 1994
Technical Report ITL-94-4	Dynamics of Intake Towers and Other MDOF Structures Under Earthquake Loads: A Computer-Aided Approach	Jul 1994
Technical Report ITL-94-5	Procedure for Static Analysis of Gravity Dams Including Foundation Effects Using the Finite Element Method - Phase 1 B	Jul 1994
Instruction Report ITL-94-5	User's Guide: Computer Program for Winkler Soil-Structure Interaction Analysis of Sheet-Pile Walls (CWALSSI)	Nov 1994

(Continued)

REPORTS PUBLISHED UNDER THE COMPUTER-AIDED STRUCTURAL ENGINEERING (CASE) PROJECT

	Title	Date
Instruction Report ITL-94-6	User's Guide: Computer Program for Analysis of Beam-Column Structures with Nonlinear Supports (CBEAMC)	Nov 1994
Instruction Report ITL-94-7	User's Guide to CTWALL - A Microcomputer Program for the Analysis of Retaining and Flood Walls	Dec 1994
Contract Report ITL-95-1	Comparison of Barge Impact Experimental and Finite Element Results for the Lower Miter Gate of Lock and Dam 26	Jun 1995
Technical Report ITL-95-5	Soil-Structure Interaction Parameters for Structured/Cemented Silts	Aug 1995
Instruction Report ITL-95-1	User's Guide: Computer Program for the Design and Investigation of Horizontally Framed Miter Gates Using the Load and Resistance Factor Criteria (CMITER-LRFD)	Aug 1995
Technical Report ITL-95-8	Constitutive Modeling of Concrete for Massive Concrete Structures, A Simplified Overview	Sep 1995
Instruction Report ITL-96-1	Use's Guide: Computer Program for Two-Dimensional Dynamic Analysis of U-Frame or W-Frame Structures (CDWFRM)	Jun 1996
Instruction Report ITL-96-2	Computer-Aided Structural Modeling (CASM), Version 6.00 　　　　Report 1: Tutorial Guide 　　　　Report 2: User's Guide 　　　　Report 3: Scheme A 　　　　Report 4: Scheme B 　　　　Report 5: Scheme C	Jun 1996
Technical Report ITL-96-8	Hyperbolic Stress-Strain Parameters for Structured/Cemented Silts	Aug 1996
Instruction Report ITL-96-3	User's Guide: Computer Program for the Design and Investigation of Horizontally Framed Miter Gates Using the Load and Resistance Factor Criteria (CMITERW-LRFD) Windows Version	Sep 1996
Instruction Report ITL-97-1	User's Guide: Computer Aided Inspection Forms for Hydraulic Steel Structures (CAIF-HSS), Windows Version	Sep 1996
Instruction Report ITL-97-2	User's Guide: Arch Dam Stress Analysis System (ADSAS)	Aug 1996
Instruction Report ITL-98-1	User's Guide for the Three-Dimensional Stability Analysis/Design (3DSAD) Program	Sep 1998
Technical Report ITL-98-4	Investigation of At-Rest Soil Pressures due to Irregular Sloping Soil Surfaces and CSOILP User's Guide	Sep 1998
Technical Report ITL-98-5	The Shear Ring Method and the Program Ring Wall	Sep 1998
Technical Report ITL-98-6	Reliability and Stability Assessment of Concrete Gravity Structures (RCSLIDE): Theoretical Manual	Dec 1998

(Continued)

6

REPORTS PUBLISHED UNDER THE COMPUTER-AIDED STRUCTURAL ENGINEERING (CASE) PROJECT

(Concluded)

	Title	Page
Technical Report ITL-99-1	Development of an Improved Numerical Model for Concrete-to-Soil Interfaces in Soil-Structure Interaction Analyses	
	Report 1: Preliminary Study	Jan 1999
	Report 2: Final Study	Aug 2000
Technical Report ITL-99-5	River Replacement Analysis	Dec 1999
ERDC/ITL TR-00-1	Evaluation and Comparison of Stability Analysis and Uplift Criteria for Concrete Gravity Dams by Three Federal Agencies	Jan 2000
ERDC/ITL TR-00-2	Reliability and Stability Assessment of Concrete Gravity Structures (RCSLIDE): User's Guide	Jul 2000
ERDC/ITL TR-00-5	Theoretical Manual for Pile Foundations	Nov 2000
ERDC/ITL TR-01-2	SOILSTRUCT-ALPHA for Personal Computers Report 1: Visual Modeler	Dec 2001
ERDC/ITL TR-01-3	Finite Element Modeling of Cooling Coil Effects in Mass Concrete Systems	Aug 2001
ERDC/ITL TR-01-4	Investigation of Wall Friction, Surcharge Loads, and Moment Reduction Curves for Anchored Sheet-Pile Walls	Sep 2001
ERDC/ITL TR-01-7	Smeared and Discrete Crack Evaluations of a Lock Exhibiting Earth Pressure-Induced Cracking	Dec 2001